IOP Publishing Nanotechnology
Nanotechnology 31 (2020) 172001 (40pp) https://doi.org/10.1088/1361-6528/ab5f29

Topical Review

3D printed nanomaterial-based electronic, biomedical, and bioelectronic devices

Samuel Hales[1,3], Eric Tokita[1,2,3], Rajan Neupane[1,3], Udayan Ghosh[1], Brian Elder[1], Douglas Wirthlin[1] and Yong Lin Kong[1]

[1] Department of Mechanical Engineering, University of Utah, Salt Lake City, UT 84112, United States of America
[2] Department of Biomedical Engineering, University of Utah, Salt Lake City, UT 84112, United States of America

E-mail: yong.kong@utah.edu

Received 1 December 2018, revised 28 October 2019
Accepted for publication 5 December 2019
Published 6 February 2020

Abstract

The ability to seamlessly integrate functional materials into three-dimensional (3D) constructs has been of significant interest, as it can enable the creation of multifunctional devices. Such integration can be achieved with a multiscale, multi-material 3D printing strategy. This technology has enabled the creation of unique devices such as personalized tissue regenerative scaffolds, biomedical implants, 3D electronic devices, and bionic constructs which are challenging to realize with conventional manufacturing processes. In particular, the incorporation of nanomaterials into 3D printed devices can endow a wide range of constructs with tailorable mechanical, chemical, and electrical functionalities. This review highlights the advances and unique possibilities in the fabrication of novel electronic, biomedical, and bioelectronic devices that are realized by the synergistic integration of nanomaterials with 3D printing technologies.

Keywords: 3D printing, nanomaterials, bioelectronics, biomedical, electronics, additive manufacturing, multiscale 3D printing

(Some figures may appear in colour only in the online journal)

1. Introduction

The ability of additive manufacturing to seamlessly interweave disparate materials into a multifunctional construct can enable the creation of unique biomedical and electronic devices. Additive manufacturing, also known as '3D printing', is defined by the American Society for Testing and Materials (ASTM) as 'a process of joining materials to make objects from 3D model data, usually layer upon layer [1].' Traditionally developed as a rapid prototyping technique, 3D printing has become increasingly accessible with the advent of low-cost desktop 3D printers [2, 3], and increasingly powerful with the development of novel printing technologies [4–9]. 3D printing has been heralded for its capability to create geometrically complex constructs with low cost and minimal material waste and has been increasingly utilized by the aerospace and automotive industries—particularly for highly customized, low-volume production where the economy of scale of conventional mass production is no longer applicable [10, 11].

3D printing is also projected to have a significant impact beyond these industries, especially in the field of medicine and personalized electronics. For example, it can address a wide range of unmet clinical needs [12, 13] with the creation of personalized implants [14], regenerative scaffolds [15, 16], and drug delivery devices [17, 18]. Furthermore, 3D printed models of patients' unique anatomy, acquired with modern medical imaging technologies, can improve surgery planning,

[3] Equal contribution.

implant design, and provide unprecedented medical training [19, 20]. In another exciting development, the 3D printing of living cells could lead to the creation of biological constructs that can regenerate or augment lost tissues or organs due to diseases, trauma or congenital disabilities [16, 21]. In the field of electronics, 3D printing can enable the creation of non-planar [22], flexible [23], wearable [24], and—more recently—ingestible gastric resident electronics [18, 25].

Nanomaterials are materials with one dimension between 1 and 100 nm. The addition of nanomaterials to 3D printed constructs can impart functional properties such as electrical [26], magnetic [27], and optical properties [22]. Importantly, at the nanometer scale, a subset of functional materials exhibit size-dependent properties; this allows for the fine-tuning of the properties by synthesizing different sizes of the nanomaterials. For example, the size dependence of the emission wavelength [22] of quantum dots (semiconducting nanoparticles) can be leveraged to create a display device with exceptionally high color purity [28]. Furthermore, a material with dimensions on this scale exhibits significant changes to its surface-to-volume ratio, allowing the fine-tuning of physical and chemical properties such as a lower melting point, higher chemical reactivity, and higher surface conductivity in comparison to the same material in its bulk form [29].

The synergistic integration of nanomaterials with a multi-material additive manufacturing approach can extend the reach of 3D printing technologies beyond the creation of passive single-material constructs [7]. The ability to seamlessly integrate functional nanomaterials with distinct materials is a compelling fabrication approach that enables the creation of freeform architectures such as three-dimensional (3D) composite structures [30–33] and multi-functional constructs with unprecedented performance and unique properties. In particular, the application of 3D printing in the creation of biomedical and electronic devices is especially attractive [34, 35] due to the inherent heterogeneity of complex biological systems and the potential to overcome planar constraints of microfabricated electronic systems [7, 12]. The field of bioelectronics, a subset of biomedical, has especially notable applications due to the ability of 3D printing to seamlessly interweave electrically conductive nanomaterials into geometrically complex, biocompatible scaffolds and devices that replicate the inherent complexity and flexibility of biological systems [36–38]. Indeed, conventional subtractive manufacturing methods—such as machining, drilling, grinding, and lithographic processes—or formative manufacturing methods, such as forging and investment casting, are inherently limited in their ability to create complex geometries and/or multifunctional, multi-material structures [11].

This review highlights the advances in the development of unique electronic, biomedical, and bioelectronic functional devices that leverage the synergistic integration of additive manufacturing with nanomaterials. We will first introduce commonly used 3D printing approaches and the ability of nanomaterials to impart functional properties. We will then highlight the development of 3D printed nanomaterial-based electronics, such as energy storage devices (figure 1(A)) and photonic devices (figure 1(B)), and discuss how these enable

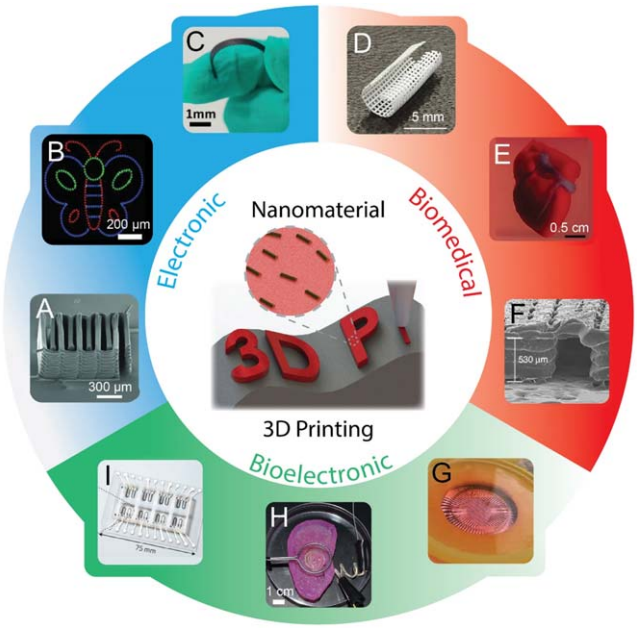

Figure 1. The synergistic integration of 3D printing with a wide range of materials enables the creation of unique electronic, biomedical, and bioelectronic functional devices. For example, electronics such as (A) interdigitated electrodes for use in a lithium-ion microbattery can be 3D printed with lithium titanate ($Li_4Ti_5O_{12}$, LTO) and lithium iron phosphate nanoparticles ($LiFePO_4$, LFP). [39] John Wiley & Sons. Copyright © 2013 WILEY-VCH Verlag GmbH & Co. KGaA, Weinheim. (B) A multicolor display can be printed with perovskite lead halide nanocrystals. [40] John Wiley & Sons. © 2019 WILEY-VCH Verlag GmbH & Co. KGaA, Weinheim. (C) A flexible electronic device can be 3D printed with reduced graphene oxide (rGO). Reprinted from [23], Copyright (2016), with permission from Elsevier. In biomedical devices, (D) hexagonal boron nitride (hBN) imparts increased mechanical flexibility to a 3D printed poly(lactic-co-glycolic acid) (PLGA) sheet. Reprinted with permission from [41]. Copyright (2018) American Chemical Society. Similarly, (E) thick vascularized tissue can be 3D printed, as shown by a biological construct immersed in a support bath mimicking a small-scale heart. Reproduced from [42]. CC BY 4.0. (F) 3D printed calvarial bone with microchannels can be fabricated using polycaprolactone (PCL) doped with tricalcium phosphate (TCP) nanoparticles to facilitate vascularization. Reprinted by permission from Springer Nature Customer Service Centre GmbH: Springer Nature, Nature Biotechnology, [43], 2016. In bioelectronic devices, (G) flexible microelectrode arrays can be 3D printed with silver nanoparticles on complex substrates such as gelatin and attached to a circuit board for action potential measurements of cell culture. Reproduced from [44]. CC BY 4.0. (H) A 3D printed bionic ear containing gold nanoparticle-infused silicone and cultured living cells (chondrocytes) demonstrates improved audio sensing over a human ear. Reprinted with permission from [45]. Copyright (2013) American Chemical Society. (I) Soft strain gauges printed with carbon nanoparticle ink guide the regeneration and measure the beating strength of cardiac tissue. Reprinted by permission from Springer Nature Customer Service Centre GmbH: Springer Nature, Nature Materials, [46], 2016.

the creation of flexible and wearable sensors (figure 1(C)) that can overcome the limitations of conventionally fabricated electronics. Next, we will review the creation of unique nanomaterial-based, 3D printed biomedical devices. These are discussed in relation to the customization of mechanical (figure 1(D)), geometric (figure 1(E)), biological (figure 1(F)),

and responsive properties, and include personalized regenerative constructs, biological implants, and drug delivery methods which possess unique properties that are endowed by nanomaterials. Finally, we will highlight the merging of biological constructs and electronics enabled by this multiscale 3D printing approach. The bioelectronic devices reviewed include microelectrodes (figure 1(G)), the interfacing point between biological electricity and fabricated electronics; bioelectronic scaffolds (figure 1(H)), which use electricity to potentially enhance cell regrowth and recovery; biosensors, which measure an array of biological organisms and molecules; and lab-on-a-chip devices (figure 1(I)), which enable the systematic study of complex biological processes.

2. 3D printing methods

3D printing, as previously described, is defined by the ASTM as 'a process of joining materials to make objects from 3D model data, usually layer upon layer [1].' 3D printed structures are first digitally constructed as 3D models with computer-aided design (CAD) software and converted into a digital approximation of the model such as a stereolithography (STL) file. This geometry is then interpreted and synthesized into machine code which the 3D printer uses to solidify regions of resins, powders, or inks layer by layer into a 3D construct [47]. 3D printing is a broad class of manufacturing technologies, which Lewis *et al* [6] categorized as light and ink-based. In this review, we will describe key technologies that can potentially be integrated with nanomaterials for the creation of functional devices.

2.1. Light-based methods

Light-based 3D printing methods use light to selectively solidify photocurable resins or sinter polymer, ceramic, or metal powders. For example, stereolithography (SLA), shown in figure 2(A), was one of the first 3D printing methods tested [48] and has a minimum feature size of down to 50 μm [49]. It uses a basin of photocurable resin which is selectively photopolymerized by ultraviolet (UV) laser one volume element (voxel) at a time. Once a layer of resin is fully solidified on the build platform, the platform retracts and a new layer of resin is introduced. Digital projection lithography (DLP) [50, 51] and continuous liquid interface production (CLIP) [4] also precisely solidify photocurable resin, but are able to solidify an entire layer of resin at a time—increasing print speeds to 6×10^{-2} ml h^{-1}. DLP accomplishes this by using a digital micromirror device [50] or a liquid crystal display [51] as a dynamic mask and projecting the mask pattern on the liquid resin, as shown in figure 2(B). CLIP further accelerates the process with an oxygen-permeable build window which enables a thin ($\sim$10 μm) layer of uncured, oxygen-containing resin to exist between the window and the part. UV images can thus be continuously projected through the window, and the part can be steadily drawn out of the resin in minutes [4]. A representation of CLIP is shown in figure 2(C). Two-photon polymerization 3D printing (2PP) is another light-based method where ultrashort IR (infrared) laser pulses are used to polymerize a tiny voxel within the reservoir of liquid resin [4]. This enables an exceptional 100 nm feature size without the need for a retractable platform. Further, the total part size can reach approximately 1 cm^3 [6]. In general, the printing materials of SLA-based techniques are limited to photocurable resins. Post-processing is also required—including post-curing with UV light and the removal of the supports generated during the printing process [49].

In selective laser sintering (SLS), instead of a photocurable resin, a bed of polymer, ceramic, or metal powder is sintered with a laser on a retractable bed [55, 56]. When a layer is completely sintered, the bed retracts into the powder and a fresh layer of powder is rolled onto the top of the part, as shown in figure 2(D). The powder bed supports the construct, hence no additional supporting structures need to be generated during the printing process. This method is limited by the size of the particles to be sintered, but can still achieve a feature size of approximately 100 μm [6]. Generally, the final parts are highly porous, and the thermal stresses from the high-temperature laser have to be considered as they can cause distortion to the printed part [56].

2.2. Ink-based methods

Ink-based 3D printing methods use inks or thermoplastic filaments which are extruded through a nozzle and selectively deposited onto a substrate [6, 7]. Ink-based 3D printing can be subcategorized into filament and droplet-based methods. Filament-based methods continuously extrude an ink or thermoplastic filament onto a build plate, while droplet-based methods deposit low-viscosity fluids (2–10^2 MPa s) [12, 57].

In fused deposition modeling (FDM) motors drive thermoplastic filament through a heated nozzle. The melted filament is selectively deposited onto a build plate, where it again solidifies—as shown in figure 2(E). Due to its relative simplicity, FDM filaments and printers can be inexpensive (printers cost as little as $200). Further, multiple heated nozzles can be integrated to achieve multi-material prints [58]. Post-processing is required to remove supports for complex structures, however, and filaments must be preformed for extrusion. Direct ink writing (DIW), another class of filament-based 3D printing, uses pneumatic pressure, a piston, or screw to extrude liquid ink through a nozzle (as shown in figure 2(F)). In some DIW, post-processing steps are used solidify the extruded ink, such as photopolymerization or thermal curing [6]. Inks can be formulated from polymeric and colloidal suspensions [59], and because no high temperatures are involved in the printing process, bioprinting (the printing of living cells) is also possible [21, 60–62].

Electrospinning is another filament-based 3D printing method, which can generate nanoscale fibers. In electrospinning, a high voltage is first applied between a nozzle containing the ink and the grounded collector. When the electrostatic repulsion within the ink becomes more significant than the surface tension at the head of the nozzle, a charged jet of liquid ejects from the nozzle towards the grounded substrate, as shown in figure 2(G). While far-field

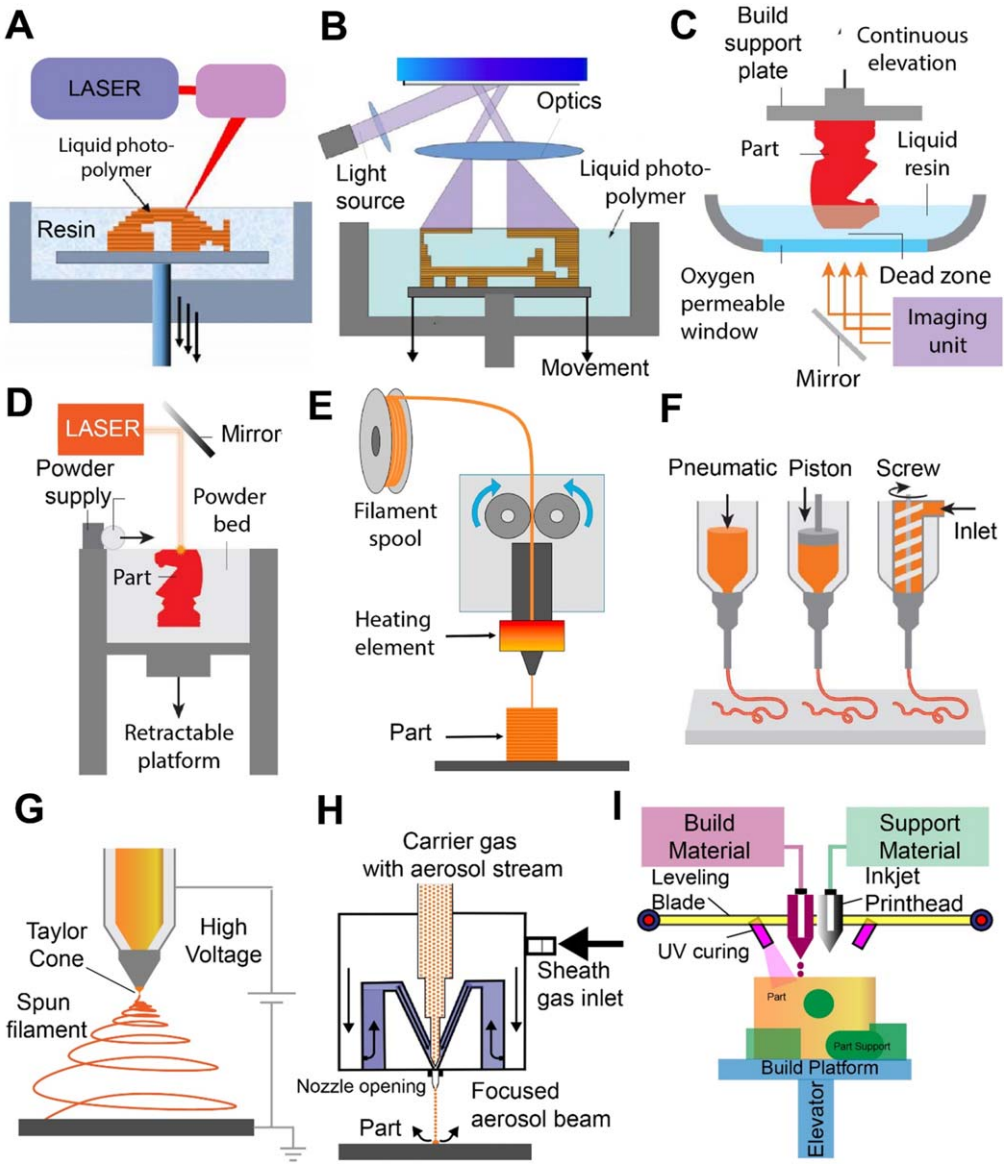

Figure 2. Representations of light and ink-based 3D printing methods. Light-based methods include (A) stereolithography (SLA), (B) digital projection lithography (DLP), (C) continuous light interface projection (CLIP), and (D) selective laser sintering (SLS). Ink-based methods include (E) fused deposition modeling (FDM), (F) direct ink writing (DIW), (G) electrospinning, (H) aerosol jet printing (AJP), and (I) direct inkjet printing. (A and E) Reprinted from [52], Copyright (2016), with permission from Elsevier. (B) [53] John Wiley & Sons. © 2018 WILEY-VCH Verlag GmbH & Co. KGaA, Weinheim. (C, D and F) Reprinted by permission from Springer Nature Customer Service Centre GmbH: Springer Nature, Nature, [6], 2016. (H) Reprinted with permission from [54]. Copyright (2013) American Chemical Society. (I) [12] John Wiley & Sons. © 2018 WILEY-VCH Verlag GmbH & Co. KGaA, Weinheim.

electrospinning (where the distance between the needle and the substrate is typically between 5 and 15 cm) forms disordered mats of nanoscale fibers that can be under 100 nm wide, near-field electrospinning (500 μm–5 cm) allows for controlled deposition of micrometer-wide fibers [63, 64]. Organic polymers are most commonly used in electrospinning, but small molecules, colloidal particles, and composites have been utilized as well [63, 65, 66].

Aerosol jet printing (AJP), as shown in figure 2(H), is also a filament-based 3D printing method. In AJP, an ink is first converted into an aerosol using an ultrasonic or pneumatic atomizer, then combined with a carrier gas for transportation, and finally compressed into a focused stream by a sheath gas just before ejection [67]. The use of a powerful aerosol stream allows this technique to print in multiple directions, including upwards, and on complex surfaces, such as on five orthogonal sides of a cube [68]. Commercial AJP systems can generate aerosol using inks with viscosities from 1 to 1000 cp, allowing a wide range of usable materials—from metals [69], ceramics [70] and polymers to biological matter [71]—to be printed at high resolution (10 μm).

Direct inkjet printing is a droplet-based 3D printing method which primarily uses piezoelectric or thermal nozzles to propel low-viscosity fluids onto a build plate [72, 73]. Thermal printers heat the ink for a few microseconds so that an expanding bubble forces a drop of ink through the nozzle,

while piezoelectric printers apply voltage to a glass tube or bending plate which then propels a droplet through the nozzle [74]. Often the resin is then UV cured, as shown in figure 2(I). Ink droplets as small as 2–12 pl can be deposited with this method [75], and multiple nozzles can be used simultaneously for multi-material printing [76]. Similar to DIW and AJP, the deposition of ink without high temperatures allows for the deposition of a wide range of polymers [77], suspensions [78], and living materials [79, 80]. However, the viscosity is limited to less than 0.25 Pa s, and the ink has to be precisely formulated to prevent nozzle clogging [81]. Using inkjet printing to actuate binding agents, binder jet 3D printing creates 3D structures by binding polymer, metal, or ceramic powder [56]. The use of binder on powder prevents the thermal stresses that can occur after SLS printing, but often requires steps such as sintering or infiltration (addition of strengthening materials) after binding to improve mechanical strength [82].

Electrohydrodynamic jet (e-jet) printing uses a similar setup as electrospinning, with a voltage applied between an ink-filled nozzle and a grounded substrate; applying this voltage creates an electrostatic charge in the ink that can overcome the surface tension of the liquid. Instead of ejecting continuous fibers, e-jet printing uses a pulsed voltage to eject droplets that can be as small as attoliters in volume, and print spots that are under 100 nm in diameter [83–85]. The materials used in e-jet printing are comparable to those used in electrospinning, including organic polymers, colloidal particles, and composites [84].

3D printer resolution can be divided into three subcategories: *Z* resolution, *XY* resolution, and minimum feature size [86]. *Z* resolution corresponds to the minimum allowable layer height in a printing method. In techniques such as SLA or FDM, this value is reported as the resolution of the motors driving the height of the build plate or printer nozzle. In contrast, for methods such as direct inkjet printing, the droplet thickness determines the *Z* resolution. Similarly, *XY* resolution corresponds to the minimum allowable horizontal movement of the build plate, nozzles, or optics. While *XY* resolution is determined by the motion of the printer, minimum feature size can be defined as the smallest horizontal feature that can feasibly be created in a printing method. In light-based 3D printing methods, this value is primarily determined by the beam size of the photocuring or sintering light. For SLA, the minimum feature size is determined by the spot size of the laser [87] and in DLP and CLIP it is based on the pixel size [53]. In SLS, this depends on both the laser spot size and the size of the particles to be sintered [6]. In filament-based 3D printing methods, feature size is determined by the diameter of the nozzle or fiber [6]. In droplet-based methods such as direct inkjet and e-jet printing, the footprint of an ink droplet determines feature size [88], and binder jet feature size is determined by both the footprint size and the particle diameters [89]. For more information regarding 3D printing technologies and applications, the reader is referred to several excellent reviews [3, 6, 12, 34, 90, 91]. Table 1 also provides a brief overview of 3D printing technologies.

3. Properties of nanomaterials

Nanomaterials are materials with one dimension of ca. 1–100 nm, and their proximity to the scale of atoms and molecules (the diameter of a DNA strand being approximately 2 nm [102]) results in properties that differ from the same material in its bulk form [103]. A material in its bulk form generally has well-defined properties, such as melting temperature, chemical reactivity, and color. Gold in its bulk form has a melting temperature of 1064 °C, is not a catalyst, and has a characteristic yellow color. In contrast, gold nanoparticles have a melting temperature of approximately 300 °C–400 °C, effectively catalyze specific reactions, and appear red to purple [104]. Indeed, a subset of material properties, such as melting point and emission spectra, can be modulated by changing the size of the particles, which enable the tuning of material properties by changing the size of the materials.

First, approaching the nanometer scale, the significantly increased surface-to-volume ratio of nanomaterials compared to that of their bulk form has an important geometrical effect [29]. For example, the greater relative number of weakly bound atoms at the surface increases the chemical reactivity of nanomaterials and allows some to be used as catalysts. Nanomaterial catalysts can be recycled multiple times (some up to 20 [105–107]) without loss of activity, and their small size allows many reactions to occur simultaneously [108, 109]. The weakly bound surface atoms in nanomaterials also result in melting-point depression due to their reduced cohesive energy. Similarly, conductive nanomaterial traces can be sintered at lower temperatures than the same material in bulk [110]. The increased surface area of metal nanomaterials has allowed for the creation of novel devices, such as micro-supercapacitors which can fully charge and discharge in seconds and operate for millions of cycles without losing energy storage capacity [111]. Ion access to supercapacitor electrodes is increased with the use of nanoparticle electrodes, allowing for a greater amount of charge to be transferred.

Second, a subset of nanomaterial properties begins to be size-dependent as they approach the nanometer scale. This size-dependency can be leveraged to fine-tune or to achieve precise properties of interest by varying the particle size. For example, for semiconducting nanomaterials, the quantum confinement effect results in the modulation of energy levels as the motion of their electrons are confined in a higher degree than their corresponding bulk counterpart [112]. Some effects of quantum confinement include the optical absorption of shorter wavelengths—such as the color shift of gold nanoparticles mentioned above—and a shift in emission wavelength of quantum dots. The extent of this absorption and emission shift depends on the size of the nanomaterials, allowing for the creation of quantum dot light-emitting diodes (LEDs) with various emission spectra by varying the size of the nanomaterials used [113, 114]. The plasmon resonance of nanomaterials is tunable as well. Plasmon resonance is the oscillation of free electrons at the surface of metals driven by the absorption of electromagnetic waves, an oscillation analogous to a simple mass-spring-damper oscillator model [115]. The electron cloud at the surface of a metal oscillates

Table 1. 3D printing methods.

Printing method	Compatible materials	Fabrication strategy	Minimum feature size	Advantages and disadvantages
Stereolithography (SLA)	Photocurable resin	Pointwise laser curing of resin, once a layer is fully printed the build plate retracts to introduce a new layer.	50–200 μm [6]	*Advantages:* Smoother surface finishing in comparison to FDM *Disadvantages:* Material selection limited to photocurable resin
Digital projection lithography (DLP)	Photocurable resin	2D pattern is projected onto resin to solidify an entire layer at a time	Pixel size-dependent, e.g. 1 μm [53]	*Advantages:* Faster than SLA; 2D projection ensures higher throughput [12] *Disadvantages:* Larger volume of photopolymer required in comparison to SLA
Continuous liquid interface production (CLIP)	Photocurable resin	Complete 2D pattern is project onto liquid resin, oxygen permeable build window allows for continuous printing	Below 100 μm [92]	*Advantages:* Faster than SLA and DLP [81, 93], can achieve relatively seamless 3D printing *Disadvantages:* Availability is limited, limited to photopolymer resins
Two-photon polymerization (2PP)	Photocurable resin	Ultrashort laser pulses polymerize a tiny voxel at the focal point of the laser	100 nm [6, 53]	*Advantages:* Highest resolution 3D printing *Disadvantages:* Costly setup due to the need for highly accurate optics and positioning stage [12]
Selective laser sintering (SLS)	Polymer, ceramic, and metal powders	Laser sinters powder on a retractable bed	100–200 μm [6, 94]	*Advantages:* No need for supporting structures or supporting materials *Disadvantages:* High temperatures result in thermal stresses [12]
Fused deposition modeling (FDM)	Thermoplastic filament	Heated nozzle deposits melted filament onto a build plate which then solidifies	100 μm [52, 95]	*Advantages:* Inexpensive printers and filaments, can be integrated to achieve multi-material printing [58] *Disadvantages:* Supporting structures required for free-standing models (in contrast with a powder bed system)
Direct ink writing (DIW)	Shear-thinning fluid, gels (etc)	Liquid ink is extruded from a nozzle	1–500 μm, ink dependent [6, 95, 96]	*Advantages:* Compatible with a wide range of materials, including biological inks *Disadvantages:* Precise ink formulation is needed to achieve small feature sizes [6]
Electrospinning	Polymers, colloidal particles, composites	High voltage causes a charged jet to eject from a nozzle towards a collector	50 nm–400 μm [63, 97]	*Advantages:* Nanoscale fibers can be fabricated *Disadvantages:* Precise control over deposition difficult with far-field electrospinning
Aerosol jet printing (AJP)	Low-viscosity fluid	Ink is converted into an aerosol, compressed into a focused stream, and ejected from a nozzle	10 μm [68]	*Advantages:* Can print in multiple directions with a wide range of materials (from polymers to metal nanoparticles) [68] *Disadvantages:* Solid content of ink must be low, small particle sizes allowed [98]

Table 1. (Continued.)

Printing method	Compatible materials	Fabrication strategy	Minimum feature size	Advantages and disadvantages
Direct inkjet printing	Low-viscosity fluid	Thermal or piezoelectric nozzles propel ink droplets onto a build plate	10–100 μm [6, 99]	*Advantages:* Multi-material printing possible, high resolution, compatible with biological inks *Disadvantages:* Printing resolution is highly dependent on ink formulation and nozzle size
Binder jet printing	Polymer powder and liquid binder	Droplets of binder are ink-jetted onto a powder bed	170 μm [95]	*Advantages:* No thermal stresses in the finished part (in contrast with SLS) *Disadvantages:* Mechanical properties inhibited by porosity, often post-processing required [82]
Electrohydrodynamic jet (e-jet) printing	Polymers, colloidal particles, composites	High voltage causes a charged droplet to eject from a nozzle towards a collector	240 nm–50 μm [100]	*Advantages:* Higher resolution in comparison to DIW and SLA *Disadvantages:* Requires carefully manufactured nozzles and precise voltages [101]

like a dipole parallel to the direction of the electric field in the driving electromagnetic waves. The resonant frequency of this oscillation in nanomaterials is determined by the size of the particles, thus allowing for tunable control [116]. Nanoparticles can absorb wavelengths that are larger than the particles themselves, and the enhanced electromagnetic field near the particle surface has several exciting applications. For instance, it enables the creation of highly sensitive biosensors [116–118], enables active targeting of nanoparticles to cancer cells [119], and improved solar cell efficiency [120, 121].

In another example, the magnetic domains and conductivity of nanomaterials are also influenced by their size. Magnetic nanomaterials on the range of 10–20 nm are comprised of a single magnetic domain and can exhibit superparamagnetism, where the magnetic field randomly switches direction under the influence of heat [122]. The ability to direct or extract magnetic nanomaterials in solution with a magnetic field has also spawned their potential use as retrievable biosensors, enzymes, and catalysts [117].

Due to the inherent porosity that is introduced in a significant subset of 3D printing methods (such as SLS), nanomaterials have also been utilized to enhance the mechanical properties of printed parts—providing increased tensile strength, for example [123]. The inclusion of nanomaterials into 3D printing processes results in devices with significantly modified material properties, tunable photonic effects [22], electrical conductivity [26], and magnetic properties [27]. Table 2 describes examples of nanomaterial integration in the modulation of the material properties of 3D printed parts. SLA and DLP are grouped in table 2 as the introduction of nanomaterials into the photocurable resins of these light-based 3D printing methods will similarly affect the properties of the finished products [124]. Additionally, the authors are not aware of achieved nanomaterial integration with CLIP due to its relatively recent development [125]. To the best of our knowledge, the company owning this patented technology does not currently offer nanomaterial resins and printers are normally available by subscription [126].

4. 3D printed devices with nanomaterials

4.1. Electronics

Printed electronics is a rapidly evolving field wherein printing technologies are applied to fabricate electronic circuits and devices [173]. Conventionally, electronic devices are manufactured on rigid substrates by planar processes such as photolithography [174], electroless plating [175, 176], or vacuum deposition [177, 178]. Fundamentally, these processes suffer from two shortcomings. First, subtractive fabrication methods are generally planar in nature, which often impedes the fabrication of enclosed geometries, voids, overhangs, or 3D structures. Second, most of these traditional methods are limited to the processing of a single material per processing step. This limits their ability to produce electronics with multifunctional properties.

On the other hand, the 3D printing of nanomaterials allows for the customization of device geometry and enables the multi-material, multiscale fabrication of electronic devices. The ability to incorporate nanomaterials in an electronic printing system can impart properties such as electrical conductivity [173] and optical properties [165, 179, 180]. High-performance energy storage devices such as lithium-ion batteries [181] and microsupercapacitors [182], flexible electronics [183] as well as photonic devices [184] have been developed by leveraging the functional properties of nanomaterials integrated with various light-based and ink-based methods.

4.1.1. Energy storage devices. A key prerequisite for the advancement of flexible and wearable devices is the development of high performance energy storage microdevices with high energy density and fast charging/discharging rates [39]. Energy storage devices typically retain energy based on the electrochemical reaction that typically occurs between two different electrodes: the anode and cathode. Nanomaterials such as graphene, graphene oxides, silver, and carbon nanotubes have been used in the fabrication of the electrodes and electrolytes of energy storage devices [185–187]. Recent development in 3D printing technologies have enabled the creation of 3D printed nanomaterial-based energy devices such as lithium-ion (Li-ion) batteries [39], microsupercapacitors [188], and pseudocapacitors [182].

The ability of additive manufacturing to print multiple materials simultaneously could reduce the number of processing steps required to fabricate energy storage devices. Unlike traditional subtractive methods which are often limited to handling a single material at a time, 3D printing allows the incorporation of multiple functional nanomaterials. Moreover, the assembly of nanomaterials with other components in an electrochemical device could be optimized to ensure that the unique properties of the nanomaterials, such as high surface area and electrical conductivity, are not compromised. Rocha *et al* [189] used a single-step DIW method with post-processing to fabricate electrodes for supercapacitors and batteries. They prepared thermo-responsive inks—inks whose properties are dependent on their temperature—to fabricate the electrodes. The electrodes consisted of chemically reduced graphene as the active material and copper as the current collecting material. The thermal reduction of the graphene-based ink and sintering conditions of copper (i.e. sintering temperature) match well so that the reduction and sintering could occur simultaneously. By using this strategy, they were able to preserve the electrical properties of the graphene ink. Figure 3(A), left shows the fabricated double-legged and single-legged electrodes assembled to create a supercapacitor, and the enhanced image shows its components. Figure 3(A), right is a scanning electron microscopy (SEM) image of the interface region between the graphene-based ink and the copper collector illustrating good physical contact, which results in enhanced performance of the device. Hence 3D printing offers the flexibility to print bespoke inks consisting of multiple materials in a single printing step,

Table 2. 3D printed nanomaterials: the effects of the addition of nanomaterials on the material properties of 3D printed constructs and on the respective printing process. Properties discussed include modulus of elasticity (E), strain to failure (ε), ultimate tensile strength (UTS), compressive strength (CS), flexural strength (FS), stiffness (k), and shear stress (τ).

3D printing method	Carbon-based	Metals	Ceramics/others
Stereolithography (SLA) and Digital projection lithography (DLP)	*Graphene*: increased UTS and ductility [127] *CNT*: increased UTS, lower max ε [132]	*Silver NPs*: increased UTS, E, and glass transition temperature; decreased ε [128, 129] *Gold NPs*: increased thermal stability and k (up to 0.16 μM gold) [133] *Iron NPs*: increased CS and E, decreased ε when combined with poly(ethylene glycol) diacrylate (PEGDA) [134]	*Silica*: increased UTS, E, and ε, printing accuracy not affected [130, 131] *Attapulgite (ATP)*: increased TS and E, printing accuracy significantly reduced [131] *Montmorillonite*: increased UTS and E, printing accuracy significantly reduced [131] *Hydroxyapatite* (nHa): comparable CS, increased E [135]
Two-photon polymerization (2PP)	*CNT*: spontaneous alignment of CNT observed along nanowire axis which could potentially result in programmable anisotropic properties [136]	*Gold NRs*: increased storage modulus and hardness [137] *Titanium dioxide NPs*: tunable refractive index, high concentrations of nanoparticles made polymerization difficult [139, 140] *Magnetite NPs*: superparamagnetic actuation abilities [141]	*CdSe-ZnS*: fluorescent [138]
Selective laser sintering (SLS)	*MWCNT*: increased UTS and E, decreased ε, greater fatigue strength [142]	*Silver NPs*: resistivity (3.0×10^{-5} Ω cm) close to that of bulk (1.59×10^{-6} Ω cm), significant heat-affected zone [143] *Copper NPs*: resistivity less than 3× that of bulk copper (depending on the laser irradiance levels) with minimal oxidation [145] *Iron NPs*: decreased creep and shrinkage [123, 146]	*Calcium phosphate*: slightly increased CS (from ~0.48 to ~0.57 MPa for nanocomposite scaffolds, compared to pure polymer scaffolds in dry conditions), biocompatible [144]
Fused deposition modeling (FDM)	*Graphene*: increased E (0–8 wt% graphene), decreased UTS and ε, excessive wear on print nozzles [147, 148] *CNTs and Carbon nanofibers*: increased UTS, E, and k; decreased ε compared to virgin polymer matrix, excessive wear on print nozzles [148, 150, 151]	*Iron NPs*: increased compression modulus, decreased CS and comparable max ε [134]	*Silica*: increased UTS, FS, max ε, improved heat flow and isotropy of part [149] *Montmorillonite*: increased UTS, E, FS; decreased thermal expansion coefficient and max ε [149, 152] *Calcium carbonate*: increased UTS, FS, ε, improved heat flow and isotropy of part [149]
Direct ink writing (DIW)	*Graphene*: increased E (0%–20% graphene), increased ε (>210% for 20% graphene), increased conductivity (~600 S m^{-1} at 40% particle loading) [153] *CNT*: increased CS to ~9 MPa compared to ~4 MPa for polymers without CNT [155]	*Silver NPs*: maintained conductivity over many loading cycles [154] *Iron NPs*: increased E (83 MPa) in comparison to divalent cations (17 MPa), imparts magnetic properties [156]	*CdSe-ZnS*: fluorescent [22]
Electrospinning	*Graphene*: controllable swelling, no negative effects on the nanofibers' morphology [157] *CNT*: biocompatible, increased cell alignment, decreased cellular attachment [159]	*Gold NRs*: act as a photothermal agent, biocompatible [158], increased storage modulus (at 1, 2, and 3 wt% gold) [137]	

Table 2. (Continued.)

3D printing method	Carbon-based	Metals	Ceramics/others
Aerosol jet printing (AJP)	*Graphene*: maintained conductivity over 1000 bending cycles [160] *CNT*: adjustable conductivity (conductivity of composite increases from insulating to conductive at 1.64 wt% to 3.22 wt% of CNTs) [162]	*Silver NPs*: maintained conductivity over 1000 bending cycles, enhanced conductivity with addition of CNTs [160, 161]	
Direct inkjet printing	*Graphene*: annealing improves conductivity of graphene/nitrocellulose films (to $\sim$40 000 S m^{-1}), negligible change in resistance over 2000 bending cycles [163] *CNT*: average carrier mobility of 4 cm^2 V^{-1} s^{-1} and ON/OFF current ratios of 10^4 in thin film transistors [166]	*Silver NPs*: reduced shrinkage and distortion, maintained mechanical stability over 1000 bending cycles [164] *Gold NPs*: sintering improves conductivity, stable resistance over 1000 bending cycles [110]	CsPbBr3 *NCs*: fluorescent [165]
Binder jet printing		*Copper*: increased green strength and density, decreased shrinkage, increased porosity and some foaming observed at high concentrations (20%–40% vol.) [167, 168]	*Alumina*: increased CS and density (from 76 to 641 kPa for 0%–15% Alumina), decreased porosity [169]
Electrohydrodynamic jet (e-jet) printing		*Silver NPs*: thermal curing of NP at 200 °C for one hour decreased resistivity (by $\sim$95%) [170] *Gold NPs*: maintained mechanical integrity with bending, can be printed with no permanent solvent [84, 171, 172]	

which could reduce the fabrication time of energy storage devices. Additionally, Kim *et al* utilized novel material combinations to develop a fully-3D printed aqueous zinc-ion battery [190]. Their studies used polyaniline-coated carbon fiber cathodes, zinc anodes and an SLA-printed porous separator to fabricate rechargeable batteries. The SLA printer constructed different battery geometries with variable charge-discharge curves, highlighting an advantage of 3D printed, electronic devices.

Extrusion-based 3D printing allows for the fabrication of energy storage device components with hierarchical geometries that could facilitate rapid ion transport in the interface between electrode and electrolyte, ultimately enhancing the charging/discharging rate [193, 194]. Hierarchy in a geometrical context refers to the presence of typical feature sizes that span across orders of magnitude. A structure possessing pore sizes that range from the nanoscale to the macroscale is said to have a hierarchical structure. In printed electronics, devices having components that exhibit hierarchical dimensions typically display enhanced performance compared to those with stochastic feature sizes. The presence of a hierarchy in pore sizes in an electrode of an electrochemical storage device could enhance charge transfer and diffusion of ions [195]. For example, holey graphene oxide, a nanoporous graphene-based material, was used to synthesize printable ink for the electrodes of a battery [191]. Figure 3(B), left shows the preparation of holey-graphene ink. Pore sizes from a few nanometers (4–25 nm through holes) to hundreds of micrometers ($<$500 μm square pores) were obtained in the printable ink. Figure 3(B), right shows the deep discharge curve of the printed parts with porous and nonporous features. The porous electrode of the holey graphene shows an increased areal capacitance ($\sim$13 mAh cm^{-2}) in comparison to the parts made up of graphene oxides such as Vor-X graphene ($\sim$10 mAh cm^{-2}) and natural graphite ($\sim$3 mAh cm^{-2}). Recently, Zhu *et al* fabricated supercapacitors based on hierarchical graphene aerogels with periodic macropores by using DIW [193]. These macropores facilitate mass transport, ultimately enabling the fabrication of supercapacitors with superior rate capability (ca. 90% from 0.5 to 10 A g^{-1}) compared to the other carbon-based electrodes [196]. In a

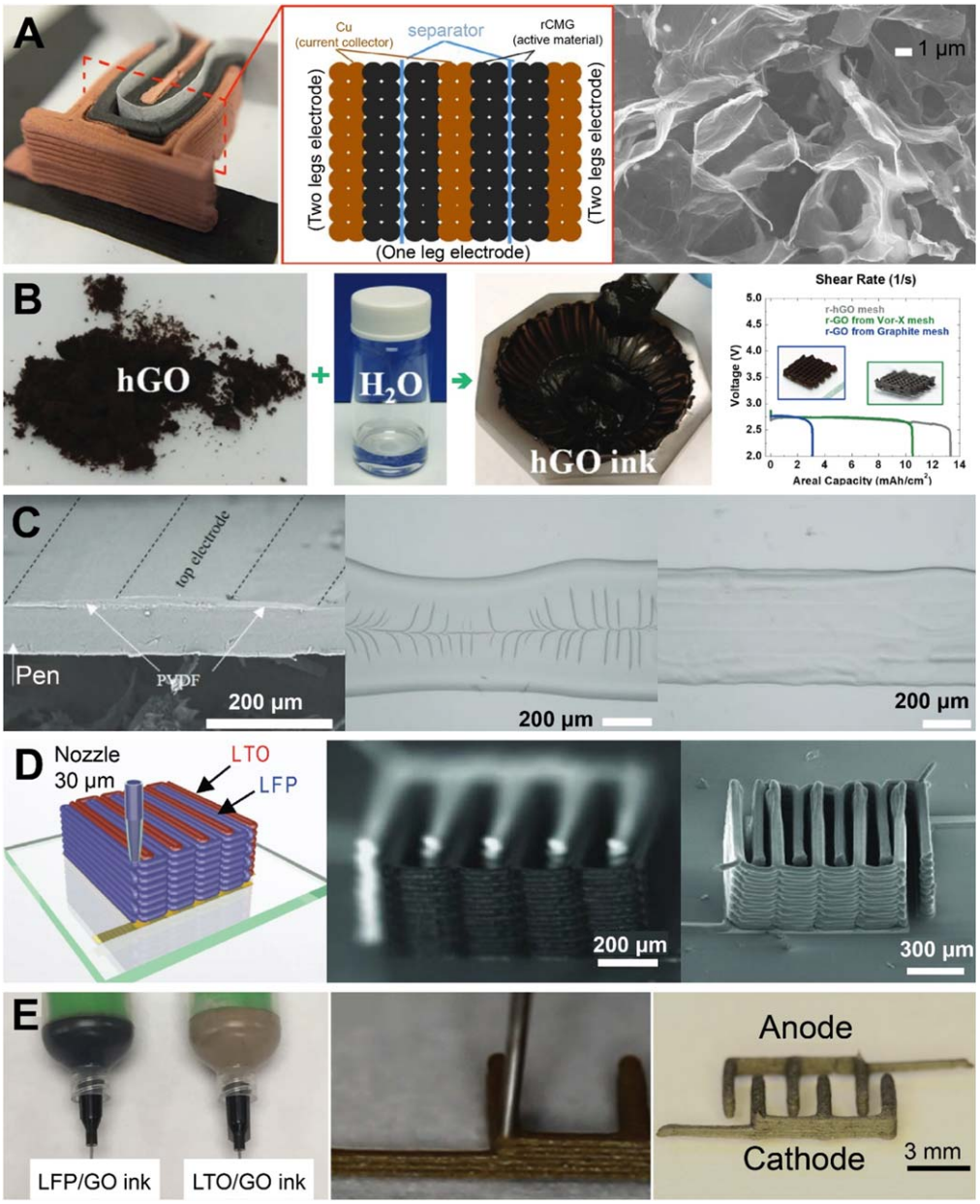

Figure 3. Energy storage devices fabricated by the 3D printing of nanomaterials: (A) 3D printing allows the fabrication of interdigitated nanomaterial architectures for supercapacitors. Image of an assembled supercapacitor where the electrodes are printed using a graphene-based ink and a copper-based collector (left). The middle image shows the cross-sectional scheme of the device with a copper (Cu) current collector, separators, and reduced chemically modified graphene (rCMG). Right is a scanning electron microscopy (SEM) image of the interface region of copper and rCMG showing good physical contact. Reprinted with permission from [189]. Copyright (2017) American Chemical Society. (B) Preparation of a hierarchically porous graphene ink by dissolving holey graphene oxide in water for 3D printing. The right image shows the discharge performance of the printed mesh (insets show the printed meshes). It is shown that meshes using holey graphene ink result in superior performance when compared to meshes printed with other graphene-based inks. [191] John Wiley & Sons. © 2018 WILEY-VCH Verlag GmbH & Co. KGaA, Weinheim. (C) A cross-sectional image of a printed micro-capacitor (left), an optical image of the dielectric layer with a mixture of polyvinylidene difluoride (PVDF) and polyvinyl alcohol (PVA) at 30 °C (center), and 70 °C which shows a defect-free layer of PVA and PVDF (right). [188] John Wiley & Sons. © 2019 WILEY-VCH Verlag GmbH & Co. KGaA, Weinheim. (D) Direct ink writing of the interdigitated electrodes for a lithium-ion (Li-ion) battery (left) and optical images of a printed and annealed interdigitated electrode. [39] John Wiley & Sons. Copyright © 2013 WILEY-VCH Verlag GmbH & Co. KGaA, Weinheim. (E) Graphene-based inks stored in two different syringes for the fabrication of interdigitated electrodes of a lithium ion battery (left). The center image shows the printing of the electrodes and right shows an optical image of the interdigitated electrodes. [192] John Wiley & Sons. © 2016 WILEY-VCH Verlag GmbH & Co. KGaA, Weinheim.

recent development, Brown *et al* [197] printed hybrid molybdenum disulfide (MoS_2)-graphene aerogels to fabricate porous electrode materials for sodium-ion battery anodes. The ink consisted of a mixture of a MoS_2 precursor and graphene oxide nanosheets (300–800 nm in average size). Brown *et al* used freeze-drying and reductive thermal

annealing to fabricate the hybrid structures [197]. In this process, the inkjet-printed droplets were readily frozen as ice, using a cold substrate plate at −30 °C. After this, the aerogels were thermally annealed in 3% hydrogen and 97% argon. The hybrid structure consisted of MoS_2 nanoparticles embedded in reduced graphene oxide (rGO) [197]. The pore size, ranging from 3 to 5 μm, facilitated the ion transport while the interconnected graphene network enhanced the electrical conductivity. Saleh *et al* printed hierarchically porous microlattices of silver nanoparticles using aerosol jet printing to fabricate electrode materials for lithium ion batteries [198]. The microlattice not only enhanced the areal capacitance, but it also resulted in a structure having enhanced strain tolerance when swelling occurs in the battery under frequent charge/discharge cycles. The areal capacitance of the structure with a hierarchically porous structure showed four times the areal capacity of the structure without hierarchically porous geometry.

The low temperature operating conditions inherent to 3D printing processes such as stereolithography (SLA) allows for the printing of energy storage devices based on polymer nanocomposites. Printing polymers in a dielectric film is important because they can impart a high polarization effect for energy storage devices such as capacitors. Yang *et al* used SLA to print a polymer composite containing silver (Ag) decorated lead zirconate titanate composites (PZT@Ag) to fabricate capacitors [199]. However, an adjustment had to be made in the printing process because the incorporation of Ag nanoparticles substantially increased the refractive index, decreasing the cure depth. In comparison to the pure Flex resin, the polymer nanocomposite exhibited a 30-fold increase in dielectric permittivity and hence an enhanced specific capacitance (63 F g^{-1} at the current density of 0.5 A g^{-1}). Recently, Torres-Canas *et al* used inkjet printing to fully print a microcapacitor on a poly(ethylene naphthalate) (PEN) substrate (figure 3(C)) [188]. The printable ink consisted of a mixture of polyvinylidene difluoride (PVDF) latex particles and polyvinyl alcohol (PVA) in water. The ink leverages the high polarization of PVDF and high breakdown dielectric of the PVA in order to obtain high energy density. The electrodes were made up of inkjet-printed carbon nanotubes (CNTs). Figure 3(C), center and right are the optical images of the dielectric layer with a mixture of PVDF and PVA at 30 °C and 70 °C, respectively. The microcapacitor had an energy density of around 12 J cm^{-3} at 550 MV m^{-1} and an efficiency of 74%. The capacitance could be tuned by changing the thickness of the sandwiched layer between the electrodes, allowing for the potential creation of rapidly customized capacitors with various capacitance values.

The 3D printing of nanomaterials allows for the customization of energy storage device geometries such as interdigitated electrodes, the precise manufacturing of which can result in improved areal energy density with a smaller capacitor footprint [200]. Sun *et al* [39] fabricated 3D interdigitated microbattery architectures (3D-IMA) where the cathode and anode inks were prepared by suspending the lithium titanate ($Li_4Ti_5O_{12}$, LTO) and lithium iron phosphate ($LiFePO_4$, LFP) nanoparticles in water, ethylene glycol, and glycerol. Ethylene glycol and glycerol were used to improve adhesion between individual layers. The inks were highly concentrated, having 57 and 60 wt% for the cathode and anode inks respectively. Using this highly concentrated ink, they were able to print structures with high aspect ratios (∼0.8 to 11) wherein the areal energy density and power density were reported to be 9.7 J cm^{-2} and 2.7 mW cm^{-2} respectively. Figure 3(D), left demonstrates the printing strategy with different components such as cathodes and anodes, whereas figure 3(D), right shows the printed battery architecture and the structure after sintering respectively. However, an entirely 3D printed battery was not demonstrated until Fu *et al* used a graphene oxide-based nanomaterial ink to 3D print the cathode, anode, and the solid-state electrolyte of a lithium ion-based battery (figure 3(E), right) [192]. The inks for the anode and cathodes consisted of graphene oxide sheets with LFP and LTO, respectively (figure 3(E), left). They demonstrated a specific capacitance of ∼160 mAh g^{-1} and ∼170 mAh g^{-1} for the cathode and anode respectively. The optimum viscoelastic nature of graphene oxide-based ink enabled the patterning of anode and cathode electrodes in an interdigitated architecture. In addition, the solid-like electrolytes offer the advantage of not potentially leaking or combusting like their fluidic electrolyte counterparts.

4.1.2. Flexible electronics. Flexible electronics are capable of maintaining their stability and shape under mechanical bending and twisting while retaining their functional properties, such as electrical conductivity [173, 201]. To attain this flexibility, nanomaterials such as graphene and CNTs have been utilized [202, 203]. In recent decades, research has been focused on the scalable fabrication of flexible devices which have applications as pressure sensors [204], electronic skin [205], optoelectronic devices [206], and energy harvesting devices [207].

3D printing allows for the fabrication of electrical circuits on soft and flexible substrates, such as papers and polyamides, to fabricate flexible electronic devices. Substrates such as paper offer the ability to create devices that are lightweight, cost-effective, and biodegradable. Zhang *et al* [23] used a composite filament made up of chemically and thermally reduced graphene oxide and polylactic acid (PLA) to fabricate flexible electronic circuits on paper and polyimide (PI). The synthesized graphene could reach up to 600 S cm^{-1} in electrical conductivity. Figure 4(A), left shows the printed flexible circuit with its enlarged cross-section in the middle. Figure 4(A), right shows the ability of the fabricated electronic circuit to endure bending. They reported that there was no post-print shrinkage or extrusion swelling in the printed part. This is important in order to realize compact, flexible devices with uniform lateral dimensions.

The ability to use natural products to fabricate flexible devices is one of the many advantages of 3D printing with nanomaterials. Le *et al* [208] patterned graphene on wood and leaves for electronics on paper and wood with an ultrashort laser pulse technique. The fabricated graphene is termed 'laser-induced graphene' (LIG). This method is generally

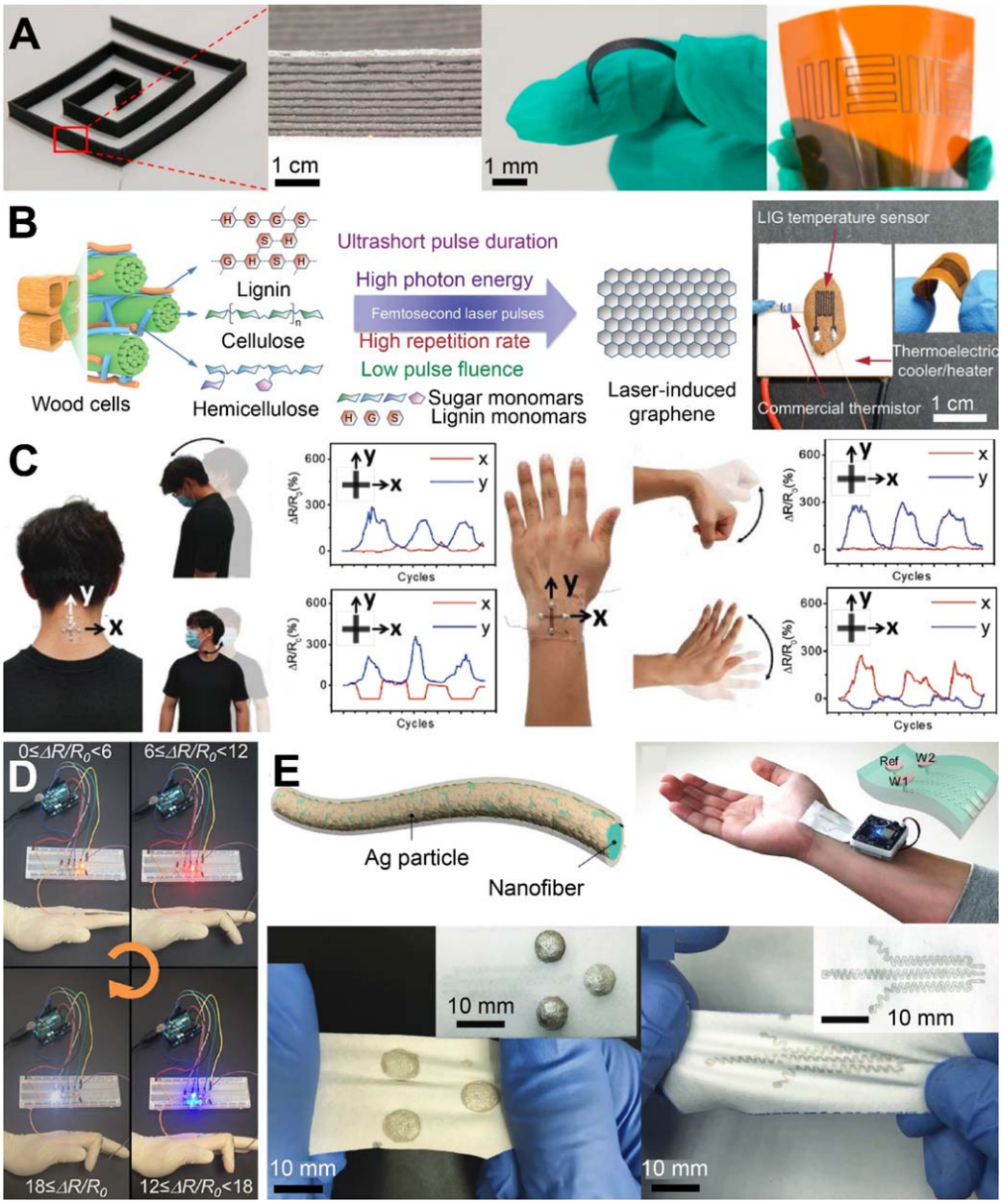

Figure 4. Nanomaterials can be used to 3D print flexible and wearable electronic devices. (A) From left to right, a flexible electronic circuit 3D printed with reduced graphene oxide, a magnified image of the circuit, a demonstration of the flexibility of the printed material, and a flexible circuit pattern in a polyimide substrate. Reprinted from [23], Copyright (2016), with permission from Elsevier. (B) 3D printing can be used to fabricate flexible electronics using natural materials such as leaves and wood. Laser induced graphene (LIG) can be synthesized with ultrashort laser pulses (left) and can be used in printing temperature sensors (right). [208] John Wiley & Sons. © 2019 WILEY-VCH Verlag GmbH & Co. KGaA, Weinheim. (C) Wearable devices with applications in strain sensing and healthcare. Printed strain sensors attached to the neck (left) and wrist (right) to detect multi-degree-of-freedom motions. The graphs show the high selectivity of the sensors to anisotropically detect strain in multiple directions. [209] John Wiley & Sons. © 2019 WILEY-VCH Verlag GmbH & Co. KGaA, Weinheim. (D) Flexible electronic sensors can be used to detect strains corresponding to the various configurations of a human hand. The left image shows the strain response of CNT-based strain sensors with the corresponding illumination of LEDs for a specific range. Reprinted with permission from [210]. Copyright (2018) American Chemical Society. (E) Flexible electronics can be leveraged to create electronic textiles (e-textiles), having numerous pressure sensors to detect human bodily movement. Top left image shows the schematic of a single cladded nanofiber of a printed e-textile. Top right image shows a surface electromyography (sEMG) sensor on a wrist. The bottom images show the sensor electrodes of the sEMG device (left) and the serpentine traces on the opposite side of e-textile. [211] John Wiley & Sons. © 2018 WILEY-VCH Verlag GmbH & Co. KGaA, Weinheim.

termed 'green manufacturing,' because the use of toxic solvents (often associated with synthesized graphene) is avoided and the fabricated parts are often biologically degradable, making them environmentally friendly. Figure 4(B), left, shows the strategy wherein natural products such as wood and leaves are exposed to laser radiation to fabricate LIG. The use of ultrashort laser pulses avoids laser-induced ablation and can convert several components such as lignin, phenolic groups, and cellulose into LIG. Using this strategy, Dinh Le *et al* fabricated temperature sensors,

electrical interconnects, and a pseudocapacitor. Figure 4(B), right shows a temperature sensor fabricated on a naturally dried leaf, which exhibited a retained flexibility, good sensitivity, and good recovery behavior. Cellulose nanofibers have also been used as the substrate in the fabrication of flexible electronics. Nge *et al* used cellulose nanofibers as a substrate for inkjet printing of silver conductive lines [212]. The nanoporous structure inherent to the nanostructured paper, made up of cellulose nanofibers, allowed the smooth deposition of silver nanoparticles. The conductive silver patterns showed a slight increase (110%) in electrical resistance when bent at a bend radius of 6 mm. This shows that 3D printing can be used with natural products to fabricate flexible devices. This also offers an alternative approach to fabricate flexible electronics without the need for harsh chemicals and sophisticated ink synthesizing steps.

3D printed nanomaterial strain sensors possess the advantages of being flexible, low cost, and highly sensitive [210]. The concept of 'electronic skin' encompasses devices that strive to mimic the multivariate sensors in human skin, including (but not limited to) strain and pressure sensors, which could potentially mimic the sensitivity and flexibility of typical human skin. Wei *et al* printed an electronic skin that constituted both strain and pressure sensors [24]. The ink consisted of Ecoflex0030 as the matrix for carbon nanoparticles. Printed pressure and strain sensors were shown to have promising applications in complex gesture recognition, hardness sensing of an object, and arterial pulse measurement. An alternative pressure sensor was developed by Visser *et al*, who utilized direct bubble writing to fabricate a foam with variable conductance [213]. Using a core–shell extruder and rapid-polymerization, they were able to produce foams with engineered bubble size and volume fraction. Due to the rapid-polymerization process, these bubbles were stable even when pressure was applied. When mixed with silver nanoparticles, the compression of the foams could be measured as a function of the electrical resistance. Lee *et al* used carbon nanofiber-PDMS composites to develop highly flexible anisotropic strain sensors (figure 4(C)) [209]. They devised a unique electrospinning setup where the collectors were angled at an angle of 15° relative to each other, causing the electric field to split and align the fibers across the inclined gap. The highly aligned carbon nanofibers allowed the detection of multidirectional strains. The graphs shown in figure 4(C), right display the ability of the device to selectively detect strain in two perpendicular directions. Wajahat *et al* fabricated a strain sensor by meniscus guided 3D printing of CNT-based ink on a curved surface [210]. By using this strategy, they were able to develop a movement-sensitive strain sensor that could be utilized as a gesture-based human-machine interface. Figure 4(D) shows the strain response of fabricated strain sensors, demonstrating the ability to sense strain during various configurations of a human hand by the corresponding illumination of LEDs.

The ability of 3D printing to fabricate complex geometries could enable the fabrication of textile-based electronics. An e-textile is a type of electronic device wherein electronics are embedded in textiles for wearable applications [214–216]. E-textiles have the advantage of being porous, lightweight, soft, and breathable, which are important attributes for a wearable device. La *et al* printed e-textile patches using a nanocomposite ink consisting of silver particles and silver flakes [211]. The e-textile patch consists of permeated silver (Ag) particle/fluoropolymer composite ink in a porous textile (figure 4(E), top left). Figure 4(E), top right shows the surface electromyography (sEMG) sensor on a wrist muscle. The patch consists of electrodes on one side and serpentine traces on the other side (figure 4(E), bottom). The authors reported a conductivity of $\sim$3200 S cm^{-1} and demonstrated that the sEMG sensor could be worn on different parts of the body including the submental space, elbow, calf, and ankle to monitor muscle movement and send information to an external device. Carey *et al* fabricated field-effect transistors by inkjet printing graphene/hexagonal-boron-nitride (hBN) based ink on textiles [217]. The fabricated e-textile could be bent to small bending radii (as small as 8 mm) without compromising its mobility. It was also shown that the textile could retain its functionality up to at least 20 washing cycles.

4.1.3. Photonic devices. Photonic devices are another class of electronics that benefit from the 3D printing of nanomaterials. Photonic devices either produce, manipulate, or detect light, and include LEDs [22, 218] and solar and photovoltaic cells and displays [179, 219, 220]. Typically, semiconducting nanomaterials such as quantum dots, quantum dot nanocomposites, and perovskite crystals are used as the active layer in the fabrication of photonic devices [22, 221]. For example, semiconductor quantum dots (QDs) are a class of nanomaterials whose optoelectronic properties, such as photoluminescence (PL) emission spectra, are often dictated by size-dependent quantum confinement effects [222]. This offers the ability to tune their optoelectronic properties by changing their size.

3D printing allows for precise patterning of semiconductor nanomaterials such QDs, which could enable the fabrication of LEDs for display applications [223, 224]. The exotic optical properties of QDs, such as size-controlled tunable emission wavelength, narrow emission spectra, and high luminescent efficiency, are desirable in such applications [114, 225]. Moreover, the solution processability of quantum dots in colloidal solution renders them highly compatible with extrusion-based 3D printing processes. The two most desirable properties of LEDs in display applications are their high brightness and color purity [226], the maximum brightness of conventional displays (such as smartphones and monitors) being approximately 600 cd m^{-2} [226]. The 3D printing of nanomaterials seeks to achieve these properties by carefully depositing semiconductor nanomaterials in a 3D printed construct. Kong *et al* fabricated a fully 3D printed QD-LED by using different classes of materials in each layer of the LED [22]. The diode consisted of emissive semiconductive quantum dots, an elastomeric matrix, organic polymer, solid and liquid metals, and an ultraviolet (UV)-adhesive transparent substrate. In order to circumvent the so-called coffee-ring effect [227], the QDs were dispersed in a binary solution of toluene and dichlorobenzene to induce

Marangoni flow. The coffee-ring effect is often observed when a colloidal solution is left to dry on a surface, and its non-uniformity often deteriorates the performance of printed electronics [228]. Marangoni flow tends to mitigate the coffee-ring effect and hence results in a uniformly deposited active layer [229]. Figure 5(A), left shows a schematic of the different layers in the printed QD-LED. The QD-LED had a maximum brightness of $250\,\mathrm{cd\,m^{-2}}$ at 5 V in green. Figure 5(A), bottom shows the schematic of a QD-LED printed on a non-planar substrate. Future studies on the complex soft matter physics phenomena, such as with confined constructs [230] and the characterization of drying-induced stress [231], could provide critical insights that can lead to improved printing performance. This ability to print on non-planar surfaces has potential applications in biological inspection, process monitoring, and optoelectronic devices [232]. Jiang *et al* [233] fabricated coffee-ring free quantum dot film by inkjet printing quantum dots dissolved in dichlorobenzene (DCB) and cyclohexylbenzene (CHB). In order to mitigate the coffee-ring effect, they printed a solution of 20:80 DCB and CHB on a modified zinc oxide layer. The printing of a binary mixture of QDs on a chemically modified ZnO layer enhanced the evaporation rate, ultimately suppressing the coffee-ring effect. Xiong *et al* [234] created a binary mixture of cyclohexylbenzene (CHB) and indane to inkjet print an emissive layer of red cadmium zinc selenide/zinc sulfide (CdZnSe/ZnS core/shell QDs) of a LED. They printed three different materials as the hole transport layer and found that the hole transport (HTL) of polyvinyl carbazole (PVK) exhibited excellent solvent resistance, which mitigates the layer erosion and optimizes the device performance. It was found that this configuration exceeded 17.0% external quantum efficiency (EQE) and current efficiency of 28.8 cd A^{-1}. Azzellino *et al* patterned colloidal QDs of lead sulfide/cadmium sulfide (PbS-CdS) core–shell quantum dots to create LEDs having an EQE of 2% by inkjet printing [235]. The process included inkjet printing of the QD ink on lithographically patterned microwells after spin coating zinc oxide (ZnO) and photoresist on an indium tin oxide electrode.

Recently, 3D printing technologies have also been leveraged to fabricate photonic devices based on perovskite quantum dots (PQDs). The typical formula of perovskite is AMX_3, where A may be calcium ion (Ca^{2+}), strontium ion (Sr^{2+}), barium ion (Ba^{2+}) etc, M may be titanium ion (Ti^{4+}), zirconium ion (Zr^{4+}) , and X may be oxygen (O_2) [221]. Metal halide perovskites [237] have found applications in solar cells [220, 238], X-ray detectors [239], lasers [221], security labels [240], and LEDs [221, 241]. On the other hand, hybrid perovskite contains organic and inorganic components where A may be organic, divalent metal cations around M site and halides such as chlorine (Cl), bromine (Br) and iodine (I) at X-site [221]. Typically, halide perovskite materials such as cesium lead halides ($CsPbX_3$, $CsPb_2X_5$, and Cs_4PbX_6, X = Cl, Br, and I) have attracted increasing attention due to their high photoluminescence yield, tunable light emission wavelength, and emission spectra with a narrow full width at half maximum [180, 221, 242]. Moreover, it has been shown that perovskite materials can be synthesized from a low-temperature processing in a scalable fabrication process. Zhu *et al* [40] used electrohydrodynamic printing to pattern a halide perovskite solution in order to fabricate devices that could potentially be used in electronic displays. The inks were crystallized *in situ* after printing. Figure 5(B), top shows the microlines and microarray patterns formed by $CsPbBr_3$ dots. The color of the perovskite inks is dependent on their halide content. Figure 5(B), bottom left shows the red, green, and blue (RGB) pattern, and the bottom-right images show the printed tree and butterfly patterns. It was also demonstrated that the photoluminescence quantum yield of the printed films, especially for the bromide containing ink, could be more than 75%. Shi *et al* used *in situ* inkjet-printing of a PQD precursor solution to fabricate quantum dot patterns [180]. The *in situ* preparation of the PQDs obviate the need for preforming colloidal solution before printing—a process which often requires functionalization of nanoparticles in order to ensure uniform dispersion. *In situ* inkjet printing is particularly important because it avoids challenges such as ink agglomeration and photoluminescence (PL) quenching. A perovskite precursor ink consisting of perovskite dissolved in *N*, *N*-dimethylformamide (DMF) or dimethyl sulfoxide (DMSO) was inkjet printed on a polymer film on a heated substrate. The precursor solution partially dissolves or swells the underlying polymer thin film to form a colloidal microarray. For example, Shi *et al* used DMF to dissolve or swell the polymer film such as polymethyl methacrylate (PMMA), polystyrene (PS), polyvinyl chloride (PVC), and PVDF [180]. The crystallization of the PQDs results in a formation of microdisks at locations determined by the printing program. It was shown that the emission from the microdisk arrays could be changed from blue to red by varying the halide content in the perovskite precursor solution from chlorine to bromine. The left image in figure 5(C) shows a typical clover pattern of the printed PQDs layer under UV-365 nm illumination, and the middle and right images show the dark field optical images of the highlighted section on the left. It was also reported that these printed microdisk arrays could have potential applications in flexible devices because the perovskite layer patterns and polymer film can be easily peeled off from the substrates. Finally, Zhou *et al* DIW printed perovskite nanowires to fabricate photonic devices [243]. They found that altering the nanowire's print orientation facilitated the programming of optoelectric devices, such as RGB displays, optical strain sensors, and optical information storing devices. These studies demonstrate the application of 3D perovskite printing in functional photonic devices.

The integration of nanomaterials and 3D printing can potentially improve the performance of solar cells [244]. Recent reports have shown that some printed solar cell devices have outperformed spin-coated counterparts [236]. Huckaba *et al* [236] fabricated perovskite solar cells where the TiO_2 acted as the perovskite absorber layer possessing a mesoporous structure, enhancing the carrier mobility. Huckaba *et al* demonstrated that inkjet printing could develop a scalable and commercial platform for the fabrication of perovskite solar cells. The fabricated device was >1 cm^2 in

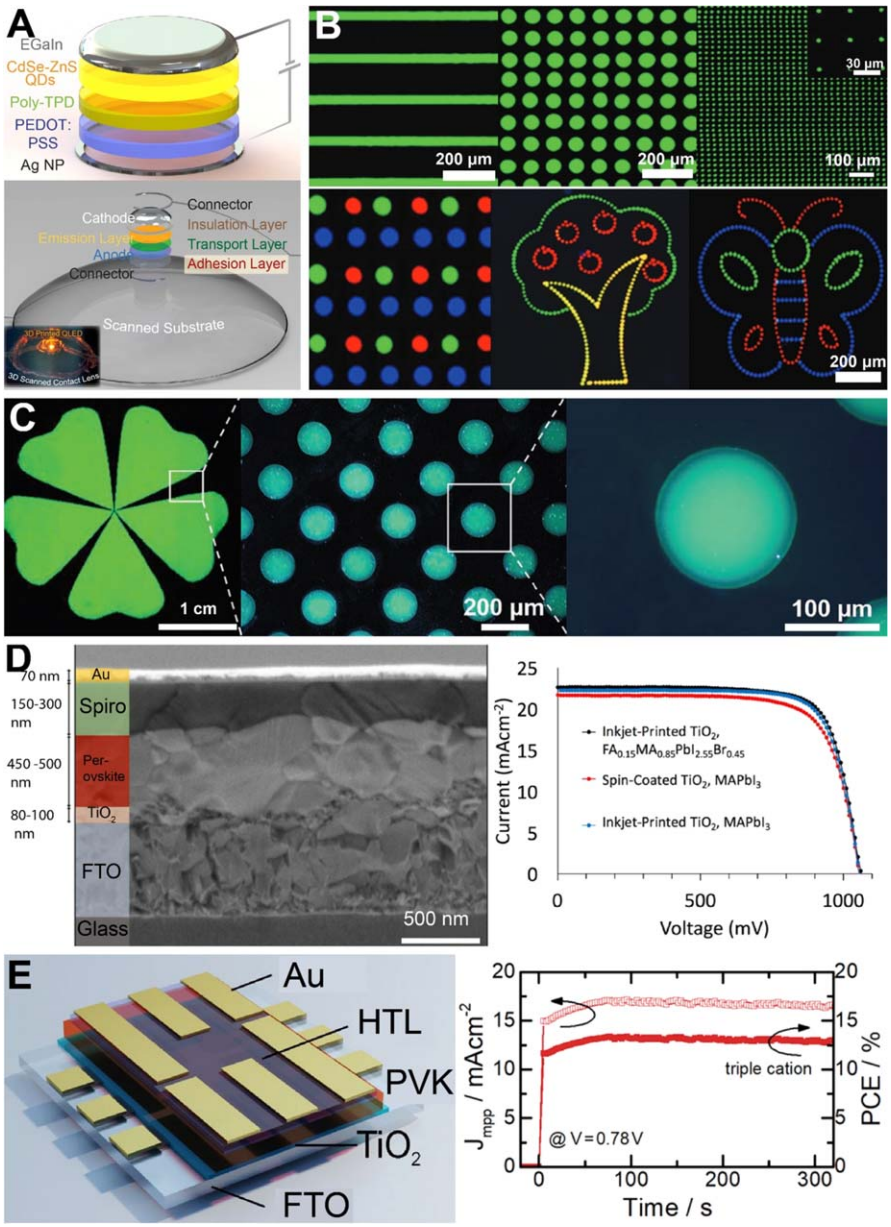

Figure 5. Photonic devices fabricated by the 3D printing of nanomaterials. (A) A fully 3D printed light-emitting diode (LED) is fabricated with different classes of materials, from an elastomeric matrix to semiconductor quantum dots. Top image shows the schematic of a 3D printed quantum dot LED. Moreover, 3D scanning enables the printing of photonic devices on non-planar surfaces. Bottom image shows the printed LED on a curvilinear surface and printed QD-LED on a 3D scanned contact lens is shown in the inset. Reprinted with permission from [22]. Copyright (2014) American Chemical Society. (B) Perovskite lead halides can be successfully printed to fabricate highly saturated display devices. Top image shows photoluminescence images of microlines, microarrays, and a high-resolution dot matrix of cesium lead halide ($CsPbBr_3$) with dot diameters of $\sim$5 μm. Bottom-left image shows the printed microdisk RGB (red, green, and blue) patterns. Bottom-right image shows a colorful tree and butterfly pattern made by lead perovskite halide. [40] John Wiley & Sons. © 2019 WILEY-VCH Verlag GmbH & Co. KGaA, Weinheim. (C) *In situ* inkjet printing could enable the fabrication of perovskite quantum dot arrays for display applications. Left is an optical image of *in situ* printed perovskite quantum dot patterns under ultraviolet (UV) 365 nm illumination. [180] John Wiley & Sons. © 2019 WILEY-VCH Verlag GmbH & Co. KGaA, Weinheim. (D) Inkjet printing can be used to fabricate perovskite solar cells with a mesoporous electron transport layer having enhanced efficiency. Left shows a cross-sectional transmission electron microscopy image with a deposited TiO_2 layer. Right shows the current density–voltage (J–V) curve showing that the performance of a mesoporous structure (blue) is comparable to the spin-coated (red) layer. [236] John Wiley & Sons. © 2019 Wiley-VCH Verlag GmbH & Co. KGaA, Weinheim. (E) Inclusion of triple cations in a perovskite layer could potentially increase the thermal stability and the moisture-resistant properties of a photovoltaic device. Left shows the schematic of a triple cation solar cell architecture. The graph on the right shows the current density and power conversion efficiency with respect to time for the triple cation solar cell, indicating its consistent performance. Reprinted with permission from [179]. Copyright (2018) American Chemical Society.

area and reported to have greater than 18% conversion efficiency. Figure 5(D), left shows the cross-sectional SEM image of the perovskite solar cell, where the mesoporous titanium dioxide (TiO_2) and perovskite absorber were inkjet-printed and HTL was spin coated. They optimized the drop spacing between the inkjet-printed droplets, temperature, and percent of titanium di-isopropoxide bis(acetylacetonate) (TAA) in TiO_2 ink to enhance the short circuit current and open circuit voltage between the electrodes. Figure 5(D), right shows the comparison of photovoltaic performance of inkjet-printed TiO_2 in mixed $(FA_{0.15}MA_{0.85})Pb(I_{2.55}Br_{0.45})$, spin coated TiO_2, and inkjet-printed TiO_2 in pure methylammonium lead iodide ($MAPbI_3$). Mesoporous films for pure $MAPbI_3$ absorber layers enhance the device performance due to improved short circuit current.

In addition, 3D printing can offer control over the crystallization behavior of perovskite layers, which is critical for the performance and lifetime of a solar cell device—such as in the creation of air-stable solar cell devices [245, 246]. Typically, perovskite solar cells are sensitive to moisture and illumination to UV light, which are found to decrease their lifespan. The use of triple cation perovskite with a small amount of cesium (15%) added to the perovskite is found to improve the thermal stability and moisture resistivity. For example, Mathies *et al* [179] inkjet printed a mixed cation perovskite layer on top of an electron transport layer, namely TiO_2. The schematic diagram shown in figure 5(E), left shows the schematic of a stack of layers, including glass, fluorine-doped tin oxide (FTO), TiO_2, triple cation perovskite (PVK)/spiro-MeOTAD as the hole transport layer, and Au electrode. The right image shows that the power conversion efficiency of the triple cation perovskite solar cells remains unaltered at 23 °C for 300 s. For further details and discussion on the enhancement of the stability of solar cells, the reader is referred to several excellent reviews [245–248] which provide in-depth discussion.

In summary, the 3D printing of nanomaterials is a promising approach to complement microfabrication processes and enable the creation of unique electronic devices, such as high performing energy storage devices; photonic devices; and flexible, wearable, and textile electronics. For example, 3D printing allows for the customization of device geometries, the integration of hierarchical geometries, and direct printing on flexible substrates and materials which are otherwise incompatible with a conventional fabrication approach.

4.2. Biomedical devices

A biomedical device is defined as any instrument, apparatus, machine, appliance, or implant intended for medical purposes [249]. They are used for diagnosis, monitoring, or treatment of diseases as well as the support of vital functions. Some examples of biomedical devices include cardiac pacemakers, vascular stents, and surgical sutures. The biomedical device industry is massive, expected to be valued at 409.5 billion dollars by 2023 [250]. 3D printing has enabled the creation of biomedical devices that are capable of addressing a wide range of unmet clinical needs due to its ability to fabricate personalized constructs and prototypes [34]. For example, 3D printing has enabled the creation of biosensors [251], implants [252], prosthetics [253], and tissue engineering constructs [254]. Recent advances in novel 3D printing technologies have vastly expanded the capability to fabricate novel biomedical devices. In particular, the incorporation of nanomaterials to the 3D printing process is an attractive approach to modulate mechanical, geometric, biological, or responsive properties in biomedical devices.

4.2.1. Customization of mechanical properties. Mechanical properties such as elasticity, stiffness, and tensile strength are important considerations for biomedical devices. For example, achieving mechanical properties that match that of native tissues has been a longstanding goal in tissue engineering [255]. In orthopedics, significant interest has been devoted to developing specialized implants with engineered Young's modulus that match the mechanical properties of bones [256]. Stress shielding occurs when the mechanical strength of an implant surpasses that of bone, which leads to bone resorption and an increased risk of future fracture [257]. In order to remedy this issue, implants with mechanical properties that are similar to bone are desirable. While these examples are not the only applications of mechanical properties in biomedical devices, they highlight the need to engineer the mechanical properties of medical devices.

Nanomaterials are capable of modulating the mechanical properties, such as tensile strength, of 3D printed biomedical devices [258–260]. For example, Sezer *et al* demonstrated that the integration of multiwall carbon nanotubes (MWCNTs) into acrylonitrile butadiene styrene (ABS) polymers could produce prints with superior tensile strength [261]. Varying concentrations of MWCNTs were tested for tensile strength (figure 6(A)). Their findings demonstrated that the dispersion of MWCNTs resulted in superior mechanical strength up to 7 wt%. This improved tensile strength expands the applications of this material to more loadbearing uses. Other studies paired MWCNTs with polybutylene terephthalate [148] and thermoplastic polyurethane [262] and reported similar improvements in mechanical properties. In addition, nanofillers such as calcium carbonate and montmorillonite have been shown to improve the mechanical strength of 3D printed structures as well [149]. The addition of nanomontmorillonite to ABS increased tensile strength from 29.5 to 37.1 MPa while the flexural strength increased from 54.8 to 64.2 MPa. These results were consistent with those obtained from injection-molded composites, suggesting that this reinforcement method is comparable to similar methods used in traditional manufacturing.

Nanomaterials can also be used to enhance the mechanical strength of 3D printed hydrogels. Zhai *et al* used nanoclay-embedded poly (N-acryloyl glycinamide) to 3D print a bone scaffold [263] where the incorporation of nanoclays increased the physical cross-linking of the polymer chains. This crosslinking improved the tensile strength,

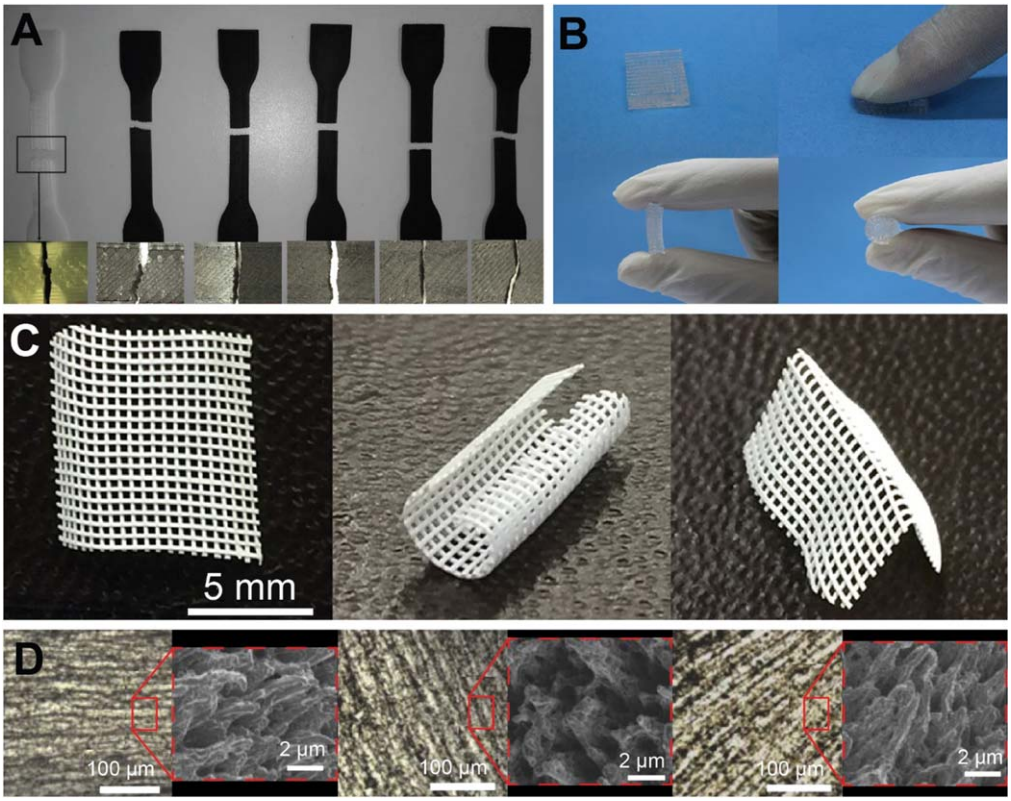

Figure 6. Nanomaterials can provide function mechanical properties to 3D printed constructs. (A) Acrylonitrile butadiene styrene (ABS) polymer embedded with MWCNT's exhibit superior tensile strength up to 7 wt%. Reprinted from [261], Copyright (2019), with permission from Elsevier. (B) 3D printed hydrogel scaffold exhibiting enhanced mechanical strength due to nanomaterials can be integrated into load-bearing applications such as bone. The N-acryloyl glycinamide hydrogel and nanoclay composite displayed properties that improve load-bearing applications. Reprinted with permission from [263]. Copyright (2017) American Chemical Society. (C) A poly(lactic-*co*-glycolic acid) (PLGA) sheet with hexagonal boron nitride maintains mechanical stability when bent. Reprinted with permission from [41]. Copyright (2018) American Chemical Society. (D) Electrically assisted 3D printed multi-walled carbon nanotubes (MWCNTs) are oriented in different directions in each layer, resulting in customizable, biomimetic mechanical properties. [264] John Wiley & Sons. © 2017 WILEY-VCH Verlag GmbH & Co. KGaA, Weinheim.

Young's modulus, and maximum strain of the 3D printed hydrogel construct (figure 6(B)). Hydrogels have long been investigated for use in tissue scaffolds due to their biocompatibility; however, many hydrogels were unable to support significant weight. The incorporation of nanomaterials into 3D printed hydrogels is an important advancement in biomedical implants as it expands the applications of these scaffolds.

Improved flexibility of printed devices is another advantage that nanomaterial 3D printing can provide. Flexibility is an important quality for some devices in order to function within the dynamic body without failing. Guiney *et al* printed a poly(lactic-co-glycolic acid) sheet with hexagonal boron nitride nanoparticles [41]. This sheet was flexible and could be bent while still maintaining mechanical stability (figure 6(C)). When testing different concentrations of hBN, 3D printed structures showed an increase in strain to failure percentage until 60% hBN. The authors suggest that the composite's modular mechanical properties can have applications in many bioelectric technologies. When applying these findings to the broader 3D printing field, nanomaterials can provide an important tool in developing 3D printed constructs with desirable flexible properties.

In tissue engineering, the 3D printing of nanomaterials can help replicate the mechanical properties of native tissues. Xu *et al* demonstrated how 3D printed nanocellulose could be used to create compressible cell scaffolds for wound healing [265]. Cellulose nanofibrils were integrated with gelatin to create noncytotoxic scaffolds that promote cell growth. Achieving this mechanical property is important in wound healing because cell growth only occurs under specific conditions. Additionally, this study demonstrated that modifying the ratio of cellulose nanofibrils and gelatin methacrylate allowed for a tunable Young's modulus, suggesting that medical devices with engineered compressive properties can be created for specific applications.

The integration of magnetic particles in a 3D printing process also provides an additional degree of control over the mechanical properties in the pursuit of biomimetic mechanical properties [266]. Utilizing magnetic fields that orient anisotropic, magnetic nanoparticles in uniform directions, Martin *et al* fabricated architecture with supporting fibers that displayed different responses to stress depending on the orientation of the nanoparticles [266]. High strength alumina nanoparticles were coated with magnetic iron oxide particles. These nanomaterials were added to the printing reservoir of a

DLP printer. Prior to polymerization, the field strengths of three orthogonal electromagnets were adjusted to create a 3D magnetic field. The magnetically active nanoparticles then align their long axis with the magnetic field vector. This method facilitated the production of a heterogeneous structure with anisotropic nanoparticles that were aligned in varying spatial orientations. The manipulation of the physical structure produced constructs with nanomaterial alignment that could mimic biological architectures such as cortical bone. Such findings suggest the incorporation of external magnetic fields with 3D printing technologies can fabricate constructs with mechanical properties similar to biological tissues.

In a similar mechanism to magnetically-oriented printing, electrically and shear-assisted 3D printing of nanomaterials can be used to achieve biomimetic properties. In one example, electrically-assisted, nano-composite polymers were used to develop personalized intervertebral disks [267]. Adjustment of polymer composition with the electrical field allowed for optimization of compressive properties that closely align with that of trabecular bone. Applications of this concept could inform medical implants that have personalized mechanical properties. Yang *et al* altered the mechanical properties of an artificial meniscus by using CNTs and electrically-assisted 3D printing to create a radially-aligned fibrous architecture (figure 6(D)) [264]. Specifically, they printed sheets of alternatingly aligned MWCNT-embedded polymer. The alternating orientation resembled that of a meniscus and prevented cracks from easily passing from layer to layer, effectively improving the impact resistance. Using shear-induced alignment of anisotropic cellulose nanocrystals, Siqueira *et al* replicated the directional mechanical reinforcement observed in cell walls [268]. They found that the orientation of the cellulose nanocrystal alignment played a role in the mechanical properties of printed matrices, including increased elastic modulus and tensile strength in the direction of shear alignment. This finding suggests that shear-induced patterning can be used to develop products with direction-specific mechanical properties.

4.2.2. Customization of geometric properties. Additive manufacturing methods have the ability to fabricate unique geometries that are not possible with conventional subtractive or formative manufacturing techniques [34]. The geometry of a printed product can dictate many functional properties of a device, so the ability to fabricate precise geometries is an interest for medical devices. For example, Lee *et al* demonstrated the versatility of 3D printing by using PEG sacrificial scaffold to develop complex geometries with overhanging architecture and porous regions [269]. In addition, computer imaging such as CT scans can be used in conjunction with 3D printing to produce personalized, anatomic models [270]. These models can inform personalized medical devices that match the anatomy of individuals [271]. The incorporation of nanomaterials further extends the versatility of 3D printing in these aspects. For example, it can expand the range of practical materials, generate high-resolution structures, and produce customized medical devices.

First, incorporation of nanomaterials can enable the 3D printing of complex structures with materials that otherwise cannot be practically 3D printed. Abouzeid *et al* used cellulose nanofibrils in conjunction with alginate hydrogels to create scaffolds with complex geometries [272]. As pure alginate hydrogels often do not have the viscosity necessary to sustain self-supporting complex structures, the nanoparticles play an important role in enabling this feat. This composite has been used to replicate the structures of ear and bone, as shown in figure 7(A). Similarly, Wilson *et al* used nano silicates in a printable bioink that enable the 3D printing of both an ear and a nose [273] (figure 7(B)). Indeed, the incorporation of nanomaterials enables the creation of a self-supporting structure with a wider range of materials, enabling the fabrication of more complex architecture.

Second, the 3D printing of nanomaterials can also allow for the construction of high-resolution freeform architectures. Saleh *et al* utilized aerosol jet printing to 3D print metal nanoparticles into a well-defined, micro lattice architecture. For example, lattice structures with octahedral and hexagonal unit cells were constructed with a total length of 100, 200, and 300 μm. They also demonstrated the versatility of this printing technique by building spatial interconnects, columns, and a dome. The applications of this printing method and materials could be extended to many fields such as tissue engineering, microfluidics, and microelectronics, which require precise architectures.

When combined with advanced medical imaging, 3D printing of nanomaterials can create personalized medical implants. These implants may include cardiac patches, prosthetics, or implants. The anatomy of each individual varies, which limits the effectiveness of 'one-size-fits-all' medical devices. Noor *et al* demonstrated the applicability of 3D printing nanomaterials by developing a personalized cardiac patch [42]. A cardiac patch is a tissue engineering construct that replaces damaged tissue in patients [276]. It must be elastic in order to withstand the movement of the heart, and it must allow cell growth and vascularization. Using CT scans of the patient's heart, Noor *et al* used major blood vessels to orient the heart and 3D print a cardiac patch specific to that patient [42]. This collagenous nanofiber scaffold was seeded with cells from the patient, creating a construct that addresses both geometric and biochemical requirements. Computer modeling complemented the printing processing by preparing appropriate spacing for vascularization. Noor *et al* also used the same bioprinting technique with collagenous nanofibers to produce a miniaturized heart of thick vascularized tissue (figure 7(C)). The proof of concept was printed in a supporting bath and exhibited cellularization.

3D printing of a nanomaterial-based medical device also enables the creation of personalized prosthetics. In a paper by Tong *et al*, a customized arm prosthetic is designed for a patient with an upper limb deformation [274]. 3D scans of the patient's limb informed the modeling of the implant and pressure sensors. After a prosthetic was designed to conform to the patient's unique anatomy, a customized sensor was

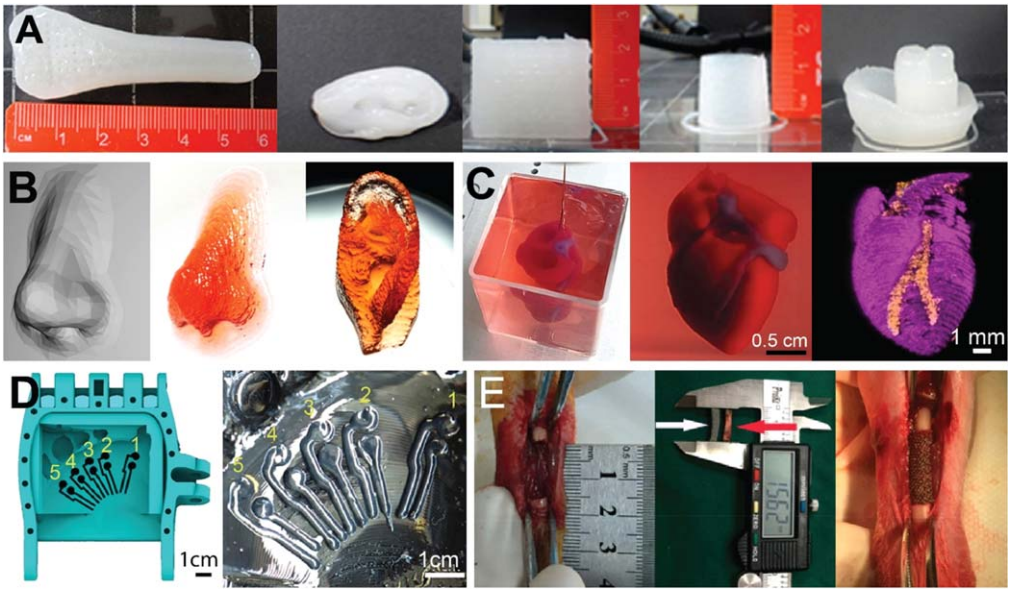

Figure 7. 3D printed constructs with complex geometric properties fabricated using nanomaterials. (A) Cellulose nanofiber prints can produce a variety of complex geometric products. Structures include the bone, ear, cube, cylinder, and boat. Reprinted with permission from [272]. Copyright (272) American Chemical Society. (B) Bioink containing nanosilicates and kappa-carrageenan can print self-supporting anatomical structures such as a nose or ear. Reprinted with permission from [273]. Copyright (3017) American Chemical Society. (C) Bioprinted thick-vascularized tissue in a support bath mimics the shape of a miniature heart. Leftmost image shows the printing in a support bath. Center image shows the heart, and the right image is a confocal image which demonstrates cellularization. Reproduced from [42]. CC BY 4.0. (D) 3D printed prosthetic for a patient with an upper limb deformity using CNT ink as a pressure sensor. The patient had a unique hand deformity, but 3D printing the prosthetic allowed for customized sensors for improved control. Reproduced from [274]. CC BY 4.0. (E) Customized titanium implant coated with nanohydroxyapatite made to fit bone defects. CT scans were used to inform the geometric design of the implant, improving the fit within the body. Reprinted with permission from [275]. Copyright (2018) American Chemical Society.

printed to improve patient control. Multi-walled carbon nanotube ink was designed to conform to the shape of the patient's limb, and this paste could detect patient movement and facilitate control of the implant. Figure 7(D) shows how the customizability of 3D printing conformed to the unique anatomy of the patient. The personalized interface between arm and prosthetic showed a 408% improvement in contact area compared to non-personalized designs, which resulted in improved control by the patient.

Finally, the 3D printing of nanomaterials can fabricate customized support structures. Ma *et al* added nanohydroxyapatite crystals to 3D printed titanium alloys to develop personalized implants for orthopedic healing [275]. Traditional titanium implants often vary from complex native bones in terms of mechanical strength and geometric shape. 3D printing of titanium alloy supplemented with nanohydroxyapatite can address both issues. The product exhibited Young's modulus like bone, and CT scans informed designs that geometrically matched personalized injuries. Figure 7(E) demonstrates how 3D imaging can inform the design of implants for improved geometric fit. The application of personalized devices could be expanded to general populations to ensure that every patient is receiving optimal healthcare.

4.2.3. Customization of biological properties. Early generations of biomedical implants relied on bioinert materials to improve biocompatibility. Current biomedical devices can be designed to elicit specific biological responses [277]. This has potential applications in the field of regenerative medicine [12, 43]. Implantable scaffolds can be designed to provide the necessary environment for cell differentiation and proliferation and to restore the functionality of the tissue [12]. Utilizing nanomaterials, 3D printed constructs can mimic biological tissues, improve cell viability, and illicit specific biological activities.

The integration of nanomaterials with 3D printing could fabricate constructs that mimic specific biological structures. Apelgren *et al* used bacterial nanocellulose to 3D print a replacement for human cartilage [278]. They found that structures produced by this method resembled the mechanical and biological conditions found in natural cartilage. In another example, Markstedt *et al* [279] prepared bioink with nanofibrillated cellulose (NFC) and alginate. By combining the shear-thinning capability of NFC and fast curing cross-linking property of alginate, they successfully 3D bioprinted a sheep meniscus with soft tissue and cells. Figure 8(A) illustrates the cell viability of human chondrocytes. This method could lend itself to other bioprinting techniques, expanding the viability of 3D printed tissues. Also, Narayanan *et al* combined geometric and biologic 3D bioprinting to develop an artificial meniscus seeded with human adipose-derived stem cells [280]. A PLA nanofiber-alginate hydrogel was used as the scaffold material and printed into the shape of a human meniscus. Figure 8(B) shows the final print as well as images of the scaffold structure and cell staining. These images, which were taken four weeks after seeding, provide evidence that nanomaterial

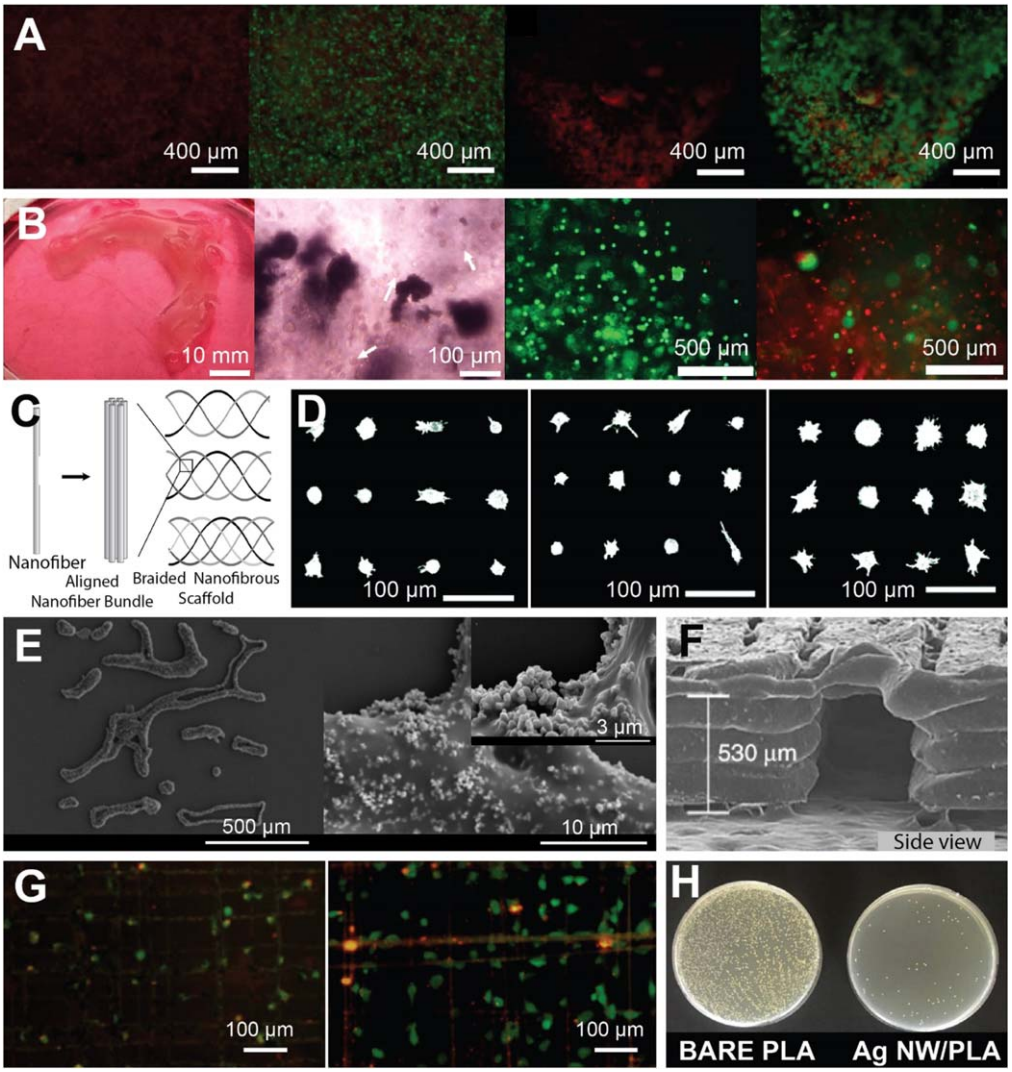

Figure 8. 3D printing of nanomaterials influences the biological properties of the construct. (A) Bioprinting of human chondrocytes with nanocellulose (hNC). Viability of hNC before (left and middle right) and after (right and middle left) 3D bioprinting. Here, red indicated dead cells, and green indicates live cells. Images demonstrate the feasibility of bioprinting living cells. Reprinted with permission from [279]. Copyright (2015) American Chemical Society. (B) 3D printing of meniscus using alginate nanofiber bioink supplemented with human adipose-derived stem cells. From left to right, anatomically shaped meniscus, image highlighting the distribution of cells and nanofibers, the cell viability on the external region of the construct after four weeks in culture, and the cell viability on the internal region of the construct after four weeks in culture. Reprinted with permission from [280]. Copyright (2016) American Chemical Society. (C) Illustration of a braided nanofibrous scaffold. Electrospun poly(lactic acid) (PLLA) was used to mimic biological tendons and could support the growth of human mesenchymal stem cells. The mechanical strength of the scaffold was dependent on the combination of nanofibers and number of nanofibers in a bundle. Therefore, these structures can be designed to match specific mechanical properties within the body. Reproduced with permission from [281]. © Copyright 2013, Mary Ann Liebert, Inc. (D) Bioactive gold nanoparticles enhance human adipose-derived stem cell growth in 3D printed scaffolds 24 h after seeding. From left to right, cell growth on gelatin hydrogel, cell growth on gelatin hydrogel supplemented with gold nanoparticles, and cell growth on gelatin hydrogel supplemented with peptide conjugated gold nanoparticles. Reproduced from [282] with permission of The Royal Society of Chemistry. (E) SEM imaging of piezoelectric nanocomposite (left). In the closeup image of the Osteo-Print (right), barium titanite nanoparticles (BTNPs) on the surface of the 3D structure is observed. These nanoparticles give the composite piezoelectric properties which can be exploited by ultrasonic waves to improve osteogenesis. Reprinted with permission from [283]. Copyright (2015) American Chemical Society. (F) SEM image of 3D printed calvarial bone construct. The construct included human amniotic fluid-derived stem cells that were cultured for 10 d. After five months of implantation, the implant exhibited vascularized bone tissue. Reprinted by permission from Springer Nature Customer Service Centre GmbH: Springer Nature, Nature Biotechnology, [43], 2016. (G) SEM image of the PEO-PCL scaffolds with selective cell attachment. The construct was printed using a solvent-based electrohydrodynamic 3D printing process which allowed for high-resolution printing of polymer. Left figure shows scaffold embedded with MWCNTs with reduced cell adhesion. Right figure shows improved cell adhesion without MWCNTs. Reproduced from [284]. © IOP Publishing Ltd. All rights reserved. (H) 3D printed silver nanowire composites limit E. coli bacterial growth after 2 h. Applications onto implantable medical devices could help reduce infection. Reprinted from [285], Copyright (2019), with permission from Elsevier.

3D printing has applications in facilitating cell growth on printed scaffolds.

3D printed nanofibers can also enable the creation of tendon and ligament (T/L) tissue scaffolds. Indeed, the slow natural recovery of T/L injuries often results in scar-like tissue with poor performance. Current surgical treatment such as tissue gaping [286] and synthetic or allografting [287] exhibit limited long-term biocompatibility, durability, and functionality [281]. Barber *et al* [281] fabricated braided nanofibrous scaffolds (BNFSs) for constructing T/L tissue by electrospinning poly(L-lactic acid) (PLLA). The printed nanofibers were braided into 3, 4, or 5 aligned bundles to construct T/L tissue engineering scaffolds (figure 8(C)). The authors highlight the applicability of BNFSs to replace specific tendons and ligaments, as the range of Young's moduli for the tissue engineering scaffolds (47.6–55.0 MPa) could match the requirements of various native tendons and ligaments. Additionally, the cell alignment of human mesenchymal stem cells that were seeded onto the scaffold aligned parallel with the nanofibers similar to tendons and ligaments, suggesting that this scaffold design could assist in programmed cell growth.

Nanomaterials can also improve cell viability of bioinks formulated for 3D printing. For tissue scaffolds to attain widespread use, they must support the growth of embedded cells. Heo *et al* developed a bioactive bone scaffold constructed of polylactic acid (PLA), gelatin hydrogel, and peptide-conjugated gold nanoparticles (RGNPs) [282]. *In vitro* studies suggest that (RGNPs) enhanced cell adhesion and proliferation on the construct as the cell area of the gel embedded with RGNPs had almost double the cell area after 24 h of seeding and exhibited significantly higher stem cell proliferation rates (figure 8(D)). Another group used bioactive nanoparticles embedded in a cell scaffold to improve cell viability [135]. Poly(lactide-co-glycolic) acid (PLGA) nanospheres encapsulated with transforming growth factor β1 (TGF-β1) functioned as bioactive nanomaterials, which were embedded into a polyethylene glycol diacrylate (PEG-Da) scaffold. This scaffold was SLA printed and seeded with human mesenchymal stem cells (hMSC). When measuring the growth of hMSC *in vitro*, Castro *et al* found that these nanomaterials helped facilitate chondrogenic differentiation, as the TGF-β1 sample showed 25% increase in type II collagen—a marker of chondrogenic differentiation. The authors speculate that the flexible nature of their 3D printing process could readily fabricate a variety of tissue scaffolds, demonstrating its applicability in tissue engineering.

In another example, piezoelectric nanoparticles can be co-printed to augment cell growth in the scaffold. Marino *et al* [283] printed a bio-inspired 3D scaffold via two-photon polymerization using piezoelectric barium titanite nanoparticles (BTNPs) embedded in the Ormocorp resist structure (figure 8(E)). In this study, ultrasound waves served as a piezoelectric stimulator, and this stimulation combined with BTNP's suggested increased rates of osteogenesis based on the expression of a protein that is upregulated during osteogenesis. The structure with BTNPs and ultrasound stimulation exhibited protein deposits on approximately 0.7% of the surface area while the sample without the BTNPs had 0.3% of the surface area.

3D printing with nanoparticles could also provide a fabrication approach to create microchannels to mimic vascular constructs. Indeed, vascularization remains a prominent challenge to achieve successful tissue regeneration in a 3D construct. Kang *et al* [43] have developed a custom bioprinting technique for fabricating human-scale tissue constructs in which microchannels are co-printed in tissue scaffolds to ensure diffusion of nutrients for cell viability. As an example, they successfully fabricated calvarial bone made of polycaprolactone (PCL) doped with tricalcium phosphate (TCP) nanoparticles (figure 8(F)). This structure was designed to improve vascularization, which is achieved after 5 months. Similar methods can be incorporated into other tissue scaffolds in order to improve biocompatibility.

Other studies have used nanoparticles integrated with 3D printed tissue scaffolds to elicit specific biological responses. In these examples, specific bioactive nanoparticles were used to generate bioactive scaffolds. Kolan *et al* demonstrated the efficacy of using 3D printed bioactive borate glass in cell scaffolds [288]. Bioactive glass facilitated binding between implants and the body and is resorbed back into the body at a faster rate compared to other scaffolds. Implementing bioactive glass into the cell scaffold increased the porosity of the print and accelerated weight loss *in vitro*, both of which are desirable qualities. This allowed for quicker healing and decreased dependence on the implant. To promote stem cell proliferation, Jakus *et al* used an extrusion method to fabricate a graphene scaffold [153]. This method used 60 vol% of graphene in polylactide-co-glycolide (PLGA) to support human mesenchymal stem cells *in vitro*. When comparing biological markers of glial and neurogenic cells, Jakus *et al* found that after 14 d, the scaffold with graphene exhibited between 2 and 6 times the amount of these markers compared to a 20 vol% graphene scaffold, suggesting that the concentration of this nanomaterial could regulate stem cell proliferation.

Integrating nanomaterials with electrospinning can yield the creation of multi-scale tissue scaffolds with selective cell attachments. He *et al* [284] fabricated a microscale poly (ε-caprolactone) (PCL) scaffold with multi-walled carbon nanotubes (MWCNTs) reinforcement (figure 8(G)) in which the addition of polyethylene oxide (PEO) to PCL was studied to achieve an optimal PEO-PCL composition. This printing process controlled the area of cell growth on scaffold constructs as they found that cells on the PEO-PCL-MWCNTs scaffold only attached cells along the printed microfibers, while the PEO-PCL scaffold did not show this selectivity. The authors hypothesized that the agglomeration of MWCNTs in the microscale fibers might have prevented cell attachment. This selective cell activity can be utilized in future scaffolds that wish to constrain cell growth to certain areas.

Infection is a serious risk that implantable medical devices carry [289]; however, 3D printing of nanomaterials can help restrict bacterial growth on printed surfaces. Bayraktar *et al* demonstrated how silver nanowire PLA nanocomposites effectively protected implants against *S. aureus* and *E. coli* bacteria (figure 8(H)) [285]. Specifically,

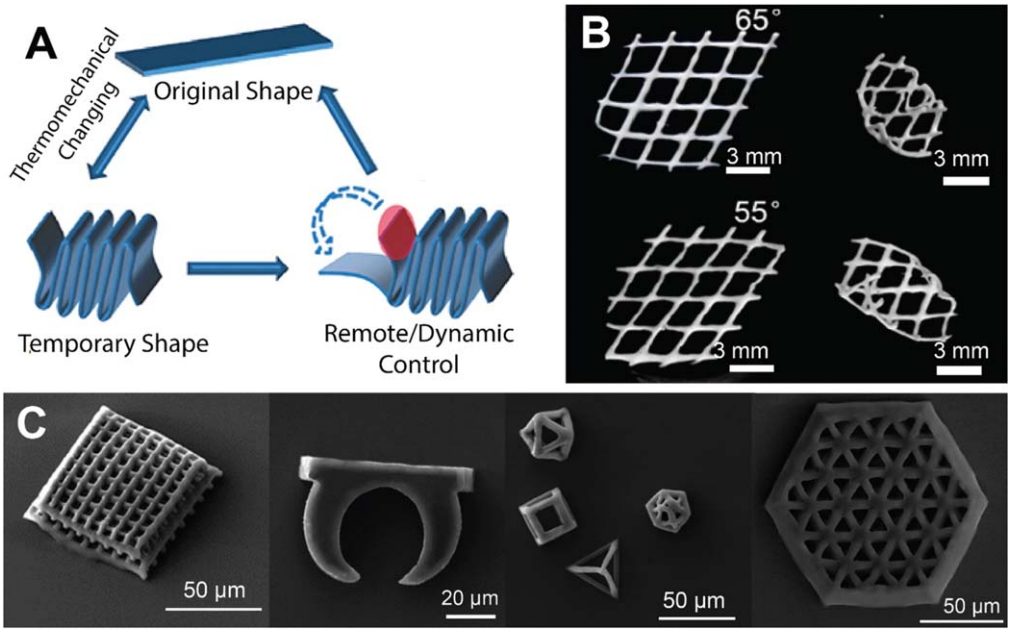

Figure 9. 4D properties can be achieved by 3D printing of nanomaterials (A) Schematic of the general mechanism for polymer shape memory. (B) A lattice structure with silica nanoparticles that improves the mechanical properties of the poly(N-isopropyl acrylamide) (PNIPAM), which is thermoresponsive and can produce a 4D effect. (C) Micro-sized structures that possess actuation properties due to the photo responsive properties of gold nanorods incorporated in the structures. (A) Reprinted by permission from Springer Nature Customer Service Centre GmbH: Springer Nature, Nano Research, [293], 2019. (B) [294] John Wiley & Sons. © 2019 WILEY-VCH Verlag GmbH & Co. KGaA, Weinheim. (C) Reprinted with permission from [137]. Copyright (2019) American Chemical Society.

silver nanowires with only 1 wt% were able to kill 100% of *S. aureus* up to four hours; however, increasing the silver concentration to 2 or 4 wt% could extend this duration. When applied to a 3D printing process, these methods are promising to minimize opportunistic infections of medical implants, such as total joint replacement prosthesis, by coating the surfaces of medical devices with bactericidal nanocomposites.

4.2.4. Customization of responsive properties. 4D printing, a process by which 3D printed structures can change shape after fabrication, has been shown to have many potential applications in the biomedical field [290]. Materials and devices fabricated by 4D printing demonstrate responsive properties to certain stimuli. The mechanism for inducing a 4D effect in a 3D printed product relies upon the use of smart materials, which can change shape when introduced to an external stimulus [291]. Nanomaterials can be incorporated in a 3D printing method to develop 4D properties within printed constructs. When an appropriate force or an external stimulus, such as optical illumination or electrical actuation, is imposed in a nanomaterial, a change in shape or a change of the construct can be induced.

Nanomaterials such as graphene, carbon nanotubes (CNTs) and silica can be incorporated in 3D printing to induce 4D effects [290]. Among other materials, polymers are an attractive smart material for 3D printed biomedical devices because of their biocompatibility and printability [292]. During printing, crosslinking develops within the polymer, which forms a permanent structure. After printing, the material can be molded to a different temporary shape. The polymer will maintain this temporary shape until it is heated above its glass transition temperature, at which point it will return to its original shape. This property can be used to design structures that move in response to certain stimulations. For a schematic explanation, see figure 9(A). Nanomaterials can be incorporated into 3D printing to develop 4D properties within printed constructs. This section will review how these constructs could inspire unique biomedical devices when stimulated by heat, light, water, or magnetism.

First, temperature-responsive nanomaterials can be used to induce 4D properties in 3D printed products. Mechanical properties are highly dependent on the material temperature, and this quality can be exploited to produce products which have dynamic mechanical properties. When Guo *et al* incorporated silica nanoparticles with poly (N-isopropyl acrylamide) PNIPAM, the composite experienced a solid to rubber transition at higher temperatures [294]. Both storage and loss modulus increased dramatically with the addition of 10 wt% silica nanoparticles, which allows for the printing of complex geometries. As seen in figure 9(B), the addition of silica nanoparticles alters PNIPAM's mechanical properties. Temperature-dependent 4D properties can also be used to make water harvesting devices. Thakur *et al* used thermoresponsive nanomaterials to create water harvesting nanofibers [295]. Two different fibers were made with cellulose acetate (CA) and PNIPAM: one fiber was printed using coaxial electrospinning, which uses two materials to create a core and shell structure, and the other fiber was blended and electrospun. The water harvesting effect is dependent upon the ability of PNIPAM to make a conformational change that exposes more hydrophilic functional groups at lower temperatures. As such, both core–shell and blended

nanofibers were shown to have 190% and 30% weight gain respectively. When the temperature was increased from 25 °C to 40 °C, the core–shell fibers lost moisture and resulted in a 57% weight loss. This tunability demonstrates how heat could be used in 3D printing of nanomaterials to induce changes after printing.

Second, light-responsive drug delivery devices can be fabricated with 3D printing of nanomaterials. Light responsive nanomaterials can endow the ability to induce shape change by photothermally heating materials [296]. Light is an attractive stimulation method because it enables high tunability and precision via the regulation of intensity and wavelength [297–299]. Tiwari *et al* used electrospinning to create drug-loaded polycaprolactone (PCL) nanofibers [298]. The PCL-drug composite nanofibers allowed for a greater surface area to be covered with the photothermally active polypyrrole (PPy) because of favorable electrostatic interactions. They reported up to 60% drug release after four periods of near-infrared (NIR) light exposure, which demonstrates how light can be used to stimulate 4D printed constructs. This precise drug release could also improve antibiotic treatments [300]. Altinbasak *et al* used an electrospinning technique to fabricate mats from poly(acrylic acid) nanofibers and reduced graphene oxide nanoparticles [157]. Photostimulation induced swelling of the nanofibers which released the drug. *In vivo* skin infection experiments in mice confirmed that the mats released enough antibiotic to induce wound healing and prevent bacterial growth of *Staphylococcus aureus*. This study suggests that future drug delivery systems could localize release to predetermined locations. Choi *et al* used gold nanorods (AuNRs) and poly(d,l-lactic-co-glycolic acid) (PLGA) to fabricate electrospun, drug-releasable nanofibers [158]. AuNRs can convert photonic energy into thermal energy, thus heating PLGA crosslinks with photonic stimulation. The heated crosslinks allowed for a 20% release of doxepin hydrochloride after 12 h. The nature of these AuNRs also allowed for the modulation of fiber temperature based on the power density of the light. Such customizability is very attractive for drug delivery vehicles, where it can be difficult to release specific amounts of drug into a system.

Light-sensitive AuNRs also have also shown to have applications in functional devices. Using two-photon polymerization, Chen *et al* fabricated ornate, micro-sized structures with AuNRs and a liquid crystalline elastomer matrix that rapidly changed shape upon photo stimulation [137]. The mechanism of actuation, however, is different from the previously described mechanism because it utilizes liquid crystals (LC). Upon printing, LCs are aligned. During NIR stimulation, the LCs lose their alignment, allowing for movement of the elastomer. As seen in figure 9(C), the direct laser printing technique allows for the fabrication of micro-sized structures that possess actuation properties. Tissue engineering is another field of interest for 4D printing light-responsive nanomaterials. Cui *et al* created a polymer/graphene nanocomposite using FDM and extrusion techniques [293]. Graphene is an attractive nanomaterial for neural cell proliferation as it is conductive and optoelectronic. Under a NIR stimulation, they reported a photocurrent of 0.3 μA within the scaffold. This has potential applications in physiological systems that utilize electric currents such as neural cells and cardiomyocytes.

Third, water-induced swelling can produce printed objects with responsive properties. Gladman *et al* utilized a hydrogel composite to develop 4D architectures that could fold and twist when placed in water [301]. The hydrogel ink was composed of N,N-dimethylacrylamide, photoinitiator, nanoclay, glucose oxidase, glucose, and nanofibrillated cellulose. When printed with shear-induced alignment, these inks exhibited anisotropic swelling behavior. Applying these properties to a bilayer structure with variable print orientations allowed for the fabrication of structures that would fold into specific flower morphologies when wet. This study demonstrates how the design of printing materials and methods can be used to design responsive architectures.

Fourth, magnetic nanomaterials can provide 4D properties for 3D printed drug delivery devices. Magnetic-responsive materials function similarly to light-responsive materials as they both induce temperature change upon stimulation. Niiyama *et al* used this strategy to achieve highly localized chemotherapeutic drug release [302]. Magnetic nanoparticles were combined with poly(NIPAAm-co-HMAAm) and printed. The localized 18% drug release was achieved by changing the frequency of an alternating magnetic field about the device, which led to a movement among the magnetic nanoparticles, increasing the temperature of the nanofibers. They reported several advantages to this chemotherapeutic technique, including controllable heating at the tumor site and localized drug delivery.

4D properties that are stimulated by magnetic fields also have applications in soft robotics. Zhu *et al* used a non-uniform magnetic field to impart 4D characteristics. They fabricated a poly(dimethyl siloxane) nanocomposite with iron nanoparticles and printed it using DIW [303]. Upon application of a magnetic field, they found that a temporary shape was achieved in 0.7 s. This fast response time was attributed to a low magnetic coercive force and high magnetic permittivity. These findings could impact the field of biomedical devices where faster actuation times are desired. Wei *et al* utilized a DIW printing method and printed a multilayered rectangular scaffold with composite poly(lactic acid)-based inks containing BP/PLA/DCM c-PLA and FeO_3. They reported that the addition of FeO_3 nanoparticles to cPLA ink increased its shape recovery ratio, magnetically stimulated functionality, and localized temperature control compared to standard PLA ink [304]. The improved shape recovery ratio is due to the addition of cross-linking structures in the nanocomposite. They proposed that their findings could be applied to an intravascular stent, which would shrink when heated. After this stent is implanted, it would cool, expanding the stent into position.

4.3. Bioelectronic devices

Electricity is an essential part of bodily function, ranging from the electrical signals sent from the brain via nerves to every part of an organism, to the electrical signals that regulate the

activity of each cell or group of cells [305, 306]. With so much of the body utilizing electrical signals to communicate and function, the ability to interface with biological electricity has significant potential in the regulation and observation of physiological functions, as well as an unraveling the complex mechanisms of the biological system [307, 308]. Bioelectronics is a field generally defined as the merging of electronics with biology, where electronic signals are exchanged between electronic devices and biology [309, 310]. The field was pioneered in the 1970s by Luigi Galvani when he first actuated a frog leg with an applied voltage [310] and has since introduced devices such as cardiac pacemakers and deep brain stimulators [311].

One of the key challenges in most bioelectronics is maintaining long-term biocompatibility: protecting cell viability and the health of the organism, as well as preserving the performances of the electronics in a complex and dynamic biological microenvironment [312, 313]. This is especially challenging with conventional electronics where mechanical, material, and geometrical dichotomies prevent a seamless merging of the electronic devices with biological constructs. For example, biological organs generally have Young's moduli 3–6 orders of magnitude smaller than that of microfabricated electronics [7, 312]. Furthermore, seamless interfacing of bioelectronics with complex, non-planar biological geometry [7] requires devices of similar or smaller scale than biological cells and tissues [309].

Nanomaterials can be integrated with a 3D printing process to enable the creation of devices with highly tunable functional properties [309, 314, 315] which overcome the dichotomy described above. For example, the multi-scale additive manufacturing approach enables a facile route to print electronic elements that can be integrated with flexible and biocompatible materials in complex geometries [7]. This section highlights the unique capability of this approach in integrating biological systems with electronics. We will first discuss the 3D printing of microelectrodes to interface electronics with biological electrical signals. Next, we will describe the 3D printing of nanomaterial-based bioelectronic scaffolds that can potentially improve tissue and organ regeneration. Finally, we will highlight how this multi-scale approach can create unique nanomaterial-based biosensors and lab-on-a-chip devices which would otherwise be challenging to fabricate.

4.3.1. Microelectrodes. Microelectrodes can interface with the body's neural pathways to either acquire electrical signals or to provide electrical stimulation [310]. To maximize biocompatibility in a complex biological microenvironment, microelectrodes need to be mechanically compliant and chemically inert [316, 317] which is challenging to be achieved with a microfabrication approach. This review focuses primarily on the 3D printing of nanomaterial-based microelectrode arrays (MEA), which can be fabricated with reduced production times, increased customization, improved biocompatibility, and at lower cost than traditional devices.

3D printing can significantly reduce the production time of MEAs and enable significant customization. In contrast to a single microelectrode, MEAs are often preferred due to their improved mass transport, response times, sensitivities, and lower limit of detection (LOD—the smallest amount of a substance that can be detected in a solution) [318]. Yang *et al* fabricated aerosol jet printed MEAs using silver nanoparticle ink and polymer traces [318]. They accurately controlled the spacing between conductive traces at 30, 100, and 180 μm, demonstrating the ease of customization with 3D printing in stark contrast to a micromachining approach. Kundu *et al* developed a process where complete 8 $\times$ 8 MEAs could be assembled in under 4 d [319] which otherwise would take up to four months with a conventional fabrication approach. This is achieved with an SLA printed clear base which is subsequently subjected to ink casting of a silver nanoparticle ink, pulsed electroplating of either a gold or platinum solution, and laser micromachining to produce the finished part. Although this approach is not entirely 3D printed and yields a lower resolution than traditional lithographic methods, the incorporation of a 3D printing process enables a rapid fabrication and prototyping approach (as shown in figure 10(A)), allowing a faster possible implementation into customized medical devices and constructs. The authors also demonstrated that the nanoporous platinum and nano-gold layers can achieve a measured impedance and double-layer capacitance similar to commercially available MEAs (1 kHz impedance of 36.8/16 kΩ and double layer capacitance of 400 nF cm^{-2}/520 nF cm^{-2} for nanoporous platinum/nano-gold, respectively).

A 3D printing approach, such as inkjet printing of nanomaterial-based inks, can enable the creation of biocompatible and flexible MEAs. Khan *et al* designed fully biocompatible MEAs with inkjet-printed gold nanoparticle conductive traces, shown in figure 10(B) [110]. Gold is desirable for biological applications due to its superior stability when in contact with biological fluids and tissues. The use of gold nanoparticles also allowed them to selectively sinter the traces on plastic substrates below the melting points of the plastics themselves. Low-temperature sintering was performed at approximately 200 °C and sintering time was carefully tuned to ensure all traces were properly fused, as traces of different widths sinter at noticeably different speeds at low temperatures. After the inkjet traces were sintered, the MEAs were coated with a thin layer of fluoropolymer and then plasma-etched to expose the electrode contacts. The fluoropolymer provided additional protection for the vias from biological fluids [321].

Indeed, integrating a complete multi-material additive manufacturing approach with nanomaterials can lead to reduced fabrication times, cost, and improved MEA biocompatibility without compromising electrical performance. Although exhibiting unique performance, the 3D printed MEAs described earlier require conventional fabrication techniques for a subset of the processes (e.g. post-processing) and are not entirely 3D printed. Recently, Schnitker *et al* leveraged a complete 3D printing approach to create highly customized MEAs in less than 60 min per chip and costing only a few cents per chip [320]. Silver nanoparticles and nanoporous carbon conductive traces were printed on a

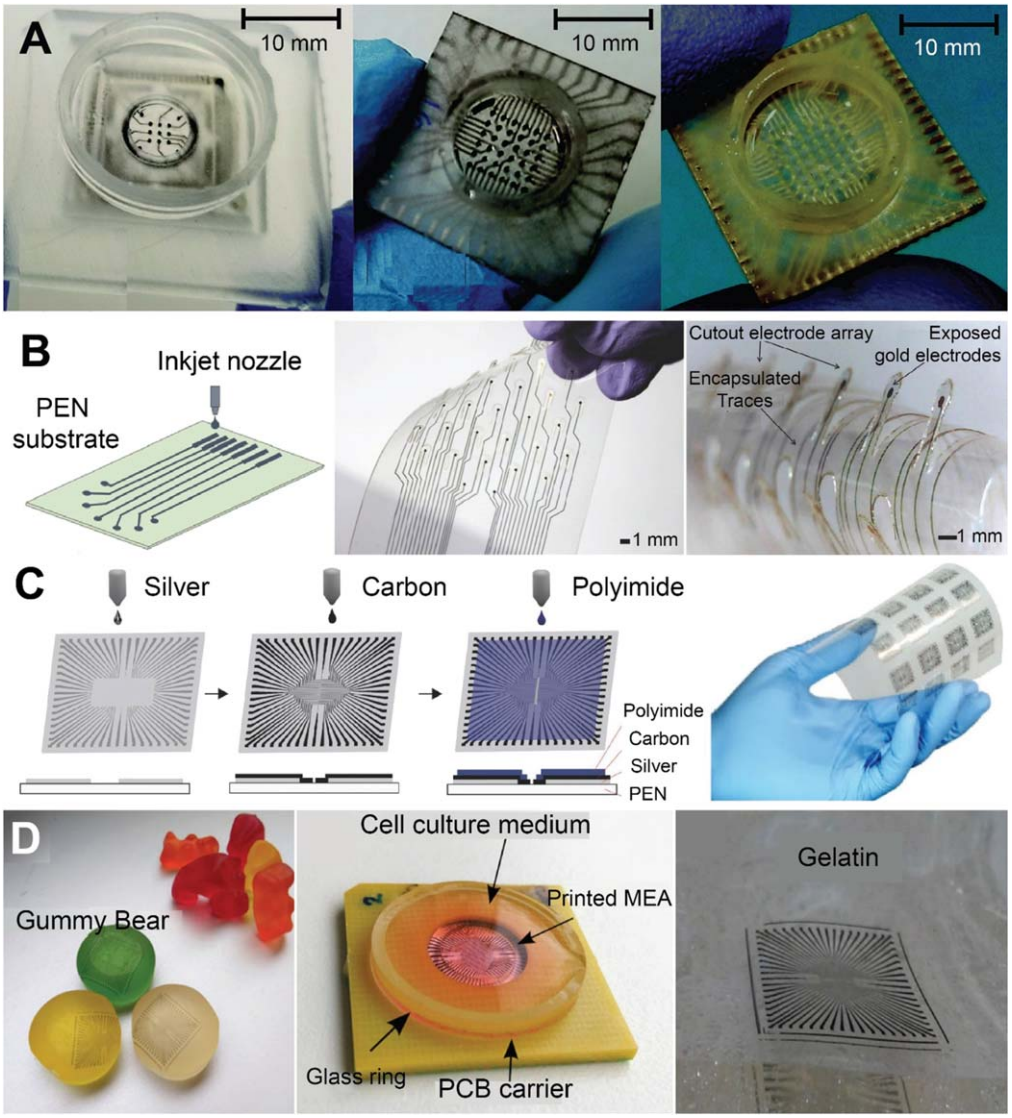

Figure 10. 3D printed, nanomaterial-based microelectrode arrays (MEAs) can be fabricated with greater customization and improved biocompatibility than devices constructed using a conventional fabrication approach. (A) Rapidly prototyped 3 × 3, 6 × 6, and 8 × 8 MEAs, respectively. The arrays consist of an SLA printed base and silver nanoparticle traces. Reproduced from [319]. CC BY 2.0. (B) Flexible inkjet-printed MEAs. Gold nanoparticle traces are printed on a polyethylene naphthalate (PEN) substrate and encapsulated in a protective fluoropolymer. Left shows the first step in the fabrication process, right and center show the completed MEAs. [110] John Wiley & Sons. © 2015 WILEY-VCH Verlag GmbH & Co. KGaA, Weinheim. (C) Flexible and fully inkjet-printed MEAs consist of silver nanoparticle traces, exposed nanoporous carbon electrodes, and a polyimide protective layer. [320] John Wiley & Sons. © 2018 WILEY-VCH Verlag GmbH & Co. KGaA, Weinheim. (D) Fully inkjet-printed MEAs on complex substrates such as gummy bears and gelatin. Center image shows an MEA printed on hydrogel and attached to a circuit board for action potential measurements of cell culture. Reproduced from [44]. CC BY 4.0.

polyethylene naphthalate base; these were coated with a dielectric polyimide in the final step to provide a protective layer, as shown in figure 10(C). The silver ink provided a useful conductive layer, but to avoid biological harm, it was not printed near the sensing area. Nanoporous carbon ink provided superior biological compatibility as an interfacing material, and can maintain electrical performance due to its chemical stability, low impedance, and large electrochemical water window (voltage range in which a chemical neither oxidizes nor reduces) [44, 322]. Impressively, the authors demonstrated the versatility of their approach by 3D printing MEAs on a variety of materials including PDMS, agarose, and complex gelatin structures (gummy bears) as shown in figure 10(D) [44].

4.3.2. Bioelectronic scaffolds. The integration of electrical components with biological regenerative scaffolds could have a significant impact on the creation of biomedical devices. For example, studies have suggested the use of electrostimulation as a potential approach to promote the regeneration of biological tissues [323–325]. The incorporation of electronics into biological scaffolds could potentially enhance, modulate or even enable regenerative processes. Indeed, the merging of

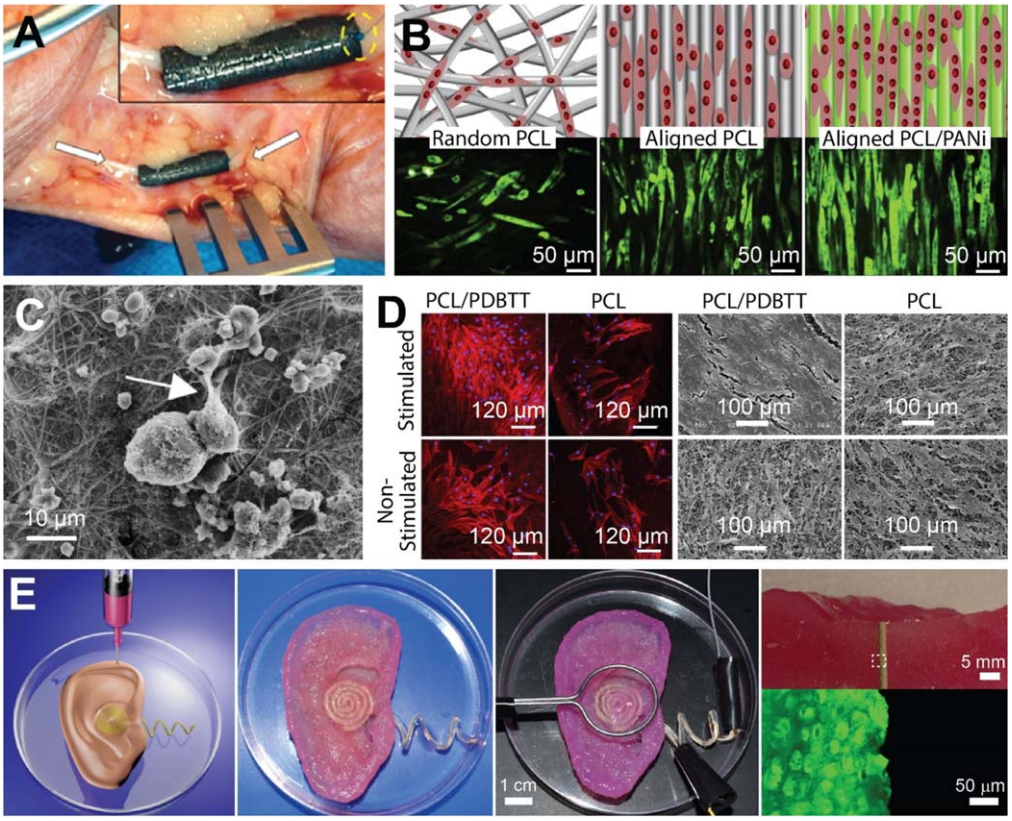

Figure 11. 3D printed bioelectronic scaffolds can aid in the regeneration of biological tissues and cells. (A) A 3D printed graphene scaffold promotes regeneration of the ulnar nerve, indicated by arrows, in a human cadaver. Reprinted with permission from [153]. Copyright (2015) American Chemical Society. (B) Electrospun nanofibers provide electrical and topographical cues to assist in the alignment and maturation of mouse skeletal myoblasts. Reprinted from [326], Copyright (2013), with permission from Elsevier. (C) A neurite, indicated by the arrow, growing on a conductive electrospun scaffold. Reprinted from [327], Copyright (2009), with permission from Elsevier. (D) Electrospun, semiconductive, photosensitive PCL/PDBTT nanofibrous scaffolds for skin regeneration result in greater cell density with light stimulation than do normal PCL scaffolds. Reprinted from [328], Copyright (2017), with permission from Elsevier. (E) A 3D printed bionic ear. Left to right shows a schematic, prototyped ear, and then the prototyped bionic ear experimental setup which is used to characterize the audio sensing of the ear. Far right shows a photographed cross section of the ear (top), and a fluorescent close-up image (bottom) showing the viability of the living chondrocytes that are in contact with the conductive electrodes. Reprinted with permission from [45]. Copyright (2013) American Chemical Society.

electrical components with biological constructs is of significant interest but has yet to be achieved due to the aforementioned challenges in merging conventional electronics with biological constructs. 3D printing of nanomaterial-based devices is a promising approach that can potentially enable a better incorporation of electronics into a complex regenerative system.

One approach to achieve such integration is through the creation of biocompatible scaffolds with imparted electrical conductivity. For example, Jakus *et al* developed a graphene-based polylactide-*co*-glycolide (PLG) scaffold [153] using DIW 3D printing. The scaffold demonstrated electrical conductivities above 800 S m^{-1} and *in vivo* biocompatibility with a mouse subcutaneous implant model for 30 d. As a proof of concept, a nerve conduit was 3D printed and characterized, as shown in figure 11(A). It was found that the shear alignment of the graphene flakes during printing improves the electrical conductivity and tensile strength (210 MPa at 20 vol% graphene) of the structure.

In addition to electrically conductive biomanufactured scaffolds, a multiscale 3D printing approach also enables the creation of electrically conductive devices into bioprinted constructs, which can improve cell adhesion and proliferation over passive scaffolds. For example, using magnetic field-assisted electrospinning, Chen *et al* studied the effect of aligned nanofibers by seeding mouse skeletal muscle tissue (myoblasts) on poly(e-caprolactone) (PCL) and PCL with polyaniline (PCL/PANi) electrospun nanofibers [326]. Intriguingly, they have shown that aligned, electrically conductive PCL/PANi nanofibers further increased myoblast number and maturation index over aligned, nonconductive PCL nanofibers by approximately 30% and 3% respectively, as shown in figure 11(B). Similarly, Bolin *et al* coated electrospun nanofibers with conductive poly(3,4-ethylenedioxythiophene) (PEDOT) and observed excellent adhesion and proliferation of neuronal cells on the scaffold, as shown in figure 11(C) [327]. Electrical stimulation further induced Ca^{2+} signaling between the cells.

In another example, Wang *et al* show that electrospun PLA/PANI conductive nanofibrous sheets can promote cell viability of cardiomyocytes (cardiac tissue) [329]. Cardiomyocytes seeded on conductive nanofibers had a higher

maturation index and fusion index than ones seeded on non-conductive PCL nanofibers. The fibers also beat synchronously with the cardiomyocytes, the cells stimulating the scaffold, an effect that could enable other bioelectronic applications [330–332]. Liu *et al* electrically stimulated MC3T3-E1 cells (bone tissue cells) on aniline pentamer-graft-gelatin (AP-*g*-GA) and poly(L-lactide) (PLLA) electrospun nanofibers [333]. Although significant differences in the cells seeded on various nanofiber mats were not observed, a higher $[Ca^{2+}]_I$ (measured value to quantify the total population of cells) was observed for cells exposed to electrical stimulation than for those that were not, and good biocompatibility was observed for all.

Photosensitive elements can also be 3D printed to enable light-induced electrical stimulation. For example, Jin *et al* found that the cell proliferation of human dermal fibroblasts (skin cells) increases on PCL/PDBTT electrospun nanofibers [328]. The photosensitive poly (N,N-bis(2-octyldodecyl)-3,6-di(thiophen-2-yl)-2,5-dihydropyrrolo[3,4-*c*]pyrrole-1,4-dione-alt-thieno[3,2-*b*]thiophene) (PDBTT) was stimulated with a red LED for one hour every 24 h, resulting in higher cell–cell communication and proliferation over PCL nanofibers. Figure 11(D) shows a comparison between stimulated and non-stimulated human dermal fibroblasts on PCL and PCL/PDBTT nanofibers.

An entirely 3D printed electronic and regenerative scaffold can also be achieved with a multiscale 3D printing process. As a proof of concept, Mannoor *et al* fabricated a bionic ear with DIW 3D printing [45]. Living chondrocytes were seeded in a hydrogel matrix, printed in the shape of an ear and co-printed with silver nanoparticles as a coiled antenna inside the ear, as shown in figure 11(E). This suggests the possibility to integrate biological constructs with functional electronics using a multi-scale 3D printing approach, allowing the creation of regenerative constructs integrated with functional electronics.

4.3.3. Biosensors. Biosensors are devices that sense the presence of a specific substance and produce a recognizable electrical signal in response [334]. Although not all biosensors interface with the body's electrical signals, bioelectronics and biosensors are often treated together due to how closely intertwined the fields are [335–337]. Glucose biosensors are bioelectronic, for example, because they utilize electrodes to detect the number of electron transfers in a catalyzed glucose reaction [309, 338, 339].

The integration of nanomaterials into 3D printed constructs can leverage their size-dependent functional properties to create tunable chemosensors. 3D printed nanomaterial-based sensors have been demonstrated to be able to detect chemicals such as glucose [340], biomarkers [341–343], herbicides [343], and bacteria [344, 345]. For example, Su *et al* fabricated a multi-well glucose sensor by FDM printing two composite filaments consisting of acrylonitrile butadiene styrene (ABS) and magnetite nanoparticles, as well as polyvinyl alcohol (PVA) and o-phenylenediamine (OPD) [340]. They achieved this by leveraging the water solubility of PVA to gradually incorporate chromogenic OPD into the mixture. When exposed to hydrogen peroxide, OPD will undergo oxidation on the surface of the magnetite—used here as a nanoparticle catalyst. The production of hydrogen peroxide from the oxidation of glucose provided a means of colorimetric observation without the addition of other reagents to the sample (figure 12(A)). The further optimization of the microstructures of the two-part plates, the incubation pH (∼5 pH), and temperature (∼40 °C) enables the creation of a reliable (∼±4.4% error) glucose monitoring device.

3D printing can also leverage the biocompatibility and chemical sensitivity of metallic nanomaterials to form flexible electrode arrays with a variety of uses, from amplifying electrical signals [346] to the detection of cancer markers [341, 342] and antioxidants [343, 347]. Using the precision and multi-material capability of inkjet printing, complex electrode arrays can be quickly fabricated using minimal materials, and customized to tune the sensor's response. For example, Adly *et al* fabricated microgap electrodes for redox-cycling biosensors with carbon and silver nanoparticles coated with polyimide ink [346]. The spacing between electrodes determines the redox-cycling amplification of electrochemical signals and, subsequently, device sensitivity (figure 12(B)). Electrode spacing down to 1 μm was achieved by carefully controlling droplet ejection frequency, translational velocity, and substrate temperature. Utilizing the sensitivity of the redox current to surface blocking, Adly *et al* successfully demonstrated the electrochemical biosensing of human immunodeficiency virus (HIV)-related DNA strands with their device. The high sensitivity of the electrode array was made possible by the single-droplet precision of inkjet printing. Similarly, Pavinatto *et al* inkjet-printed antioxidant biosensors with precisely sintered, interdigitated gold electrodes (figure 12(C)) [343]. The gold nanoparticle traces were printed on plastic substrates and sintered at 200 °C for 6 h, the finalized flexible sensors showing a limit of detection (LOD) of 200 μM. Furthermore, Jović *et al* inkjet-printed silver nanoparticles and CNTs to form an electrode array, which could detect thyroid-stimulating hormone (TSH) in an aqueous solution and atrazine (ATR) in urine with a sensitivity as high as 0.5 $\mu U\,ml^{-1}$ (TSH) and 0.01 $\mu g\,l^{-1}$ (ATR) [348].

Functionalized gold nanoparticle electrodes can be used to detect cancer biomarkers. For example, Otieno *et al* inkjet-printed electrode arrays to detect parathyroid hormone-related peptides (PTHrP), which have been utilized as biomarkers for a variety of cancers [341]. Biocompatible gold nanoparticles were used in the eight-electrode array, which was able to detect both PTHrP and its fragments with an LOD of 150 aM —approximately 1000 times lower than conventional methods. This impressive array was printed using only $0.20 of materials, and 56 arrays could be printed in a single run. Carvajal *et al* used a similarly inexpensive method to print eight-electrode arrays for sensing HER-2, a breast cancer biomarker [342]. They printed silver nanoparticle traces, gold nanoparticle electrodes, and coated the sensor with a biocompatible polyimide substrate, completely inkjet printing

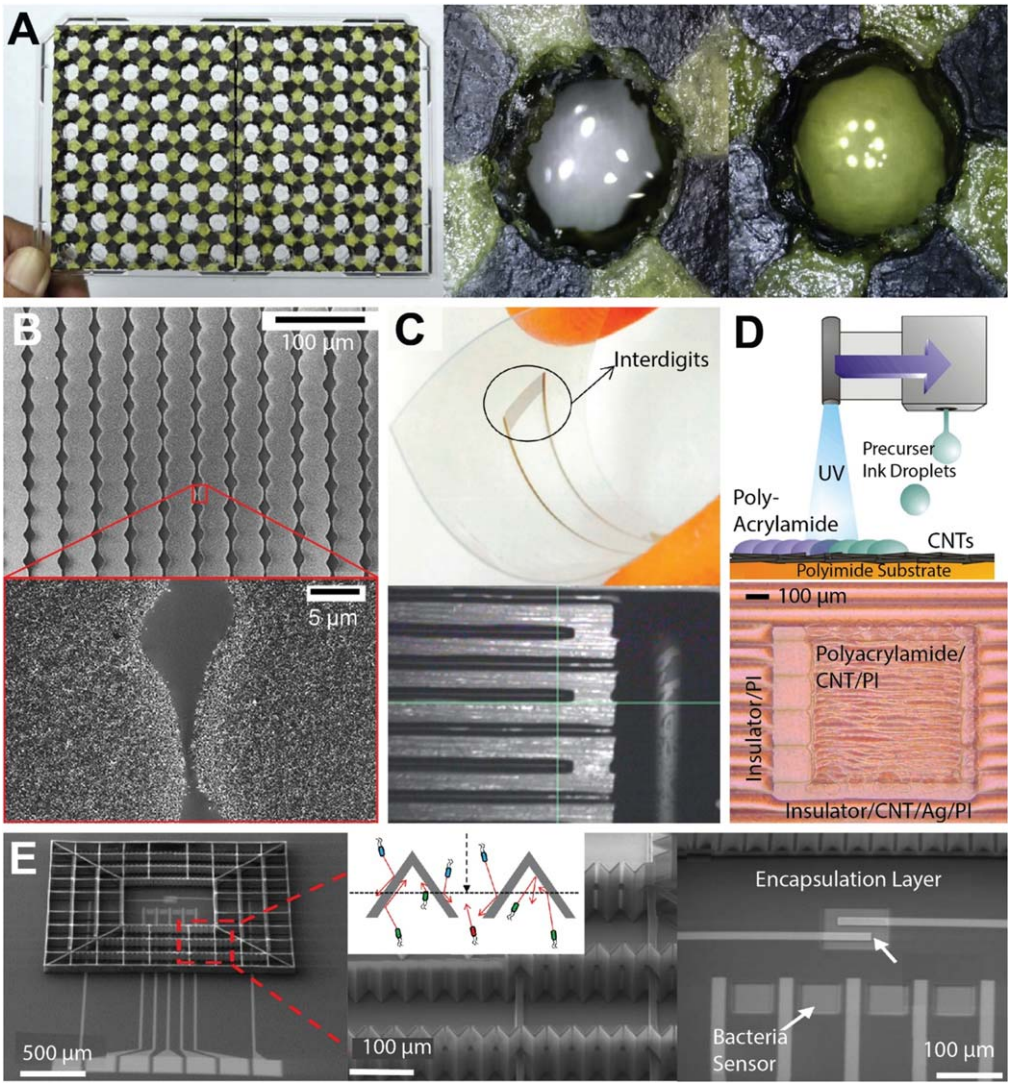

Figure 12. 3D printed nanoparticles enable the creation of biosensors with tunable properties, that are mechanically flexible, and that can detect in a variety of assay environments. (A) FDM printed multi-well, glucose determining plates allow for colorimetric differentiation between urine from a healthy person (center), and urine from a diabetic person (right). Iron magnetite nanoparticles act as reusable catalysts imbedded in the wells. Reprinted from [340], Copyright (2018), with permission from Elsevier. (B) High-resolution inkjet-printed lines for redox cycling, with spacing controlled down to 1 μm. [346] John Wiley & Sons. © 2017 WILEY-VCH Verlag GmbH & Co. KGaA, Weinheim. (C) Flexible, inkjet-printed, interdigital electrodes for antioxidant sensing. Bottom shows a magnified view of the gold nanoparticle electrodes. Reprinted from [343], Copyright (2015), with permission from Elsevier. (D) Simultaneous inkjet printing and UV photopolymerization of polyacrylamide ink on CNTs and polyimide for the creation of antioxidant-sensing electrodes. Silver nanoparticles, CNTs, an insulator, and then polyacrylamide are printed sequentially to form the biosensors (shown below). Reprinted with permission from [347]. Copyright (2015) American Chemical Society. (E) A 2PP printed microscopic cage for motile bacteria. Center inset shows the bacteria concentration mechanism, right shows the sensors at the center of the cage. Reproduced from [345]. CC BY 4.0.

the electrodes with the successful method discussed in the microelectrode section above. The sensor had an assay time of only 15 min and a LOD of 12 pg ml^{-1}. Both devices behave similarly—rather than directly detecting the biomarkers, the gold electrodes detect ferrous molecules in solution through redox reactions at the electrodes' surface. Both the electrodes and the ferrous molecules (Otieno used iron beads, Carvajal used heme) are functionalized with antibodies, so that the biomarkers will bridge the two and cause a redox current to flow. These 3D printed biosensors offer many advantages over conventional biosensors: they are inexpensive, exhibit small LODs, and their sensitivity can be tuned.

In addition to the functional properties of nanomaterials, the rapid prototyping ability of 3D printing enables the optimization of biosensor performance in a variety of assay environments. CAD can be used to maximize the efficiency of the nanomaterial biosensor through techniques such as sorting bacteria and filtering complex mixtures. For example, size-based separation can be used to maintain the biosensor's performance when using suboptimal mixtures. Lesch *et al* were able to produce an antioxidant biosensor that could operate in unfiltered, complex mixtures such as orange juice and red wine [347]. Matrix effects normally necessitate the treating of such samples with dilution or filtering before

sensing, however a thin layer (50 nm–1 μm) of polyacrylamide hydrogel (PA) acted as a screen for the CNT electrodes. Nanopores (∼13 nm) within the film permitted the passing of antioxidant molecules while blocking unwanted substances such as pulp and fibers. The hydrogel film was optimized by tuning the surface tension and viscosity of the hydrogel, along with *in situ* UV curing. The entire device was inkjet printed with four ink compositions (Ag, CNT, insulator, and PA). The multi-material inkjet process and finalized electrodes are shown in figure 12(D).

Intriguingly, a similar size-based sorting concept can be applied to bacteria assays by integrating 3D printed microfluidics and magnetic nanoparticles. This approach enables the ability to actively remove and sort *E. coli* bacteria from a solution [344]. Specifically, magnetic nanoparticle clusters (MNCs) made of 15 nm magnetite nanoparticles are functionalized with antibodies which will bind onto the bacteria to form MNC-*E. coli* complexes (MNC-EC). The magnetic properties of the magnetite particles allow the MNC-ECs to be separated from the food analog using a magnetic field. The solution of MNCs and MNC-ECs are then forced through a 3D printed, helical microfluidic channel to separate the MNC-ECs. The helical channel produces Dean vortices in the moving fluid which causes the smaller MNCs to migrate toward the outer edge of the helix. This allows the separation of a concentrated MNC solution and a concentrated MNC-EC solution. Thus, the mechanical removal of *E. coli* bacteria from food is possible, as well as collection of samples for analysis. The authors show that this approach enables detection limits as low as 10 cfu ml^{-1} in buffer and 100 cfu ml^{-1} in milk for *E. coli* with ultraviolet–visible spectroscopy. Furthermore, the optimization of device morphology can be used to passively sort bacteria. For example, Li *et al* utilized two-photon polymerization (2PP) to create a microscopic cage for motile bacteria (figure 12(E)) to improve the sensitivity of a graphene-based biosensor [345]. Inspired by venous valves, selective photopolymerization was used to fabricate a customized, directional valve system. The morphology of the valve system facilitates the motion of bacteria in only one direction, causing the bacteria to concentrate in the sensing area. As the sensor detection is due to the charge carrier density change when bacteria bind to the surface, increasing the concentration of the bacterial enhances the detection rate. Indeed, electrical measurements demonstrated signal enhancement up to 27 fold. These examples of 2PP, SLA, and inkjet 3D printed biosensors show the variety of applications and the robustness of 3D printing technology. Inexpensive and mechanically flexible sensors can be printed quickly and with excellent final sensitivities, and the 3D printing process allows for rapid customization.

4.3.4. Lab on a chip. Lab on a chip is generally defined as research with the goal of miniaturizing biological or chemical processes, such as microfluidic chips or miniaturized sensors and arrays (biochips) [349]. The fabrication of labs on a chip typically utilize time-consuming, multi-step lithographic processes [350]. The ability to seamlessly 3D print lab-on-a-chip devices could revolutionize biomedical and chemical research, allowing for rapid customization and improved cell monitoring.

The 3D printing of nanomaterial-based lab-on-a-chip devices allows for rapid customization and increased biocompatibility. For example, Moya *et al* utilized the rapid customization of inkjet printing to fabricate a dissolved oxygen sensor for a liver-on-a-chip device [351]. The low temperatures of inkjet printing allowed them to print on delicate substrates with gold and silver nanoparticle inks. The sensors were thin, flexible, and biocompatible, integrating seamlessly with the liver cell culture and microfluidics required for the device. Although the microfluidic channels were not 3D printed, the 3D printing of this portion could enable faster fabrication times and customization of the device as a whole [352–354]. An entirely DIW printed lab on a chip was achieved by Lind *et al* which demonstrates both the customization and biocompatibility achievable with this technology [46]. They printed soft strain gauge sensors in a micro-architecture that allows the growth of cardiac tissues. The printed device successfully measured the spontaneous beating of seeded cardiac tissue over the course of a month as well as the increasing strain exerted by the tissue as it grew and strengthened. During fabrication, a sacrificial 0.5 μm thick dextran film layer was printed first that would allow the strain-gauge cantilevers printed next to detach for unconstrained movement. 6.5 μm thick conductive carbon black nanoparticles mixed in thermoplastic polyurethane (TPU) were then printed as the strain gauge wires within two insulating layers of plain TPU. Polydimethylsiloxane (PDMS) was printed next as a thicker supporting layer, followed by electrical leads and contact pads printed with silver-nanoparticle polyamide (Ag:PA) ink. An insulating layer and eight individual wells were assembled on the sensors for separate tissue examination. The entire process was completed in a single continuous procedure with a four-nozzle DIW printer, with only some curing at 100 °C and subsequent cell seeding following the printing. This study illuminates the possibilities afforded by completely 3D printed lab-on-a-chip devices.

3D printed nanoparticles also allow for improved cell monitoring. Apart from the various sensors that have already been discussed, nanoparticles have also been used as markers in oxygen and pH sensors [355], DNA sensors [356], and immunoassays [357, 358]. One such nanoparticle sensor was demonstrated by Trampe *et al* through the bioprinting of living cells with oxygen sensing nanoparticles [359], which allowed for effective cell monitoring. Luminescent styrene maleic anhydride copolymer (PSMA) nanoparticles containing an O_2 luminescent indicator were DIW printed with green microalgae and mesenchymal stem cells in basic scaffolds; this allowed for online monitoring of the metabolic activity of the cells using a simple single-lens reflex camera. The 3D printing process allows for the customized integration of biosensors with lab-on-a-chip devices, allowing for the rapidly customized integration of different cell cultures and indicators into a single printed device.

5. Conclusion

This review highlights the advances of 3D printed nanomaterial-based electronic, biomedical, and bioelectronic devices. First, we discussed the creation of 3D printed electronics allowing their integration with complex geometries and on non-planar, flexible and stretchable substrates. Second, we explored how a nanomaterial-based 3D printing approach can impart mechanical, geometric, biological, and responsive properties to biomedical devices, which enable the creation of tissue scaffolds, personalized medical devices, and drug delivery devices. Third, we highlighted the creation of 3D printed bioelectronic devices such as microelectrodes, electrically stimulated tissue-regenerating scaffolds, and biosensors with enhanced sensitivity to describe the potential impact of this approach in the creation of highly integrated multifunctional constructs. In summary, the advances of a multi-scale, multi-material 3D printing approach can enable the freeform fabrication of nanomaterial-based devices by endowing unique optical, chemical, mechanical, and electrical properties to otherwise passive constructs.

Acknowledgments

The authors acknowledge funding support in part from the Department of Mechanical Engineering of the University of Utah as well as the National Science Foundation under Emerging Frontiers in Research and Innovation (EFRI) Program (Grant No. EFRI 1830958).

ORCID iDs

Yong Lin Kong https://orcid.org/0000-0003-0270-2068

References

[1] Frazier W E 2014 Metal additive manufacturing: a review *J. Mater. Eng. Perform.* **23** 1917–28
[2] Rayna T and Striukova L 2016 From rapid prototyping to home fabrication: how 3D printing is changing business model innovation *Technol. Forecast. Soc. Change* **102** 214–24
[3] Ngo T D, Kashani A, Imbalzano G, Nguyen K T Q and Hui D 2018 Additive manufacturing (3D printing): a review of materials, methods, applications and challenges *Composites B* **143** 172–96
[4] Cumpston B H *et al* 1999 Two-photon polymerization initiators for three-dimensional optical data storage and microfabrication *Nature* **398** 51–4
[5] Kelly B E, Bhattacharya I, Heidari H, Shusteff M, Spadaccini C M and Taylor H K 2019 Volumetric additive manufacturing via tomographic reconstruction *Science* **363** 1075–9
[6] Truby R L and Lewis J A 2016 Printing soft matter in three dimensions *Nature* **540** 371–8
[7] Kong Y L, Gupta M K, Johnson B N and McAlpine M C 2016 3D printed bionic nanodevices *Nano Today* **11** 330–50
[8] Mcalpine M C and Kong Y L 2018 *3D printed active electronic materials and devices* US20160218287A1
[9] McAlpine M C, McAlpine M C, Sebastian-Mannoor M, Kong Y L and Johnson B N 2016 *Multi-functional hybrid devices/structures using 3D printing* US9517128B2
[10] Joshi S C and Sheikh A A 2015 3D printing in aerospace and its long-term sustainability *Virtual Phys. Prototyp.* **10** 175–85
[11] Attaran M 2017 The rise of 3D printing: the advantages of additive manufacturing over traditional manufacturing *Bus. Horiz.* **60** 677–88
[12] Ghosh U, Ning S, Wang Y and Kong Y L 2018 Addressing unmet clinical needs with 3D printing technologies *Adv. Healthcare Mater.* **7** 1800417
[13] Guzzi E A and Tibbitt M W 2019 Additive manufacturing of precision biomaterials *Adv. Mater.* 1901994
[14] Martelli N, Serrano C, Van Den Brink H, Pineau J, Prognon P, Borget I and El Batti S 2016 Advantages and disadvantages of 3-dimensional printing in surgery: a systematic review *Surgery* **159** 1485–500
[15] Patra S and Young V 2016 A review of 3D printing techniques and the future in biofabrication of bioprinted tissue *Cell Biochem. Biophys.* **74** 93–8
[16] Schubert C, Van Langeveld M C and Donoso L A 2014 Innovations in 3D printing: a 3D overview from optics to organs *Br. J. Ophthalmol.* **98** 159–61
[17] Ursan I, Chiu L and Pierce A 2013 Three-dimensional drug printing: a structured review *J. Am. Pharm. Assoc.* **53** 136–44
[18] Kong Y L *et al* 2019 3D-Printed gastric resident electronics *Adv. Mater. Technol.* **4** 1800490
[19] Rengier F, Mehndiratta A, Von Tengg-Kobligk H, Zechmann C M, Unterhinninghofen R, Kauczor H U and Giesel F L 2010 3D printing based on imaging data: review of medical applications *Int. J. Comput. Assist. Radiol. Surg.* **5** 335–41
[20] Randazzo M, Pisapia J, Singh N and Thawani J 2016 3D printing in neurosurgery: a systematic review *Surg. Neurol. Int.* **7** 801
[21] Heinrich M A *et al* 2019 3D bioprinting: from benches to translational applications *Small* **15** 1970126
[22] Kong Y L, Tamargo I A, Kim H, Johnson B N, Gupta M K, Koh T W, Chin H A, Steingart D A, Rand B P and McAlpine M C 2014 3D printed quantum dot light-emitting diodes *Nano Lett.* **14** 7017–23
[23] Zhang D, Chi B, Li B, Gao Z, Du Y, Guo J and Wei J 2016 Fabrication of highly conductive graphene flexible circuits by 3D printing *Synth. Met.* **217** 79–86
[24] Wei P, Yang X, Cao Z, Guo X L, Jiang H, Chen Y, Morikado M, Qiu X and Yu D 2019 Flexible and stretchable electronic skin with high durability and shock resistance via embedded 3D printing technology for human activity monitoring and personal healthcare *Adv. Mater. Technol.* **24** 1900315
[25] Kong Y L 2019 Transforming military medicine with 3D printed bioelectronics *Homel. Def. Inf. Anal. Cent.* **6** 34–8
[26] Mohammed M G and Kramer R 2017 All-printed flexible and stretchable electronics *Adv. Mater.* **29** 1604965
[27] Yu F *et al* 2019 Real-time manipulation of intestinal peristalsis by enteric-encapsulated magnetic nanoparticles & wearable 3D-printed devices *NPG Asia Mater.* **11** 33
[28] Talapin D V and Steckel J 2013 Quantum dot light-emitting devices *MRS Bull.* **38** 685–91
[29] Goesmann H and Feldmann C 2010 Nanoparticulate functional materials *Angew. Chem., Int. Ed.* **49** 1362–95
[30] Kokkinis D, Schaffner M and Studart A R 2015 Multimaterial magnetically assisted 3D printing of composite materials *Nat. Commun.* **6** 8643

[31] Koopmann J, Voigt J and Niendorf T 2019 Additive manufacturing of a steel-ceramic multi-material by selective laser melting *Metall. Mater. Trans.* B **50** 1042–51

[32] Singh R, Kumar R, Farina I, Colangelo F, Feo L and Fraternali F 2019 Multi-material additive manufacturing of sustainable innovative materials and structures *Polymers* **11** 62

[33] Bandyopadhyay A and Heer B 2018 Additive manufacturing of multi-material structures *Mater. Sci. Eng.* R **129** 1–16

[34] Ventola C L 2014 Medical applications for 3D printing: current and projected uses *P T* **39** 704–11

[35] Tofail S A M, Koumoulos E P, Bandyopadhyay A, Bose S, O'Donoghue L and Charitidis C 2018 Additive manufacturing: scientific and technological challenges, market uptake and opportunities *Mater. Today* **21** 22–37

[36] Lee S J, Esworthy T, Stake S, Miao S, Zuo Y Y, Harris B T and Zhang L G 2018 Advances in 3D bioprinting for neural tissue engineering *Adv. Biosyst.* **2** 1700213

[37] Choi S, Lee H, Ghaffari R, Hyeon T and Kim D H 2016 Recent advances in flexible and stretchable bio-electronic devices integrated with nanomaterials *Adv. Mater.* **28** 4203–18

[38] Lee Y, Kim J, Koo J H, Kim T H and Kim D H 2018 Nanomaterials for bioelectronics and integrated medical systems *Korean J. Chem. Eng.* **35** 1–11

[39] Sun K, Wei T S, Ahn B Y, Seo J Y, Dillon S J and Lewis J A 2013 3D printing of interdigitated Li-ion microbattery architectures *Adv. Mater.* **25** 4539–43

[40] Zhu M *et al* 2019 Electrohydrodynamically printed high-resolution full-color hybrid perovskites *Adv. Funct. Mater.* **29** 1903294

[41] Guiney L M, Mansukhani N D, Jakus A E, Wallace S G, Shah R N and Hersam M C 2018 Three-dimensional printing of cytocompatible, thermally conductive hexagonal boron nitride nanocomposites *Nano Lett.* **18** 3488–93

[42] Noor N, Shapira A, Edri R, Gal I, Wertheim L and Dvir T 2019 3D Printing of personalized thick and perfusable cardiac patches and hearts *Adv. Sci.* **6** 1970066

[43] Kang H W, Lee S J, Ko I K, Kengla C, Yoo J J and Atala A 2016 A 3D bioprinting system to produce human-scale tissue constructs with structural integrity *Nat. Biotechnol.* **34** 312–9

[44] Adly N, Weidlich S, Seyock S, Brings F, Yakushenko A, Offenhäusser A and Wolfrum B 2018 Printed microelectrode arrays on soft materials: from PDMS to hydrogels *NPJ Flex. Electron.* **2** 15

[45] Mannoor M S, Jiang Z, James T, Kong Y L, Malatesta K A, Soboyejo W O, Verma N, Gracias D H and McAlpine M C 2013 3D printed bionic ears *Nano Lett.* **13** 2634–9

[46] Lind J U *et al* 2017 Instrumented cardiac microphysiological devices via multimaterial three-dimensional printing *Nat. Mater.* **16** 303–8

[47] Wong K V and Hernandez A 2012 A review of additive manufacturing *ISRN Mech. Eng.* **2012** 1–10

[48] Hull C W and Arcadia C 1984 *Apparatus for production of three-dimensional objects by stereolithography* US4575330A

[49] Melchels F P W, Feijen J and Grijpma D W 2010 A review on stereolithography and its applications in biomedical engineering *Biomaterials* **31** 6121–30

[50] Sun C, Fang N, Wu D M and Zhang X 2005 Projection micro-stereolithography using digital micro-mirror dynamic mask *Sensors Actuators* A **121** 113–20

[51] Zheng X, Deotte J, Alonso M P, Farquar G R, Weisgraber T H, Gemberling S, Lee H, Fang N and Spadaccini C M 2012 Design and optimization of a light-emitting diode projection micro-stereolithography three-dimensional manufacturing system *Rev. Sci. Instrum.* **83** 125001

[52] Stansbury J W and Idacavage M J 2016 3D printing with polymers: challenges among expanding options and opportunities *Dent. Mater.* **32** 54–64

[53] Hwang H H, Zhu W, Victorine G, Lawrence N and Chen S 2018 3d printing: 3D-printing of functional biomedical microdevices via light- and extrusion-based approaches *Small Methods* **2** 1870021

[54] Mahajan A, Frisbie C D and Francis L F 2013 Optimization of aerosol jet printing for high-resolution, high-aspect ratio silver lines *ACS Appl. Mater. Interfaces* **5** 4856–64

[55] Kodama H 1981 Automatic method for fabricating a three-dimensional plastic model with photo-hardening polymer *Rev. Sci. Instrum.* **52** 1770–3

[56] Shirazi S F S, Gharehkhani S, Mehrali M, Yarmand H, Metselaar H S C, Adib Kadri N and Osman N A A 2015 A review on powder-based additive manufacturing for tissue engineering: selective laser sintering and inkjet 3D printing *Sci. Technol. Adv. Mater.* **16** 033502

[57] Calvert P 2001 Inkjet printing for materials and devices *Chem. Mater.* **13** 3299–305

[58] Farahani R D, Dubé M and Therriault D 2016 Three-dimensional printing of multifunctional nanocomposites: manufacturing techniques and applications *Adv. Mater.* **28** 5794–821

[59] Lewis J A 2006 Direct ink writing of 3D functional materials *Adv. Funct. Mater.* **16** 2193–204

[60] Feinberg A W and Miller J S 2017 Progress in three-dimensional bioprinting *MRS Bull.* **42** 557–62

[61] Placone J K and Engler A J 2018 Recent advances in extrusion-based 3D printing for biomedical applications *Adv. Healthcare Mater.* **7** 1701161

[62] Murphy S V and Atala A 2014 3D bioprinting of tissues and organs *Nat. Biotechnol.* **32** 773–85

[63] Xue J, Wu T, Dai Y and Xia Y 2019 Electrospinning and electrospun nanofibers: methods, materials, and applications *Chem. Rev.* **119** 5298–415

[64] Huang Y, Bu N, Duan Y, Pan Y, Liu H, Yin Z and Xiong Y 2013 Electrohydrodynamic direct-writing *Nanoscale* **5** 12007–17

[65] Xue J, Xie J, Liu W and Xia Y 2017 Electrospun nanofibers: new concepts, materials, and applications *Acc. Chem. Res.* **50** 1976–87

[66] Huang Z M, Zhang Y Z, Kotaki M and Ramakrishna S 2003 A review on polymer nanofibers by electrospinning and their applications in nanocomposites *Compos. Sci. Technol.* **63** 2223–53

[67] Wilkinson N J, Smith M A A, Kay R W and Harris R A 2019 A review of aerosol jet printing—a non-traditional hybrid process for micro-manufacturing *Int. J. Adv. Manuf. Technol.* **105** 1–21

[68] Paulsen J A, Renn M, Christenson K and Plourde R 2012 Printing conformal electronics on 3D structures with aerosol jet technology *FIIW 2012–2012 Future of Instrumentation Int. Workshop Proc.* pp 47–50

[69] Saleh M S, Hu C and Panat R 2017 Three-dimensional microarchitected materials and devices using nanoparticle assembly by pointwise spatial printing *Sci. Adv.* **3** e1601986

[70] Folgar C E, Suchicital C and Priya S 2011 Solution-based aerosol deposition process for synthesis of multilayer structures *Mater. Lett.* **65** 1302–7

[71] Grunwald I, Groth E, Wirth I, Schumacher J, Maiwald M, Zoellmer V and Busse M 2010 Surface biofunctionalization and production of miniaturized sensor structures using aerosol printing technologies *Biofabrication* **2** 014106

[72] Martin G D, Hoath S D and Hutchings I M 2008 Inkjet printing—the physics of manipulating liquid jets and drops *J. Phys.: Conf. Ser.* **105**

[73] Le H P 1998 Progress and trends in ink-jet printing technology *J. Imaging Sci. Technol.* **42** 49–62

[74] Raje P V and Murmu N C 2014 A review on electrohydrodynamic-inkjet printing technology *Inter. J. Emerging Tech. Adv. Eng.* **4** 174–83

[75] Setti L, Fraleoni-Morgera A, Ballarin B, Filippini A, Frascaro D and Piana C 2005 An amperometric glucose biosensor prototype fabricated by thermal inkjet printing *Biosens. Bioelectron.* **20** 2019–26

[76] Ibrahim M, Otsubo T, Narahara H, Koresawa H and Suzuki H 2006 Inkjet printing resolution study for multi-material rapid prototyping *JSME Int. J.* C **49** 353–60

[77] Tekin E, Smith P J and Schubert U S 2008 Inkjet printing as a deposition and patterning tool for polymers and inorganic particles *Soft Matter* **4** 703–13

[78] Cummins G and Desmulliez M P Y 2012 Inkjet printing of conductive materials: a review *Circuit World* **38** 193–213

[79] Nakamura M, Kobayashi A, Takagi F, Watanabe A, Hiruma Y, Ohuchi K, Iwasaki Y, Horie M, Morita I and Takatani S 2006 Biocompatible inkjet printing technique for designed seeding of individual living cells *Tissue Eng.* **11** 1658–66

[80] Calvert P 2007 Materials science: printing cells *Science* **318** 208–9

[81] Wallin T J, Pikul J and Shepherd R F 2018 3D printing of soft robotic systems *Nat. Rev. Mater.* **3** 84–100

[82] Utela B, Storti D, Anderson R and Ganter M 2008 A review of process development steps for new material systems in three dimensional printing (3DP) *J. Manuf. Process.* **10** 96–104

[83] Vespini V, Coppola S, Grilli S, Paturzo M and Ferraro P 2013 Milking liquid nano-droplets by an IR laser: a new modality for the visualization of electric field lines *Meas. Sci. Technol.* **24** 045203

[84] Onses M S, Sutanto E, Ferreira P M, Alleyne A G and Rogers J A 2015 Mechanisms, capabilities, and applications of high-resolution electrohydrodynamic jet printing *Small* **11** 4237–66

[85] Park J U *et al* 2007 High-resolution electrohydrodynamic jet printing *Nat. Mater.* **6** 782–9

[86] Thornsberry C 2019 What does resolution mean in 3D printing https://3space.com/

[87] Partanen J P 1996 Lasers and optics in stereolithography *Lasers as Tools for Manufacturing of Durable Goods and Microelectronics* vol 2703 (SPIE) p 502

[88] Derby B 2010 Inkjet printing of functional and structural materials: fluid property requirements, feature stability, and resolution *Annu. Rev. Mater. Res.* **40** 395–414

[89] Moon J, Grau J E, Knezevic V, Cima M J and Sachs E M 2004 Ink-jet printing of binders for ceramic components *J. Am. Ceram. Soc.* **85** 755–62

[90] MacDonald E, Salas R, Espalin D, Perez M, Aguilera E, Muse D and Wicker R B 2014 3D printing for the rapid prototyping of structural electronics *IEEE Access* **2** 234–42

[91] Gao W, Zhang Y, Ramanujan D, Ramani K, Chen Y, Williams C B, Wang C C L, Shin Y C, Zhang S and Zavattieri P D 2015 The status, challenges, and future of additive manufacturing in engineering *CAD Comput. Aided Des.* **69** 65–89

[92] Tumbleston J R *et al* 2015 Continuous liquid interface production of 3D objects *Science* **347** 1349–52

[93] Janusziewicz R, Tumbleston J R, Quintanilla A L, Mecham S J and DeSimone J M 2016 Layerless fabrication with continuous liquid interface production *Proc. Natl Acad. Sci. USA* **113** 11703–8

[94] Sears N A, Seshadri D R, Dhavalikar P S and Cosgriff-Hernandez E 2016 A review of three-dimensional printing in tissue engineering *Tissue Eng.* B **22** 298–310

[95] Lewis J A, Smay J E, Stuecker J and Cesarano J 2006 Direct ink writing of three-dimensional ceramic structures *J. Am. Ceram. Soc.* **89** 3599–609

[96] Lewis J A 2002 Direct-write assembly of ceramics from colloidal inks *Curr. Opin. Solid State Mater. Sci.* **6** 245–50

[97] Sun D, Chang C, Li S and Lin L 2006 Near-field electrospinning *Nano Lett.* **6** 839–42

[98] Rudorfer A, Tscherner M, Palfinger C, Reil F, Hartmann P, Seferis I E, Zych E and Wenzl F P 2016 A study on aerosol jet printing technology in LED module manufacturing *SPIE* **9954** 99540E

[99] Van Osch T H J, Perelaer J, De Laat A W M and Schubert U S 2008 Inkjet printing of narrow conductive tracks on untreated polymeric substrates *Adv. Mater.* **20** 343–5

[100] Singh M, Haverinen H M, Dhagat P and Jabbour G E 2010 Inkjet printing-process and its applications *Adv. Mater.* **22** 673–85

[101] Ru C, Luo J, Xie S and Sun Y 2014 A review of non-contact micro- and nano-printing technologies *J. Micromech. Microeng.* **24** 053001

[102] Sinden R R 2012 *DNA Structure and Function* (Amsterdam: Elsevier)

[103] Roduner E 2006 Size matters: why nanomaterials are different *Chem. Soc. Rev.* **35** 583–92

[104] Daniel M C and Astruc D 2004 Gold nanoparticles: assembly, supramolecular chemistry, quantum-size-related properties, and applications toward biology, catalysis, and nanotechnology *Chem. Rev.* **104** 293–346

[105] Gröger H, Capan E, Barthuber A and Vorlop K D 2001 Asymmetric synthesis of an (R)-cyanohydrin using enzymes entrapped in lens-shaped gels *Org. Lett.* **3** 1967–71

[106] Sheldon R A and van Pelt S 2013 Enzyme immobilisation in biocatalysis: why, what and how *Chem. Soc. Rev.* **42** 6223–35

[107] Jacinto M J, Kiyohara P K, Masunaga S H, Jardim R F and Rossi L M 2008 Recoverable rhodium nanoparticles: synthesis, characterization and catalytic performance in hydrogenation reactions *Appl. Catal.* A **338** 52–7

[108] Astruc D, Lu F and Aranzaes J R 2005 Nanoparticles as recyclable catalysts: the frontier between homogeneous and heterogeneous catalysis *Angew. Chem., Int. Ed.* **44** 7852–72

[109] Corma A and Garcia H 2008 Supported gold nanoparticles as catalysts for organic reactions *Chem. Soc. Rev.* **37** 2096–126

[110] Khan Y, Pavinatto F J, Lin M C, Liao A, Swisher S L, Mann K, Subramanian V, Maharbiz M M and Arias A C 2016 Inkjet-printed flexible gold electrode arrays for bioelectronic interfaces *Adv. Funct. Mater.* **26** 1004–13

[111] Beidaghi M and Gogotsi Y 2014 Capacitive energy storage in micro-scale devices: recent advances in design and fabrication of micro-supercapacitors *Energy Environ. Sci.* **7** 867–84

[112] Kruis F E, Fissan H and Peled A 1998 Synthesis of nanoparticles in the gas phase for electronic, optical and magnetic applications—a review *J. Aerosol. Sci.* **29** 511–35

[113] Shirasaki Y, Supran G J, Bawendi M G and Bulović V 2013 Emergence of colloidal quantum-dot light-emitting technologies *Nat. Photon.* **7** 13–23

[114] Sun Q, Wang Y A, Li L S, Wang D, Zhu T, Xu J, Yang C and Li Y 2007 Bright, multicoloured light-emitting diodes based on quantum dots *Nat. Photon.* **1** 717–22

[115] Amendola V, Pilot R, Frasconi M, Maragò O M and Iatì M A 2017 Surface plasmon resonance in gold nanoparticles: a review *J. Phys.: Condens. Matter* **29** 203002

[116] Cao J, Sun T and Grattan K T V 2014 Gold nanorod-based localized surface plasmon resonance biosensors: a review *Sensors Actuators* B **195** 332–51

[117] Rocha-Santos T A P 2014 Sensors and biosensors based on magnetic nanoparticles *TrAC—Trends Anal. Chem.* **62** 28–36

[118] Luo X, Morrin A, Killard A J and Smyth M R 2006 Application of nanoparticles in electrochemical sensors and biosensors *Electroanalysis* **18** 319–26

[119] Bazak R, Houri M, El Achy S, Kamel S and Refaat T 2015 Cancer active targeting by nanoparticles: a comprehensive review of literature *J. Cancer Res. Clin. Oncol.* **141** 769–84

[120] Wu J *et al* 2015 Broadband efficiency enhancement in quantum dot solar cells coupled with multispiked plasmonic nanostars *Nano Energy* **13** 827–35

[121] Yu P, Yao Y, Wu J, Niu X, Rogach A L and Wang Z 2017 Effects of plasmonic metal core-dielectric shell nanoparticles on the broadband light absorption enhancement in thin film solar cells *Sci. Rep.* **7** 7696

[122] Lu A H, Salabas E L and Schüth F 2007 Magnetic nanoparticles: synthesis, protection, functionalization, and application *Angew. Chem., Int. Ed.* **46** 1222–44

[123] Fayazfar H, Salarian M, Rogalsky A, Sarker D, Russo P, Paserin V and Toyserkani E 2018 A critical review of powder-based additive manufacturing of ferrous alloys: process parameters, microstructure and mechanical properties *Mater. Des.* **144** 98–128

[124] Taormina G, Sciancalepore C, Messori M and Bondioli F 2018 3D printing processes for photocurable polymeric materials: technologies, materials, and future trends *J. Appl. Biomater. Funct. Mater.* **16** 151–60

[125] Desimone J M, Ermoshkin A, Ermoshkin N and Sarnulski E T 2014 *Continuous liquid interphase printing* US9360757B2

[126] Anon 2019 Carbon—the world's leading digital manufacturing platform https://www.carbon3d.com

[127] Lin D, Jin S, Zhang F, Wang C, Wang Y, Zhou C and Cheng G J 2015 3D stereolithography printing of graphene oxide reinforced complex architectures *Nanotechnology* **26** 434003

[128] Taormina G, Sciancalepore C, Bondioli F and Messori M 2018 Special resins for stereolithography: *in situ* generation of silver nanoparticles *Polymers* **10** 212

[129] Fantino E, Chiappone A, Calignano F, Fontana M, Pirri F and Roppolo I 2016 *In situ* thermal generation of silver nanoparticles in 3D printed polymeric structures *Materials* **9** 589

[130] Liu H and Mo J 2010 Study on nanosilica reinforced stereolithography resin *J. Reinf. Plast. Compos.* **29** 909–20

[131] Weng Z, Zhou Y, Lin W, Senthil T and Wu L 2016 Structure-property relationship of nano enhanced stereolithography resin for desktop SLA 3D printer *Composites* A **88** 234–42

[132] Sandoval J H and Wicker R B 2006 Functionalizing stereolithography resins: effects of dispersed multi-walled carbon nanotubes on physical properties *Rapid Prototyp. J.* **12** 292–303

[133] Abdelrasoul G N, Farkas B, Romano I, Diaspro A and Beke S 2015 Nanocomposite scaffold fabrication by incorporating gold nanoparticles into biodegradable polymer matrix: synthesis, characterization, and photothermal effect *Mater. Sci. Eng.* C **56** 305–10

[134] De Santis R, D'Amora U, Russo T, Ronca A, Gloria A and Ambrosio L 2015 3D fibre deposition and stereolithography techniques for the design of multifunctional nanocomposite magnetic scaffolds *J. Mater. Sci., Mater. Med.* **26** 250

[135] Castro N J, O'Brien J and Zhang L G 2015 Integrating biologically inspired nanomaterials and table-top stereolithography for 3D printed biomimetic osteochondral scaffolds *Nanoscale* **7** 14010–22

[136] Ushiba S, Shoji S, Masui K, Kuray P, Kono J and Kawata S 2013 3D microfabrication of single-wall carbon nanotube/polymer composites by two-photon polymerization lithography *Carbon* **59** 283–8

[137] Chen L, Dong Y, Tang C Y, Zhong L, Law W C, Tsui G C P, Yang Y and Xie X 2019 Development of direct-laser-printable light-powered nanocomposites *ACS Appl. Mater. Interfaces* **11** 19541–53

[138] Krini R, Ha C W, Prabhakaran P, El M H, Yang D Y, Zentel R and Lee K S 2015 Photosensitive functionalized surface-modified quantum dots for polymeric structures via two-photon-initiated polymerization technique *Macromol. Rapid Commun.* **36** 1108–14

[139] Vyatskikh A, Delalande S, Kudo A, Zhang X, Portela C M and Greer J R 2018 Additive manufacturing of 3D nano-architected metals *Nat. Commun.* **9** 593

[140] Guo Q, Ghadiri R, Weigel T, Aumann A, Gurevich E L, Esen C, Medenbach O, Cheng W, Chichkov B and Ostendorf A 2014 Comparison of *in situ* and ex situ methods for synthesis of two-photon polymerization polymer nanocomposites *Polymers* **6** 2037–50

[141] Suter M, Zhang L, Siringil E C, Peters C, Luehmann T, Ergeneman O, Peyer K E, Nelson B J and Hierold C 2013 Superparamagnetic microrobots: fabrication by two-photon polymerization and biocompatibility *Biomed. Microdevices* **15** 997–1003

[142] Salmoria G V, Paggi R A, Lago A and Beal V E 2011 Microstructural and mechanical characterization of PA12/MWCNTs nanocomposite manufactured by selective laser sintering *Polym. Test.* **30** 611–5

[143] Theodorakos I, Zacharatos F, Geremia R, Karnakis D and Zergioti I 2015 Selective laser sintering of Ag nanoparticles ink for applications in flexible electronics *Appl. Surf. Sci.* **336** 157–62

[144] Duan B, Wang M, Zhou W Y, Cheung W L, Li Z Y and Lu W W 2010 Three-dimensional nanocomposite scaffolds fabricated via selective laser sintering for bone tissue engineering *Acta Biomater.* **6** 4495–505

[145] Zenou M, Ermak O, Saar A and Kotler Z 2014 Laser sintering of copper nanoparticles *J. Phys. D: Appl. Phys.* **47** 025501

[146] Crane N B, Wilkes J, Sachs E and Allen S M 2005 Improving accuracy of powder sintering-based SFF processes by metal deposition from nanoparticle dispersion *16th Solid Freeform Fabrication Symp., SFF 2005* vol 12, pp 261–72

[147] Dul S, Fambri L and Pegoretti A 2016 Fused deposition modelling with ABS-graphene nanocomposites *Composites* A **85** 181–91

[148] Gnanasekaran K, Heijmans T, van Bennekom S, Woldhuis H, Wijnia S, de With G and Friedrich H 2017 3D printing of CNT- and graphene-based conductive polymer nanocomposites by fused deposition modeling *Appl. Mater. Today* **9** 21–8

[149] Meng S, He H, Jia Y, Yu P, Huang B and Chen J 2017 Effect of nanoparticles on the mechanical properties of acrylonitrile–butadiene–styrene specimens fabricated by fused deposition modeling *J. Appl. Polym. Sci.* **134** 44470

[150] Shofner M L, Lozano K, Rodríguez-Macías F J and Barrera E V 2003 Nanofiber-reinforced polymers prepared by fused deposition modeling *J. Appl. Polym. Sci.* **89** 3081–90

[151] Dul S, Fambri L and Pegoretti A 2018 Filaments production and fused deposition modelling of ABS/carbon nanotubes composites *Nanomaterials* **8** 49

[152] Weng Z, Wang J, Senthil T and Wu L 2016 Mechanical and thermal properties of ABS/montmorillonite nanocomposites for fused deposition modeling 3D printing *Mater. Des.* **102** 276–83

[153] Jakus A E, Secor E B, Rutz A L, Jordan S W, Hersam M C and Shah R N 2015 Three-dimensional printing of high-content graphene scaffolds for electronic and biomedical applications *ACS Nano* **9** 4636–48

[154] Ahn B Y, Duoss E B, Motala M J, Guo X, Park S I, Xiong Y, Yoon J, Nuzzo R G, Rogers J A and Lewis J A 2009 Omnidirectional printing of flexible, stretchable, and spanning silver microelectrodes *Science* **323** 1590–3

[155] Dorj B, Won J E, Kim J H, Choi S J, Shin U S and Kim H W 2013 Robocasting nanocomposite scaffolds of poly (caprolactone)/hydroxyapatite incorporating modified carbon nanotubes for hard tissue reconstruction *J. Biomed. Mater. Res.* A **101A** 1670–81

[156] McCracken J M, Rauzan B M, Kjellman J C E, Su H, Rogers S A and Nuzzo R G 2019 Ionic hydrogels with biomimetic 4D-printed mechanical gradients: models for soft-bodied aquatic organisms *Adv. Funct. Mater.* **29** 1806723

[157] Altinbasak I *et al* 2018 Reduced graphene-oxide-embedded polymeric nanofiber mats: an 'on-demand' photothermally triggered antibiotic release platform *ACS Appl. Mater. Interfaces* **10** 41098–106

[158] Choi J H, Seo H, Park J H, Son J H, Kim D I, Kim J, Moon G D and Hyun D C 2019 Poly(D,L-lactic-co-glycolic acid) (PLGA) hollow fiber with segmental switchability of its chains sensitive to NIR light for synergistic cancer therapy *Colloids Surf.* B **173** 258–65

[159] Rezwan K, Chen Q Z, Blaker J J and Boccaccini A R 2006 Biodegradable and bioactive porous polymer/inorganic composite scaffolds for bone tissue engineering *Biomaterials* **27** 3413–31

[160] Jabari E and Toyserkani E 2016 Aerosol-Jet printing of highly flexible and conductive graphene/silver patterns *Mater. Lett.* **174** 40–3

[161] Zhao D, Liu T, Park J G, Zhang M, Chen J M and Wang B 2012 Conductivity enhancement of aerosol-jet printed electronics by using silver nanoparticles ink with carbon nanotubes *Microelectron. Eng.* **96** 71–5

[162] Wang K, Chang Y H, Zhang C and Wang B 2016 Conductive-on-demand: tailorable polyimide/carbon nanotube nanocomposite thin film by dual-material aerosol jet printing *Carbon* **98** 397–403

[163] Secor E B, Gao T Z, Islam A E, Rao R, Wallace S G, Zhu J, Putz K W, Maruyama B and Hersam M C 2017 Enhanced conductivity, adhesion, and environmental stability of printed graphene inks with nitrocellulose *Chem. Mater.* **29** 2332–40

[164] Chung S, Lee J, Song H, Kim S, Jeong J and Hong Y 2011 Inkjet-printed stretchable silver electrode on wave structured elastomeric substrate *Appl. Phys. Lett.* **98** 153110

[165] Liu Y, Li F, Qiu L, Yang K, Li Q, Zheng X, Hu H, Guo T, Wu C and Kim T W 2019 Fluorescent microarrays of *in situ* crystallized perovskite nanocomposites fabricated for patterned applications by using inkjet printing *ACS Nano* **13** 2042–9

[166] Song D, Zare Bidoky F, Hyun W J, Walker S B, Lewis J A and Frisbie C D 2018 All-printed, self-aligned carbon nanotube thin-film transistors on imprinted plastic substrates *ACS Appl. Mater. Interfaces* **10** 15926–32

[167] Bai Y and Williams C B 2017 Binderless jetting: additive manufacturing of metal parts via jetting nanoparticles *Int. Solid Free. Fabr. Symp.* pp 249–60

[168] Bailey A, Merriman A, Elliott A and Basti M 2016 Preliminary testing of nanoparticle effectiveness in binder jetting applications *27th Annual Int. Solid Freeform Fabrication Symp.* pp 1069–77

[169] Kunchala P and Kappagantula K 2018 3D printing high density ceramics using binder jetting with nanoparticle densifiers *Mater. Des.* **155** 443–50

[170] Yu J H, Kim S Y and Hwang J 2007 Effect of viscosity of silver nanoparticle suspension on conductive line patterned by electrohydrodynamic jet printing *Appl. Phys.* A **89** 157–9

[171] Schneider J, Rohner P, Thureja D, Schmid M, Galliker P and Poulikakos D 2016 Electrohydrodynamic NanoDrip printing of high aspect ratio metal grid transparent electrodes *Adv. Funct. Mater.* **26** 833–40

[172] Galliker P, Schneider J, Eghlidi H, Kress S, Sandoghdar V and Poulikakos D 2012 Direct printing of nanostructures by electrostatic autofocussing of ink nanodroplets *Nat. Commun.* **3** 890

[173] Kamyshny A and Magdassi S 2019 Conductive nanomaterials for 2D and 3D printed flexible electronics *Chem. Soc. Rev.* **48** 1712–40

[174] Ji T, Jin S, Zhang H, Chen S and Sun X W 2018 Full color quantum dot light-emitting diodes patterned by photolithography technology *J. Soc. Inf. Disp.* **26** 121–7

[175] Lin X, Wu M, Zhang L and Wang D 2019 Superior stretchable conductors by electroless plating of copper on knitted fabrics *ACS Appl. Electron. Mater.* **1** 397–406

[176] Lai X, Guo R, Lan J, Geng L, Lin S, Jiang S, Zhang Y, Xiao H and Xiang C 2019 Flexible reduced graphene oxide/electroless copper plated poly(benzo)-benzimidazole fibers with electrical conductivity and corrosion resistance *J. Mater. Sci., Mater. Electron.* **30** 1984–92

[177] El Ajjouri Y, Palazon F, Sessolo M and Bolink H J 2018 Single-source vacuum deposition of mechanosynthesized inorganic halide perovskites *Chem. Mater.* **30** 7423–7

[178] Tong G, Li H, Li D, Zhu Z, Xu E, Li G, Yu L, Xu J and Jiang Y 2018 Dual-phase $CsPbBr_3$–$CsPb_2Br_5$ perovskite thin films via vapor deposition for high-performance rigid and flexible photodetectors *Small* **14** 1702523

[179] Mathies F, Eggers H, Richards B S, Hernandez-Sosa G, Lemmer U and Paetzold U W 2018 Inkjet-printed triple cation perovskite solar cells *ACS Appl. Energy Mater.* **1** 1834–9

[180] Shi L, Meng L, Jiang F, Ge Y, Li F, Gang W X and Zhong H 2019 *In situ* inkjet printing strategy for fabricating perovskite quantum dot patterns *Adv. Funct. Mater.* **29** 1903648

[181] Liu C, Li F, Lai-Peng M and Cheng H M 2010 Advanced materials for energy storage *Adv. Mater.* **22** E28–62

[182] Ferris A, Bourrier D, Garbarino S, Guay D and Pech D 2019 3D interdigitated microsupercapacitors with record areal cell capacitance *Small* **15** 1901224

[183] Honda W, Harada S, Arie T, Akita S and Takei K 2014 Wearable, human-interactive, health-monitoring, wireless devices fabricated by macroscale printing techniques *Adv. Funct. Mater.* **24** 3299–304

[184] Dai X, Deng Y, Peng X and Jin Y 2017 Quantum-dot light-emitting diodes for large-area displays: towards the dawn of commercialization *Adv. Mater.* **29** 1607022

[185] Guo Y G, Hu J S and Wan L J 2008 Nanostructured materials for electrochemical energy conversion and storage devices *Adv. Mater.* **20** 2877–87

[186] Pumera M 2011 Graphene-based nanomaterials for energy storage *Energy Environ. Sci.* **4** 668–74

[187] Zhao X, Sánchez B M, Dobson P J and Grant P S 2011 The role of nanomaterials in redox-based supercapacitors for next generation energy storage devices *Nanoscale* **3** 839–55

[188] Torres-Canas F, Yuan J, Ly I, Neri W, Colin A and Poulin P 2019 Inkjet printing of latex-based high-energy microcapacitors *Adv. Funct. Mater.* **29** 1901884

[189] Rocha V G, García-Tuñón E, Botas C, Markoulidis F, Feilden E, D'Elia E, Ni N, Shaffer M and Saiz E 2017 Multimaterial 3D printing of graphene-based electrodes for electrochemical energy storage using thermoresponsive inks *ACS Appl. Mater. Interfaces* **9** 37136–45

[190] Kim C, Ahn B Y, Wei T-S, Jo Y, Jeong S, Choi Y, Kim I-D and Lewis J A 2018 High-power aqueous zinc-ion batteries for customized electronic devices *ACS Nano* **12** 11838–46

[191] Lacey S D *et al* 2018 Extrusion-based 3D printing of hierarchically porous advanced battery electrodes *Adv. Mater.* **30** 1705651

[192] Fu K *et al* 2016 Graphene oxide-based electrode inks for 3D-printed lithium-ion batteries *Adv. Mater.* **28** 2587–94

[193] Zhu C, Liu T, Qian F, Han T Y J, Duoss E B, Kuntz J D, Spadaccini C M, Worsley M A and Li Y 2016 Supercapacitors based on three-dimensional hierarchical

graphene aerogels with periodic macropores *Nano Lett.* **16** 3448–56
[194] Sun H, Zhu J, Baumann D, Peng L, Xu Y, Shakir I, Huang Y and Duan X 2019 Hierarchical 3D electrodes for electrochemical energy storage *Nat. Rev. Mater.* **4** 45–60
[195] Zhang F, Liu T, Li M, Yu M, Luo Y, Tong Y and Li Y 2017 Multiscale pore network boosts capacitance of carbon electrodes for ultrafast charging *Nano Lett.* **17** 3097–104
[196] Zhang F, Wei M, Viswanathan V V, Swart B, Shao Y, Wu G and Zhou C 2017 3D printing technologies for electrochemical energy storage *Nano Energy* **40** 418–31
[197] Brown E, Yan P, Tekik H, Elangovan A, Wang J, Lin D and Li J 2019 3D printing of hybrid MoS_2-graphene aerogels as highly porous electrode materials for sodium ion battery anodes *Mater. Des.* **170** 107689
[198] Saleh M S, Li J, Park J and Panat R 2018 3D printed hierarchically-porous microlattice electrode materials for exceptionally high specific capacity and areal capacity lithium ion batteries *Addit. Manuf.* **23** 70–8
[199] Yang Y *et al* 2016 Three dimensional printing of high dielectric capacitor using projection based stereolithography method *Nano Energy* **22** 414–21
[200] Yu W, Zhou H, Li B Q and Ding S 2017 3D printing of carbon nanotubes-based microsupercapacitors *ACS Appl. Mater. Interfaces* **9** 4597–604
[201] Zou M, Ma Y, Yuan X, Hu Y, Liu J and Jin Z 2018 Flexible devices: from materials, architectures to applications *J. Semicond.* **39** 011010
[202] Secor E B, Ahn B Y, Gao T Z, Lewis J A and Hersam M C 2015 Rapid and versatile photonic annealing of graphene inks for flexible printed electronics *Adv. Mater.* **27** 6683–8
[203] Rahman M T, Cheng C-Y, Karagoz B, Renn M, Schrandt M, Gellman A and Panat R 2019 High performance flexible temperature sensors via nanoparticle printing *ACS Appl. Nano Mater.* **2** 3280–91
[204] Zang Y, Zhang F, Di C A and Zhu D 2015 Advances of flexible pressure sensors toward artificial intelligence and health care applications *Mater. Horiz.* **2** 140–56
[205] Wang B and Facchetti A 2019 Mechanically flexible conductors for stretchable and wearable E-skin and E-textile devices *Adv. Mater.* **31** 1901408
[206] Lu B-H, Lan H-B and Liu H-Z 2018 Additive manufacturing frontier: 3D printing electronics *Opto-Electronic Adv.* **1** 17000401
[207] Chen X *et al* 2019 Graphene hybrid structures for integrated and flexible optoelectronics *Adv. Mater.* 1902039
[208] Le T S D, Park S, An J, Lee P S and Kim Y J 2019 Ultrafast laser pulses enable one-step graphene patterning on woods and leaves for green electronics *Adv. Funct. Mater.* **29** 1902771
[209] Lee J H, Kim J, Liu D, Guo F, Shen X, Zheng Q, Jeon S and Kim J K 2019 Highly aligned, anisotropic carbon nanofiber films for multidirectional strain sensors with exceptional selectivity *Adv. Funct. Mater.* **29** 1901623
[210] Wajahat M, Lee S, Kim J H, Chang W S, Pyo J, Cho S H and Seol S K 2018 Flexible strain sensors fabricated by meniscus-guided printing of carbon nanotube-polymer composites *ACS Appl. Mater. Interfaces* **10** 19999–20005
[211] La T G, Qiu S, Scott D K, Bakhtiari R, Kuziek J W P, Mathewson K E, Rieger J and Chung H J 2018 Two-layered and stretchable e-textile patches for wearable healthcare electronics *Adv. Healthcare Mater.* **7** 1801033
[212] Nge T T, Nogi M and Suganuma K 2013 Electrical functionality of inkjet-printed silver nanoparticle conductive tracks on nanostructured paper compared with those on plastic substrates *J. Mater. Chem.* C **1** 5235–43
[213] Visser C W, Amato D N, Mueller J and Lewis J A 2019 Architected polymer foams via direct bubble writing *Adv. Mater.* **31** 1904668
[214] Stoppa M and Chiolerio A 2014 Wearable electronics and smart textiles: a critical review *Sensors* **14** 11957–92
[215] Gonçalves C, da Silva A F, Gomes J and Simoes R 2018 Wearable e-textile technologies: a review on sensors, actuators and control elements *Inventions* **3** 14
[216] Liao X, Song W, Zhang X, Huang H, Wang Y and Zheng Y 2018 Directly printed wearable electronic sensing textiles towards human-machine interfaces *J. Mater. Chem.* C **6** 12841–8
[217] Carey T, Cacovich S, Divitini G, Ren J, Mansouri A, Kim J M, Wang C, Ducati C, Sordan R and Torrisi F 2017 Fully inkjet-printed two-dimensional material field-effect heterojunctions for wearable and textile electronics *Nat. Commun.* **8** 1202
[218] Choi M K, Yang J, Hyeon T and Kim D-H 2018 Flexible quantum dot light-emitting diodes for next-generation displays *NPJ Flex. Electron.* **2** 10
[219] Howard I A, Abzieher T, Hossain I M, Eggers H, Schackmar F, Ternes S, Richards B S, Lemmer U and Paetzold U W 2019 Coated and printed perovskites for photovoltaic applications *Adv. Mater.* **31** 1806702
[220] Abdi-Jalebi M *et al* 2018 Maximizing and stabilizing luminescence from halide perovskites with potassium passivation *Nature* **555** 497–501
[221] Veldhuis S A, Boix P P, Yantara N, Li M, Sum T C, Mathews N and Mhaisalkar S G 2016 Perovskite materials for light-emitting diodes and lasers *Adv. Mater.* **28** 6804–34
[222] Bao B, Li M, Li Y, Jiang J, Gu Z, Zhang X, Jiang L and Song Y 2015 Patterning fluorescent quantum dot nanocomposites by reactive inkjet printing *Small* **11** 1649–54
[223] Manders J R *et al* 2015 High efficiency and ultra-wide color gamut quantum dot LEDs for next generation displays *J. Soc. Inf. Disp.* **23** 523–8
[224] Yang Z *et al* 2019 Recent advances in quantum dot-based light-emitting devices: challenges and possible solutions *Mater. Today* **24** 69–93
[225] Graham-Rowe D 2009 From dots to devices *Nat. Photon.* **3** 307–9
[226] Choi M K *et al* 2018 Extremely vivid, highly transparent, and ultrathin quantum dot light-emitting diodes *Adv. Mater.* **30** 1703279
[227] Deegan R D, Bakajin O, Dupont T F, Huber G, Nagel S R and Witten T A 1997 Capillary flow as the cause of ring stains from dried liquid drops *Nature* **389** 827–9
[228] Sun L, Yang K, Lin Z, Zhou X, Zhang Y and Guo T 2018 Effects of coffee ring via inkjet printing seed layers on field emission properties of patterned ZnO nanorods *Ceram. Int.* **44** 10735–43
[229] Hu H and Larson R G 2006 Marangoni effect reverses coffee-ring depositions *J. Phys. Chem.* B **110** 7090–4
[230] Kong Y L, Boulogne F, Kim H, Nunes J, Feng J and Stone H A 2015 Deposition of quantum dots in a capillary tube *Langmuir* **31** 12560–6
[231] Boulogne F, Kong Y L, Nunes J K and Stone H A 2016 Effect of the polydispersity of a colloidal drop on drying induced stress as measured by the buckling of a floating sheet *Phys. Rev. Lett.* **116** 238001
[232] Zhang H and Rogers J A 2019 Recent advances in flexible inorganic light emitting diodes: from materials design to integrated optoelectronic platforms *Adv. Opt. Mater.* **7** 1800936
[233] Jiang C, Zhong Z, Liu B, He Z, Zou J, Wang L, Wang J, Peng J and Cao Y 2016 Coffee-ring-free quantum dot thin film using inkjet printing from a mixed-solvent system on modified ZnO transport layer for light-emitting devices *ACS Appl. Mater. Interfaces* **8** 26162–8
[234] Xiong X *et al* 2019 Realizing 17.0% external quantum efficiency in red quantum dot light-emitting diodes by

pursuing the ideal inkjet-printed film and interface *Org. Electron. Phys., Mater. Appl.* **73** 247–54
[235] Azzellino G, Freyria F S, Nasilowski M, Bawendi M G and Bulović V 2019 Micron-scale patterning of high quantum yield quantum dot LEDs *Adv. Mater. Technol.* **4** 1800727
[236] Huckaba A J *et al* 2019 Inkjet-printed mesoporous TiO_2 and perovskite layers for high efficiency perovskite solar cells *Energy Technol.* **7** 317–24
[237] He J, Towers A, Wang Y, Yuan P, Jiang Z, Chen J, Gesquiere A J, Wu S T and Dong Y 2018 *In situ* synthesis and macroscale alignment of $CsPbBr_3$ perovskite nanorods in a polymer matrix *Nanoscale* **10** 15436–41
[238] Mei A *et al* 2014 A hole-conductor-free, fully printable mesoscopic perovskite solar cell with high stability *Science* **345** 295–8
[239] Chen Q *et al* 2018 All-inorganic perovskite nanocrystal scintillators *Nature* **561** 88–93
[240] Zhang C, Wang B, Li W, Huang S, Kong L, Li Z and Li L 2017 Conversion of invisible metal-organic frameworks to luminescent perovskite nanocrystals for confidential information encryption and decryption *Nat. Commun.* **8** 1138
[241] Lin K *et al* 2018 Perovskite light-emitting diodes with external quantum efficiency exceeding 20 per cent *Nature* **562** 245–8
[242] Bade S G R *et al* 2016 Fully printed halide perovskite light-emitting diodes with silver nanowire electrodes *ACS Nano* **10** 1795–801
[243] Zhou N, Bekenstein Y, Eisler C N, Zhang D, Schwartzberg A M, Yang P, Alivisatos A P and Lewis J A 2019 Perovskite nanowire–block copolymer composites with digitally programmable polarization anisotropy *Sci. Adv.* **5** eaav8141
[244] Green M A, Hishikawa Y, Warta W, Dunlop E D, Levi D H, Hohl-Ebinger J and Ho-Baillie A W H 2017 Solar cell efficiency tables (version 50) *Prog. Photovolt. Res. Appl.* **25** 668–76
[245] Wang D, Wright M, Elumalai N K and Uddin A 2016 Stability of perovskite solar cells *Sol. Energy Mater. Sol. Cells* **147** 255–75
[246] Rong Y, Hu Y, Mei A, Tan H, Saidaminov M I, Il S S, McGehee M D, Sargent E H and Han H 2018 Challenges for commercializing perovskite solar cells *Science* **361** 1214
[247] Wang Q, Phung N, Di Girolamo D, Vivo P and Abate A 2019 Enhancement in lifespan of halide perovskite solar cells *Energy Environ. Sci.* **12** 865–86
[248] Lira-Cantú M 2017 Perovskite solar cells: stability lies at interfaces *Nat. Energy* **2** 17115
[249] WHO 2013 Medical device—full definition https://www.who.int
[250] Wood L 2019 Global medical device market 2018 with forecasts to 2023—driven by healthcare expenditure/technological development/aging population/chronic diseases https://www.prnewswire.com
[251] Sharafeldin M, Jones A and Rusling J F 2018 3D-printed biosensor arrays for medical diagnostics *Micromachines* **9** 394
[252] Dekker T J, Steele J R, Federer A E, Hamid K S and Adams S B 2018 Use of patient-specific 3D-printed titanium implants for complex foot and ankle limb salvage, deformity correction, and arthrodesis procedures *Foot Ankle Int.* **39** 916–21
[253] ten Kate J, Smit G and Breedveld P 2017 3D-printed upper limb prostheses: a review *Disabil. Rehabil. Assist. Technol.* **12** 300–14
[254] Leukers B, Gülkan H, Irsen S H, Milz S, Tille C, Schieker M and Seitz H 2005 Hydroxyapatite scaffolds for bone tissue engineering made by 3D printing *J. Mater. Sci., Mater. Med.* **16** 1121–4
[255] Fratzl P and Weinkamer R 2007 Nature's hierarchical materials *Prog. Mater. Sci.* **52** 1263–334
[256] Niinomi M and Nakai M 2011 Titanium-based biomaterials for preventing stress shielding between implant devices and bone *Int. J. Biomater.* **2011** 836587
[257] Paul J P 1999 Strength requirements for internal and external prostheses *J. Biomech.* **32** 381–93
[258] Silvestre J, Silvestre N and De Brito J 2015 An overview on the improvement of mechanical properties of ceramics nanocomposites *J. Nanomater.* **2015** 106494
[259] Tjong S C 2007 Novel nanoparticle-reinforced metal matrix composites with enhanced mechanical properties *Adv. Eng. Mater.* **9** 639–52
[260] Tjong S C 2006 Structural and mechanical properties of polymer nanocomposites *Mater. Sci. Eng.* R **53** 73–197
[261] Sezer H K and Eren O 2019 FDM 3D printing of MWCNT re-inforced ABS nano-composite parts with enhanced mechanical and electrical properties *J. Manuf. Process.* **37** 339–47
[262] Christ J, Aliheidari N, Ameli A and Pötschke P 2017 3D printed highly elastic strain sensors of multiwalled carbon nanotube/thermoplastic nanocomposites *Annual Technical Conf.—ANTEC, Conf. Proc.* **131** 394–401
[263] Zhai X, Ma Y, Hou C, Gao F, Zhang Y, Ruan C, Pan H, Lu W W and Liu W 2017 3D-printed high strength bioactive supramolecular polymer/clay nanocomposite hydrogel scaffold for bone regeneration *ACS Biomater. Sci. Eng.* **3** 1109–18
[264] Yang Y, Chen Z, Song X, Zhang Z, Zhang J, Shung K K, Zhou Q and Chen Y 2017 Biomimetic anisotropic reinforcement architectures by electrically assisted nanocomposite 3D printing *Adv. Mater.* **29** 1605750
[265] Xu W, Molino B Z, Cheng F, Molino P J, Yue Z, Su D, Wang X, Willför S, Xu C and Wallace G G 2019 On low-concentration inks formulated by nanocellulose assisted with gelatin methacrylate (GelMA) for 3D printing toward wound healing application *ACS Appl. Mater. Interfaces* **11** 8838–48
[266] Martin J J, Fiore B E and Erb R M 2015 Designing bioinspired composite reinforcement architectures via 3D magnetic printing *Nat. Commun.* **6** 8641
[267] Serra T, Capelli C, Toumpaniari R, Orriss I R, Leong J J H, Dalgarno K and Kalaskar D M 2016 Design and fabrication of 3D-printed anatomically shaped lumbar cage for intervertebral disc (IVD) degeneration treatment *Biofabrication* **8** 035001
[268] Siqueira G, Kokkinis D, Libanori R, Hausmann M K, Gladman A S, Neels A, Tingaut P, Zimmermann T, Lewis J A and Studart A R 2017 Cellulose nanocrystal inks for 3D printing of textured cellular architectures *Adv. Funct. Mater.* **27** 1604619
[269] Lee J S, Hong J M, Jung J W, Shim J H, Oh J H and Cho D W 2014 3D printing of composite tissue with complex shape applied to ear regeneration *Biofabrication* **6** 024103
[270] Naftulin J S, Kimchi E Y and Cash S S 2015 Streamlined, inexpensive 3D printing of the brain and skull *PLoS One* **10** e0136198
[271] Xu N, Wei F, Liu X, Jiang L, Cai H, Li Z, Yu M, Wu F and Liu Z 2016 Reconstruction of the upper cervical spine using a personalized 3D-printed vertebral body in an adolescent with ewing sarcoma *Spine* **41** E50–4
[272] Abouzeid R E, Khiari R, Beneventi D and Dufresne A 2018 Biomimetic mineralization of three-dimensional printed alginate/TEMPO-oxidized cellulose nanofibril scaffolds for bone tissue engineering *Biomacromolecules* **19** 4442–52
[273] Wilson S A, Cross L M, Peak C W and Gaharwar A K 2017 Shear-thinning and thermo-reversible nanoengineered inks for 3D bioprinting *ACS Appl. Mater. Interfaces* **9** 43449–58
[274] Tong Y *et al* 2019 Low-cost sensor-integrated 3D-printed personalized prosthetic hands for children with amniotic

band syndrome: a case study in sensing pressure distribution on an anatomical human-machine interface (AHMI) using 3D-printed conformal electrode arrays *PLoS One* **14** e0214120
[275] Ma L *et al* 2018 Integrating 3D printing and biomimetic mineralization for personalized enhanced osteogenesis, angiogenesis, and osteointegration *ACS Appl. Mater. Interfaces* **10** 42146–54
[276] Qin X 2016 Coaxial electrospinning of nanofibers *Electrospun Nanofibers* (Amsterdam: Elsevier) pp 41–71
[277] Hench L L and Polak J M 2002 Third-generation biomedical materials *Science* **295** 1014–7
[278] Apelgren P, Karabulut E, Amoroso M, Mantas A, Martínez Ávila H, Kölby L, Kondo T, Toriz G and Gatenholm P 2019 *In vivo* human cartilage formation in three-dimensional bioprinted constructs with a novel bacterial nanocellulose bioink *ACS Biomater. Sci. Eng.* **5** 2482–90
[279] Markstedt K, Mantas A, Tournier I, Martínez Ávila H, Hägg D and Gatenholm P 2015 3D bioprinting human chondrocytes with nanocellulose-alginate bioink for cartilage tissue engineering applications *Biomacromolecules* **16** 1489–96
[280] Narayanan L K, Huebner P, Fisher M B, Spang J T, Starly B and Shirwaiker R A 2016 3D-Bioprinting of polylactic acid (PLA) nanofiber-alginate hydrogel bioink containing human adipose-derived stem cells *ACS Biomater. Sci. Eng.* **2** 1732–42
[281] Barber J G, Handorf A M, Allee T J and Li W J 2013 Braided nanofibrous scaffold for tendon and ligament tissue engineering *Tissue Eng.* A **19** 1265–74
[282] Heo D N, Castro N J, Lee S J, Noh H, Zhu W and Zhang L G 2017 Enhanced bone tissue regeneration using a 3D printed microstructure incorporated with a hybrid nano hydrogel *Nanoscale* **9** 5055–62
[283] Marino A, Barsotti J, De Vito G, Filippeschi C, Mazzolai B, Piazza V, Labardi M, Mattoli V and Ciofani G 2015 Two-photon lithography of 3D nanocomposite piezoelectric scaffolds for cell stimulation *ACS Appl. Mater. Interfaces* **7** 25574–9
[284] He J, Xu F, Dong R, Guo B and Li D 2017 Electrohydrodynamic 3D printing of microscale poly (ε-caprolactone) scaffolds with multi-walled carbon nanotubes *Biofabrication* **9** 1–10
[285] Bayraktar I, Doganay D, Coskun S, Kaynak C, Akca G and Unalan H E 2019 3D printed antibacterial silver nanowire/polylactide nanocomposites *Composites* B **172** 671–8
[286] Pajala A, Kangas J, Siira P, Ohtonen P and Leppilahti J 2009 Augmented compared with nonaugmented surgical repair of a fresh total achilles tendon rupture: a prospective randomized study *J. Bone Jt. Surg.* A **91** 1092–100
[287] Laurencin C T and Freeman J W 2005 Ligament tissue engineering: an evolutionary materials science approach *Biomaterials* **26** 7530–6
[288] Kolan K, Liu Y, Baldridge J, Murphy C, Semon J, Day D and Leu M 2017 Solvent based 3D printing of biopolymer/bioactive glass composite and hydrogel for tissue engineering applications *Proc. CIRP* **65** 38–43
[289] VanEpps J S and Younger J G 2016 Implantable device-related infection *Shock* **46** 597–608
[290] Choi J, Kwon O C, Jo W, Lee H J and Moon M W 2015 4D printing technology: a review *3D Print. Addit. Manuf.* **2** 159–67
[291] Kuang X, Roach D J, Wu J, Hamel C M, Ding Z, Wang T, Dunn M L and Qi H J 2019 Advances in 4D printing: materials and applications *Adv. Funct. Mater.* **29** 1805290
[292] Piedade A P 2019 4D printing: the shape-morphing in additive manufacturing *J. Funct. Biomater.* **10** 9
[293] Cui H, Miao S, Esworthy T, Jun L S, Zhou X, Hann S Y, Webster T J, Harris B T and Zhang L G 2019 A novel near-infrared light responsive 4D printed nanoarchitecture with dynamically and remotely controllable transformation *Nano Res.* **12** 1381–8
[294] Guo Y, Belgodere J A, Ma Y, Jung J P and Bharti B 2019 Directed printing and reconfiguration of thermoresponsive silica-pNIPAM nanocomposites *Macromol. Rapid Commun.* **40** 1970028
[295] Thakur N, Baji A and Ranganath A S 2018 Thermoresponsive electrospun fibers for water harvesting applications *Appl. Surf. Sci.* **433** 1018–24
[296] Lin Q, Li L, Tang M, Hou X and Ke C 2018 Rapid macroscale shape morphing of 3D-printed polyrotaxane monoliths amplified from pH-controlled nanoscale ring motions *J. Mater. Chem.* C **6** 11956–60
[297] Bozuyuk U, Yasa O, Yasa I C, Ceylan H, Kizilel S and Sitti M 2018 Light-triggered drug release from 3D-printed magnetic chitosan microswimmers *ACS Nano* **12** 9617–25
[298] Tiwari A P, Hwang T I, Oh J M, Maharjan B, Chun S, Kim B S, Joshi M K, Park C H and Kim C S 2018 PH/NIR-responsive polypyrrole-functionalized fibrous localized drug-delivery platform for synergistic cancer therapy *ACS Appl. Mater. Interfaces* **10** 20256–70
[299] Ding Y, Li W, Zhang F, Liu Z, Zanjanizadeh Ezazi N, Liu D and Santos H A 2019 Electrospun fibrous architectures for drug delivery, tissue engineering and cancer therapy *Adv. Funct. Mater.* **29** 1–35
[300] Shahriar S, Mondal J, Hasan M, Revuri V, Lee D and Lee Y-K 2019 Electrospinning nanofibers for therapeutics delivery *Nanomaterials* **9** 532
[301] Gladman A S, Matsumoto E A, Nuzzo R G, Mahadevan L and Lewis J A 2016 Biomimetic 4D printing *Nat. Mater.* **15** 413–8
[302] Niiyama E, Uto K, Lee C M, Sakura K and Ebara M 2018 Alternating magnetic field-triggered switchable nanofiber mesh for cancer thermo-chemotherapy *Polymers* **10** 1–13
[303] Zhu P, Yang W, Wang R, Gao S, Li B and Li Q 2018 4D Printing of complex structures with a fast response time to magnetic stimulus *ACS Appl. Mater. Interfaces* **10** 36435–42
[304] Wei H, Zhang Q, Yao Y, Liu L, Liu Y and Leng J 2017 Direct-write fabrication of 4D active shape-changing structures based on a shape memory polymer and its nanocomposite *ACS Appl. Mater. Interfaces* **9** 876–83
[305] Tarabella G, Coppedè N, Iannotta S, Cicoira F, Kumar P and Santato C 2013 Organic bioelectronics *Handbook of Organic Materials for Optical and (Opto) Electronic Devices: Properties and Applications* pp 597–617
[306] Parent A 2004 Giovanni Aldini: from animal electricity to human brain stimulation *Can. J. Neurol. Sci.* **31** 576–84
[307] Owens R M and Malliaras G G 2010 Organic electronics at the interface with biology *MRS Bull.* **35** 449–56
[308] Simon D T, Gabrielsson E O, Tybrandt K and Berggren M 2016 Organic bioelectronics: bridging the signaling gap between biology and technology *Chem. Rev.* **116** 13009–41
[309] Zhang A and Lieber C M 2016 Nano-bioelectronics *Chem. Rev.* **116** 215–57
[310] Denuault G 1991 Microelectrodes: theory and applications *J. Electroanal. Chem. Interfacial Electrochem.* **315** 320–1
[311] Kringelbach M L, Jenkinson N, Owen S L F and Aziz T Z 2007 Translational principles of deep brain stimulation *Nat. Rev. Neurosci.* **8** 623–35
[312] Someya T, Bao Z and Malliaras G G 2016 The rise of plastic bioelectronics *Nature* **540** 379–85
[313] Svennersten K, Larsson K C, Berggren M and Richter-Dahlfors A 2011 Organic bioelectronics in nanomedicine *Biochim. Biophys. Acta—Gen. Subjects* **1810** 276–85

[314] Duan X and Lieber C M 2015 Nanoscience and the nano-bioelectronics frontier *Nano Res.* **8** 1–22

[315] Katz E and Willner I 2004 Biomolecule-functionalized carbon nanotubes: applications in nanobioelectronics *ChemPhysChem* **5** 1084–104

[316] Khodagholy D, Doublet T, Gurfinkel M, Quilichini P, Ismailova E, Leleux P, Herve T, Sanaur S, Bernard C and Malliaras G G 2011 Highly conformable conducting polymer electrodes for *in vivo* recordings *Adv. Mater.* **23** H268–72

[317] Viventi J *et al* 2011 Flexible, foldable, actively multiplexed, high-density electrode array for mapping brain activity *in vivo Nat. Neurosci.* **14** 1599–605

[318] Yang H, Rahman M T, Du D, Panat R and Lin Y 2016 3D printed adjustable microelectrode arrays for electrochemical sensing and biosensing *Sensors Actuators* B **230** 600–6

[319] Kundu A, Nattoo C, Fremgen S, Springer S, Ausaf T and Rajaraman S 2019 Optimization of makerspace microfabrication techniques and materials for the realization of planar, 3D printed microelectrode arrays in under four days *RSC Adv.* **9** 8949–63

[320] Schnitker J, Adly N, Seyock S, Bachmann B, Yakushenko A, Wolfrum B and Offenhäusser A 2018 Rapid prototyping of ultralow-cost, inkjet-printed carbon microelectrodes for flexible bioelectronic devices *Adv. Biosyst.* **2** 1700136

[321] Ruz-Nuglo F D and Groven L J 2018 3D printing and development of fluoropolymer based reactive inks *Adv. Eng. Mater.* **20** 1700390

[322] Hayyan M, Mjalli F S, Hashim M A, AlNashef I M and Mei T X 2013 Investigating the electrochemical windows of ionic liquids *J. Ind. Eng. Chem.* **19** 106–12

[323] Qazi T H, Rai R and Boccaccini A R 2014 Tissue engineering of electrically responsive tissues using polyaniline based polymers: a review *Biomaterials* **35** 9068–86

[324] Ghasemi-Mobarakeh L, Prabhakaran M P, Morshed M, Nasr-Esfahani M H, Baharvand H, Kiani S, Al-Deyab S S and Ramakrishna S 2011 Application of conductive polymers, scaffolds and electrical stimulation for nerve tissue engineering *J. Tissue Eng. Regen. Med.* **5** e17–35

[325] Rajabi A H, Jaffe M and Arinzeh T L 2015 Piezoelectric materials for tissue regeneration: a review *Acta Biomater.* **24** 12–23

[326] Chen M C, Sun Y C and Chen Y H 2013 Electrically conductive nanofibers with highly oriented structures and their potential application in skeletal muscle tissue engineering *Acta Biomater.* **9** 5562–72

[327] Bolin M H, Svennersten K, Wang X, Chronakis I S, Richter-Dahlfors A, Jager E W H and Berggren M 2009 Nano-fiber scaffold electrodes based on PEDOT for cell stimulation *Sensors Actuators* B **142** 451–6

[328] Jin G, Li J and Li K 2017 Photosensitive semiconducting polymer-incorporated nanofibers for promoting the regeneration of skin wound *Mater. Sci. Eng.* C **70** 1176–81

[329] Wang L, Wu Y, Hu T, Guo B and Ma P X 2017 Electrospun conductive nanofibrous scaffolds for engineering cardiac tissue and 3D bioactuators *Acta Biomater.* **59** 68–81

[330] Tanaka Y, Morishima K, Shimizu T, Kikuchi A, Yamato M, Okano T and Kitamori T 2006 Demonstration of a PDMS-based bio-microactuator using cultured cardiomyocytes to drive polymer micropillars *Lab Chip* **6** 230–5

[331] Park S J *et al* 2016 Phototactic guidance of a tissue-engineered soft-robotic ray *Science* **353** 158–62

[332] Yoon J, Eyster T W, Misra A C and Lahann J 2015 Cardiomyocyte-driven actuation in biohybrid microcylinders *Adv. Mater.* **27** 4509–15

[333] Liu Y, Cui H, Zhuang X, Wei Y and Chen X 2014 Electrospinning of aniline pentamer-graft-gelatin/PLLA nanofibers for bone tissue engineering *Acta Biomater.* **10** 5074–80

[334] Malhotra B D and Pandey C M 2017 *Biosensors: Fundamentals and Applications* (Shrewsbury: Smithers Rapra)

[335] Willner I and Katz E 2005 *Biolectronics: From Theory to Applications* (New York: Wiley)

[336] Zhang D and Liu Q 2016 Biosensors and bioelectronics on smartphone for portable biochemical detection *Biosens. Bioelectron.* **75** 273–84

[337] Willner I, Katz E and Willner B 1997 Electrical contact of redox enzyme layers associated with electrodes: routes to amperometric biosensors *Electroanalysis* **9** 965–77

[338] Wang J 2008 Electrochemical glucose biosensors *Chem. Rev.* **108** 814–25

[339] Yoo E H and Lee S Y 2010 Glucose biosensors: an overview of use in clinical practice *Sensors* **10** 4558–76

[340] Su C K and Chen J C 2018 One-step three-dimensional printing of enzyme/substrate-incorporated devices for glucose testing *Anal. Chim. Acta* **1036** 133–40

[341] Otieno B A, Krause C E, Jones A L, Kremer R B and Rusling J F 2016 Cancer diagnostics via ultrasensitive multiplexed detection of parathyroid hormone-related peptides with a microfluidic immunoarray *Anal. Chem.* **88** 9269–75

[342] Carvajal S, Fera S N, Jones A L, Baldo T A, Mosa I M, Rusling J F and Krause C E 2018 Disposable inkjet-printed electrochemical platform for detection of clinically relevant HER-2 breast cancer biomarker *Biosens. Bioelectron.* **104** 158–62

[343] Pavinatto F J, Paschoal C W A and Arias A C 2015 Printed and flexible biosensor for antioxidants using interdigitated ink-jetted electrodes and gravure-deposited active layer *Biosens. Bioelectron.* **67** 553–9

[344] Lee W, Kwon D, Choi W, Jung G Y, Au A K, Folch A and Jeon S 2015 3D-Printed micro fluidic device for the detection of pathogenic bacteria using size-based separation in helical channel with trapezoid cross-section *Sci. Rep.* **5** 7717

[345] Li B, Tan H, Anastasova S, Power M, Seichepine F and Yang G Z 2019 A bio-inspired 3D micro-structure for graphene-based bacteria sensing *Biosens. Bioelectron.* **123** 77–84

[346] Adly N, Feng L, Krause K J, Mayer D, Yakushenko A, Offenhäusser A and Wolfrum B 2017 Flexible microgap electrodes by direct inkjet printing for biosensing application *Adv. Biosyst.* **1** 1600016

[347] Lesch A, Cortés-Salazar F, Amstutz V, Tacchini P and Girault H H 2015 Inkjet printed nanohydrogel coated carbon nanotubes electrodes for matrix independent sensing *Anal. Chem.* **87** 1026–33

[348] Jović M, Zhu Y, Lesch A, Bondarenko A, Cortés-Salazar F, Gumy F and Girault H H 2017 Inkjet-printed microtiter plates for portable electrochemical immunoassays *J. Electroanal. Chem.* **786** 69–76

[349] Dittrich P S and Manz A 2006 Lab-on-a-chip: microfluidics in drug discovery *Nat. Rev. Drug Discovery* **5** 210–8

[350] Herold K E and Rasooly A 2009 *Lab on a Chip Technology: Fabrication and Microfluidics* (Poole: Caister Academic Press)

[351] Moya A, Ortega-Ribera M, Guimerà X, Sowade E, Zea M, Illa X, Ramon E, Villa R, Gracia-Sancho J and Gabriel G 2018 Online oxygen monitoring using integrated inkjet-printed sensors in a liver-on-a-chip system *Lab Chip* **18** 2023–35

[352] Ho C M B, Ng S H, Li K H H and Yoon Y J 2015 3D printed microfluidics for biological applications *Lab Chip* **15** 3627–37

[353] Au A K, Huynh W, Horowitz L F and Folch A 2016 3D-printed microfluidics *Angew. Chem., Int. Ed.* **55** 3862–81

[354] Waheed S, Cabot J M, Macdonald N P, Lewis T, Guijt R M, Paull B and Breadmore M C 2016 3D printed microfluidic devices: enablers and barriers *Lab Chip* **16** 1993–2013
[355] Elgetti Brodersen K, Koren K, Lichtenberg M and Kühl M 2016 Nanoparticle-based measurements of pH and O2 dynamics in the rhizosphere of Zostera marina L.: effects of temperature elevation and light-dark transitions *Plant Cell Environ.* **39** 1619–30
[356] Cai H, Xu Y, Zhu N, He P and Fang Y 2002 An electrochemical DNA hybridization detection assay based on a silver nanoparticle label *Analyst* **127** 803–8
[357] Dequaire M, Degrand C and Limoges B 2000 An electrochemical metalloimmunoassay based on a colloidal gold label *Anal. Chem.* **72** 5521–8
[358] Yeom S H, Kang B H, Kim K J and Kang S W 2011 Nanostructures in biosensor-a review *Front. Biosci.* **16** 997–1023
[359] Trampe E, Koren K, Akkineni A R, Senwitz C, Krujatz F, Lode A, Gelinsky M and Kühl M 2018 Functionalized bioink with optical sensor nanoparticles for O2 imaging in 3D-bioprinted constructs *Adv. Funct. Mater.* **28** 1804411